

Sediment transport over sills of longitudinal training dams

Master of Science Thesis report
S.M.M. (Stefan) Jammers
April 2017



Sediment transport over sills of longitudinal training dams

by

S.M.M. (Stefan) Jammers

to obtain the degree of Master of Science

at Delft University of Technology and the National University of Singapore,

to be defended publicly on Friday April 28th, 2017 at 10:00 AM (UTC+2).

Student number: 4143353 (TUD) A0134116 (NUS)

Thesis committee:	Prof. dr. ir. W.S.J. UIJTTEWAAL,	Delft University of Technology, chair
	Dr. ir. E. MOSSELMAN,	Delft University of Technology, Deltares
	Dr. ir. R.J. LABEUR,	Delft University of Technology
	Dr. ir. A.J. PAARLBERG,	HKV Consultants
	Dr. ir. W. OTTEVANGER,	Deltares
	Dr. V. CHUA,	National University of Singapore

An electronic version of this thesis is available at <http://repository.tudelft.nl/>.

Summary

Longitudinal training dams have been constructed in the River Waal in the Netherlands in 2015. These dams separate the river in two channels: a main channel and a side channel. The design of the dam is unique in Dutch hydraulic engineering work and it is expected to fulfil multiple functions at once. This structure aims at improving ecology, high/low water safety and navigation.

At the upstream opening of the longitudinal training dam a fixed sill is situated. This sill is designed to regulate the distribution of water and sediment between both channels. However, the effect of the sills on the bed load sediment transport is not well understood. Moreover, the models that are available nowadays are not suitable to predict the sediment transport over these sills. Therefore no accurate morphological predictions of the side channel can be made.

The crest of the longitudinal-training-dam sills are aligned with the downstream direction. The bifurcation that occurs can be considered as a local widening of the river. At this bifurcation water enters the side channel and thus there is a flow component in both longitudinal direction and transverse direction. The configuration of the sill and the local flow situation affect the critical conditions under which sediment starts moving. This thesis describes how the geometry and the flow situation influence these conditions.

Once it is understood how the geometry and the flow situation affect the critical conditions of sediment transport, the next step is to investigate how the sediment is transported over the sill. The trajectory of individual sediment particles is used to develop an understanding of how the sediment is actually transported over the sill. Based on the forces that act on an individual grain, the equations of motion are established. In a so-called ‘particle model’, the equations of motion are solved and the path a sediment particle follows is predicted.

The particle model is verified with the use of a uniform flow field. In this field a constant mean flow velocity in the main channel is assumed, together with a certain flow angle and a fixed water level. It is observed that sediment motion is likely to be initiated in the River Waal for various discharges. However, transport to the side channel depends on the initial condition, the slope of the sill and the flow angle that is selected. Only for a number of combinations of the slope of the sill and the flow angle sediment transport takes place over the sill.

In reality a uniform flow field is not very realistic. Flow separation and eddy formation might induce a more ‘complicated’ flow field. The numerical flow model Delft3D is used to generate a more realistic flow field around the sill. The water levels, depth-averaged flow velocities and depth-averaged flow angles of the numerical model are coupled to the particle model to investigate how sediment is transported over the sill.

It is found that the geometry of the sill influences the conditions under which sediment is transported over the sill. An increase in the steepness of the slope of the sill reduces the sediment transport over the sill. Furthermore, for mild slopes the sediment particles need to overcome a larger distance in transverse direction to be transported over the sill. Finally, it appears that there is no linear relation between the flow and the sediment transport over the sill.

Samenvatting

In 2015 zijn in de Nederlandse rivier de Waal langsdammen aangelegd. Deze dammen scheiden de rivier in twee geulen, een hoofdgeul en een oevergeul. Het ontwerp is een uniek Nederlands waterbouwkundig ontwerp en vervult meerdere functies tegelijkertijd. Dit kunstwerk richt zich op het verbeteren van de ecologie, hoog/laagwaterveiligheid en scheepsvaart.

Aan de bovenstroomse opening van de langsdammen ligt een drempel op de bodem van de rivier. Deze drempel is ontworpen om de verdeling van water en sediment in beide geulen te reguleren. Het effect van deze drempel op het bodemsedimenttransport wordt echter tot op heden nog niet goed begrepen. De modellen die tegenwoordig gebruikt worden kunnen het sedimenttransport over de drempel ook niet goed voorspellen. Daarom kunnen er ook geen accurate morfologische voorspellingen van de oevergeul gemaakt worden.

De langsdamdrempels hebben een kruin parallel aan de benedenstroomse (longitudinale) richting van de rivier. De splitsing die ontstaat kan worden beschouwd als een lokale verwijding van de rivier. Op het splitsingspunt gaat water de oevergeul in en dus moet er een stromingscomponent in zowel longitudinale als transversale richting zijn. Gelet op de configuratie van de drempel en de lokale stromings situatie, worden de kritische condities waaronder sediment begint te bewegen aangepast. In deze thesis is beschreven hoe de geometrie en de stromings situatie deze condities beïnvloedt.

Indien eenmaal begrepen wordt hoe de kritische condities van het sediment transport veranderen, dan is de volgende stap om te onderzoeken hoe het sediment over de drempel getransporteerd wordt. Het pad van een individueel sedimentdeeltje is gebruikt om te begrijpen hoe het sediment over de drempel wordt getransporteerd. Gebaseerd op krachtenbalansen die werken op een individuele korrel zijn bewegingsvergelijkingen opgesteld. In het zogenoemde deeltjesmodel worden de bewegingsvergelijkingen opgelost en wordt daarmee het pad dat een deeltje volgt voorspeld.

Dit model is geverifieerd met behulp van een uniform stromingsveld. In dit veld is een constant gemiddelde stroomsnelheid in de hoofdgeul aangenomen samen met een bepaalde stromingshoek en een vastgesteld waterniveau. Het bleek dat begin van beweging onder alle stromingscondities in de Waal voorkomt. Desalniettemin wordt het transport naar de oevergeul over de drempel beïnvloed door de initiële condities, de steilheid van de drempel en de stromingshoek. Enkel voor een bepaald aantal combinaties van de steilheid van de drempel en de stromingshoek zal transport over de drempel plaatsvinden.

In werkelijkheid is een uniform stromingsveld niet realistisch, loslating van de stroming en wervelingen veroorzaken een meer gecompliceerd stromingsveld. Het numerieke stromingsmodel Delft3D is gebruikt om een meer realistisch stromingsveld te creëren. De waterstanden, stroomsnelheden en stromingshoeken werden bepaald om in te schatten hoe het sediment wordt getransporteerd over de drempel.

De geometrie van de drempel is van invloed is op de condities waaronder het sediment getransporteerd wordt over de drempel. Een toename van de steilheid van de drempel leidt tot een vermindering van het sedimenttransport over de drempel. Daarnaast komt naar voren dat voor

vrij vlakke hellingen de sedimentkorrels een grotere afstand afleggen om over de drempel heen getransporteerd te worden, door de geometrie van de drempel. Tenslotte blijkt dat er geen lineair verband is tussen de stroming en het sediment dat over de drempel wordt getransporteerd.

Preface

*“Do not go where the path may lead,
go instead where there is no path and leave a trail.”*

—Ralph Waldo Emerson (1803-1882)

In this master thesis, my graduation work on sediment transport over sills of longitudinal training dams is presented. This thesis is the final product of my master Hydraulic Engineering and Water Resources Management at Delft University of Technology and the National University of Singapore. I have carried out this thesis in cooperation with HKV Consultants and Deltares.

I am grateful to my academic supervisors for their guidance during the process. Wim Uijttewaal, during our discussions you inspired me by showing connections which I did not see at first sight. Thank you for your trust, patience and time. Andries Paarlberg, I really enjoyed our biweekly meetings on Monday mornings, we always started with discussing the weekend before continuing to talk about work. You encouraged me to contact people and share knowledge wherever possible. Thank you for your encouragement and understanding throughout my graduation. Robert Jan Labeur, I asked you to join my thesis committee, because I very much enjoyed our fruitful conversations during my additional thesis. Your constructive view on my work has definitely been helpful throughout the process of writing this thesis, but also in becoming an engineer. Erik Mosselman, you introduced me to the subject of longitudinal training dams. Your advise has been very helpful during the graduation and your corrections really helped to perfect my English. Willem Ottevanger, if I had numerical problems that frustrated me profoundly I could always reach out to you. Thank you for being so accessible. Vivien Chua, thank you for your involvement as my Singaporean supervisor. Your lectures formed a good basis for a proper understanding of the numerical software I used, and therefore I am glad that you joined my committee.

Thanks to HKV Consultants and Deltares for the close collaboration with you. I would like to thank all my colleagues for the nice chats we had during lunch, coffee breaks, short afternoon walks and even the drinks in the bars. A special thanks to my sparring partner Bart van Linge, whom it was great to work with. I have very fond memories of our trips to companies and the field.

The NCR-meetings have been inspiring events to me, to hear and see all the innovative ideas of the Dutch river engineers. Special thanks to Henk Eerden and Adri Wagener (Rijkswaterstaat) for providing data on the longitudinal training dams and organising visits to the field. I would also like to thank Timo de Ruijscher and Frank Collas for your involvement, it was very inspiring to talk with you about our researches.

My study has been an interesting and challenging journey, during which I have explored many different fields within civil engineering at various locations around the world. Along this exciting path I could always count on the support of my parents. You provided the financial and moral

support for all the decisions I have made throughout my study; I am greatly indebted to you, mom and dad. I also wish to express my gratitude to the rest of my family: Oma, Yvonne, Antony and Victor.

Studying in Delft and overseas has always felt as a privilege and an honour to me. I wish to thank my friends from all around the world, for the nice discussions we had about the things that matter in life. You were the ones that made every day count. A special thanks to Teije van der Horst and Odile Smith for putting so much effort in reading through my thesis and critically reviewing my work.

Finally, I want to express my deepest gratitude to my boyfriend, Timo, for your love and support. Your unyielding support pulled me through difficult times, it felt as we were in this together. Thank you for your patience to listen to my talks about longitudinal training dams, sediment transport and my frustrations with my models. Your devotion and critical questions on what I was doing, resulted in the best discussions. Sincerely thanks for everything my dear.

Stefan Jammers
Delft, April 28th, 2017

In memory of *Annelies Kolk*.

Two days we walked this path together, then we
went separate ways instead.

Thank you for your encouragement, trust and
devotion.

I dedicate my work to you.

Contents

1	Introduction	1
1.1	Context	1
1.1.1	Historical overview of Dutch river system	1
1.1.2	Problems in River Waal	1
1.1.3	Longitudinal training dams	2
1.1.4	Sill in openings of longitudinal training dam	3
1.2	Problem description	4
1.3	Research question	5
1.4	Methodology	5
1.5	Related research	5
1.6	Reading guide	6
2	Background information	7
2.1	Introduction	7
2.2	Design of longitudinal training dams	7
2.3	Flow situation in River Waal	11
2.4	Field data in River Waal	11
2.4.1	Flow in River Waal	12
2.4.2	Bed topography River Waal	12
2.5	Sediment transport in general	14
2.6	Criteria for initiation of sediment motion	14
2.6.1	Correction initiation of motion for transverse slope	16
2.6.2	Correction initiation of motion for flow alignment	18
2.7	Sediment motion	20
2.7.1	Forces on sediment particle	21
2.7.2	Streamwise side slope experiments	22
2.8	Scope of research	23
2.9	Key points of this chapter	23
3	Set-up of conceptual particle model	25
3.1	Introduction	25
3.2	Schematisation of river bed in particle model	26
3.3	Distribution of flow	27
3.4	Initiation of motion of sill slope	29
3.4.1	Relation between sill slope and flow angle	30
3.4.2	Relation between sill slope and relative depth	30
3.4.3	Intermediate conclusions	32
3.5	Particle model	32
3.6	Reflection on particle model	36
3.7	General applicability of particle model	37
3.8	Key points of this chapter	37

4	Verification of particle model with uniform flow field	39
4.1	Introduction	39
4.2	Verification cases of particle model	40
4.3	Minimum flow angle	41
4.4	Initiation of motion	42
4.5	Results	43
4.5.1	Combining initiation of motion with transport over sill	43
4.5.2	Test cases aligned flow and unaligned flow	44
4.5.3	Other results	46
4.6	Key points of this chapter	47
5	Application of particle model with non-uniform flow field	49
5.1	Introduction	49
5.2	Generating a non-uniform flow field	49
5.2.1	Boundary conditions	49
5.2.2	Water level field	50
5.2.3	Flow velocity field	51
5.2.4	Flow velocity angle field	51
5.3	Results	52
5.3.1	Water level	52
5.3.2	Flow velocity and flow angle	52
5.3.3	Bed configuration of the sill	54
5.4	Bifurcation relations	57
5.5	Key points of this chapter	58
6	Discussion	61
7	Conclusions and recommendations	65
7.1	Conclusions	65
7.2	Recommendations	67
	References	69
	Appendix	71
A	Incipient motion of sediment particles	71
A.1	Introduction	71
A.2	Incipient motion on horizontal bed	71
A.3	Incipient motion on inclined bed	74
A.4	Incipient motion on a side slope with aligned flow	76
A.5	Incipient motion on a side slope with unaligned flow	79
B	Derivations of correction factors for critical Shields parameter	83
B.1	Relative critical Shields parameter on streamwise sloping bed	84
B.2	Relative critical Shields parameter on streamwise side slope	85
B.3	Translation between two coordinate systems	87
B.4	Relative critical Shields parameter on non-streamwise side slope	88
B.5	Comparing section B.4 with literature	90
C	Additional information on particle model	93
C.1	Introduction	93
C.2	Parameters	93
C.3	Control volume	94
C.4	Velocities	95
C.5	Boundary conditions	95

D Set-up of numerical Delft3D FLOW model	97
D.1 Introduction	97
D.2 Set-up of model	98
D.2.1 Grid refinement	98
D.2.2 Time step	98
D.2.3 Spin-up time	99
D.3 Indetermination	101
D.4 Additional information	101
D.5 Coupling with particle model	103

Chapter 1

Introduction

1.1 Context

1.1.1 Historical overview of Dutch river system

The Netherlands is a country whose name already suggests that it is situated in a delta region. River deltas can be characterised as flat, have meandering rivers and form a transition of the upper reaches of a river towards the sea. Bifurcations are often found in these river deltas, which lead to a characteristic geo-morphological landscape. The rivers do not only discharge water, but they also carry sediments and ice towards the sea.

Already in the Middle Ages humans started intervening in the Dutch river system. The natural behaviour of a river delta with bifurcations and meandering rivers thereby disappeared from the landscape. River banks were fixed and land was reclaimed. This was done using so-called regulation structures (e.g. groynes) to steer the flow and keep the river navigable by increasing the flow velocity to prevent sand banks to develop. From Figure 1.1 it can be seen that the Rivers Rhine and Meuse are nowadays the most dominant rivers in the Netherlands and that there are only a few branches left.

In the 19th century groynes have become characteristic elements along the Dutch rivers. River groynes are created perpendicularly to the riverbanks and have had a major impact on the river morphology. Originally, river groynes were designed to prevent ice dams to occur in the rivers since ice dams used to be the main cause of dike failures (Rijkswaterstaat, 2012). Additional advantage of river groynes is reducing dredging works. Dredging works are usually necessary for keeping the river navigable for shipping.

1.1.2 Problems in River Waal

The River Rhine, average discharge of 2200 m³/s at Lobith, bifurcates into the River Waal and the Pannerden Canal, with a discharge distribution of approximately 2/3 and 1/3 respectively. In the River Waal the groynes keep the river in place and guarantee a navigable depth. However, over the past century a bed level degradation trend of the river bed was observed, i.e. erosion of the river bed took place and the river bed became deeper. This leads to instabilities of hydraulic structures, such as groynes.



Figure 1.1: Map of the current Dutch river system. Source: www.mapsofworld.com

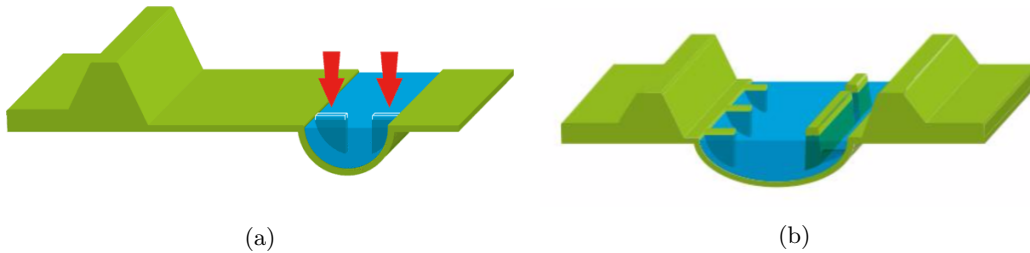


Figure 1.2: Room for the River measures in the River Waal: (a) lowering groynes and (b) construction of longitudinal training dams. Source: Room for the River.

Moreover, since the river bed became deeper, groynes emerged more often than necessary and form obstacles during high water discharges. Thereby they reduce the discharge capacity of the river (Liefveld et al., 2011). Emerged groynes result in a smaller conveyance area, leading to higher flow velocities, thereby causing more bed degradation. Eventually this leads to a positive feedback loop, in which the process of bed degradation is reinforcing itself. Therefore two substitutional measures were taken along the River Waal: (I) the crest of groynes were lowered (see Figure 1.2a) and (II) groynes were removed and longitudinal training dams were constructed (see Figure 1.2b and subsection 1.1.3). Both measures pertained to the Room for the River programme¹.

1.1.3 Longitudinal training dams

Longitudinal training dams are a unique and new type of hydraulic structure in the Dutch river system. They are located at the inner side of a river bend where the depth of the river is more shallow and hence reduces hindrance to shipping. The longitudinal training dams are made of a sand body and a top layer of rubble. They have been constructed near the toe of the former groynes. The longitudinal training dams divide the river into a main channel and side channel. In

¹The Room for the River programme started in 2006 and was completed in 2016. It aimed at creating more space for the river during high river discharges.

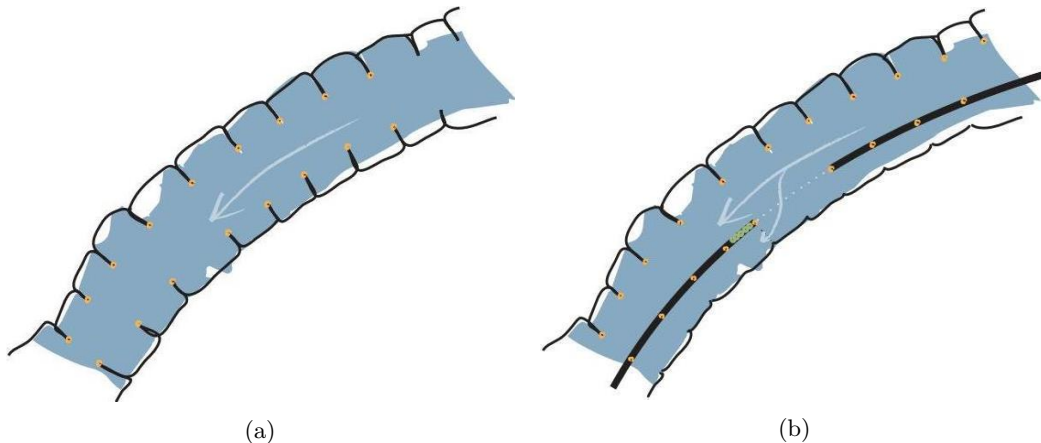


Figure 1.3: In (a) the old situation with only groynes is sketched, while in (b) longitudinal training dams have been constructed at the inner side of the river bend. Source: Rijkswaterstaat (2011).

Figure 1.3a the ‘old’ situation is schematised where there are only river groynes present, whereas Figure 1.3b shows the ‘new’ situation with the two channels separated by a longitudinal training dam. At strategic locations openings have been made to manage the distribution of water and sediments. The openings have been filled with rubble stones functioning as a sill, to keep the river navigable at low discharges. By regulating the distribution of sediments, river managers can control the morphological evolution of the river bed in both channels. Three longitudinal training dams have been completed between Tiel and Zaltbommel since 2015. Figure 1.4 shows a design sketch of an longitudinal training dam. Typical lengths of a longitudinal training dam is 3 km.

Longitudinal training dams are investigated within the scope of the ‘RiverCare’ research programme (Rivercare, 2016). This programme aims at improving the knowledge related to the consequences of the Room for the River and the Delta programmes². During the exploratory phase of the longitudinal training dams design, the effects of the openings have been investigated in a study by Huthoff et al. (2011). In this study the openings were completely opened and completely closed, to investigate the control range of the longitudinal training dams on the discharge distribution and the morphological changes.

1.1.4 Sill in openings of longitudinal training dam

Sills downstream of the inlet have a crest height below the crest of the longitudinal training dam and above OLR³. These sills are expected to be submerged only a couple of days per year. At the upstream end of the longitudinal training dam an inlet sill is located, below OLR, i.e. this inlet sill is (almost) always submerged. The current crest height of the sill is at OLR -1.25 m and has a transverse slope on both sides of 1:2.5, but in the future other configurations of this sill are also possible.

Since the inlet sill is generally submerged, it allows for the distribution of water and sediment. Understanding the distribution processes at the inlet sill is necessary in order to predict the hydraulic and morphological effect of the longitudinal training dam on the river system.

²The Dutch Delta programme started in 2010 and aims at protecting the land from flooding, reducing fresh water shortage and preparing for climate change.

³OLR means ‘Overeengekomen Lage Rivierwaterstand’ or ‘Agreed Lower River Level’ which is a minimum water level in the river that the government guarantees in the branches of the River Rhine.

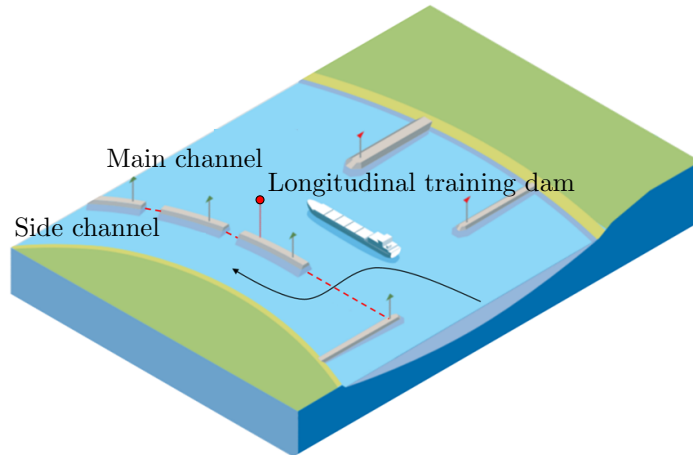


Figure 1.4: Sketch of longitudinal training dam, with side channel and main channel. Black arrow indicates the flow direction towards the side channel. The dashed line at the inlet indicates the submerged sill. Downstream of the inlet two emerged sills are sketched. Source: Ruimte voor de Rivier.

1.2 Problem description

Huthoff et al. (2011) applied the DVR model⁴ to estimate the hydraulic and morphological effects of the construction of the longitudinal training dams. This model is often applied to estimate the morphological response of the river bed, of the branches of the River Rhine and to human interventions (e.g. dredging works or construction of hydraulic structures). One of the shortcomings of this model is that some areas in the river branches have to be considered as morphologically inactive (e.g. groyne fields) since the morphological processes are not well understood at these locations. This type of model shortcomings could lead to erroneous predictions on navigability depth and dredging works, which might eventually result in unnecessary costs. To improve these model concepts it is essential to investigate the possible shortcomings.

As discussed earlier, the inlet sill is expected to be responsible for the distribution of water and sediment. According to Huthoff et al. (2011), during the modelling phase of the longitudinal training dam project it was uncertain what the effect of the sill/weir would be on the distribution of sediment. The side channel of the longitudinal training dam project was therefore considered as morphologically inactive in the DVR-model. The inlet sill was implemented as subgrid weirs. Subgrid weirs are numerical model features that are often used because the grid sizes in the DVR-model are too large (order of 40x10 m) to include the geometry of the structures in the bed topography. Sediment transport over the sill was not modelled. Monitoring would take place in the field in order to observe the effect of the sills in practice.

Monitoring is very useful in practice to get a feeling of how to steer the sediment distribution. However, the physical background concerning this distribution of sediment is unknown therefore the side channel is currently considered to be morphologically inactive. In order to understand the physical processes that play a role in the distribution, it must be understood how sediment is transported over a longitudinal-training-dam sill. This knowledge can later be implemented in numerical models, so that both channels can be considered as morphologically active.

⁴Duurzame Vaardiepte Rijndelta (DVR) stands for Sustainable Navigable depth Rhine delta which is a hydro- and morphodynamic numerical model that is specifically designed for the branches of the River Rhine.

1.3 Research question

This research aims to conduct an exploratory study to investigate the mechanisms that play a role in the sediment transport over a longitudinal-training-dam sill. In current numerical models, such as the DVR model, empirical relations are used to estimate sediment transport. It appears that these relations do not apply at longitudinal-training-dam sills. For these structures a different approach in modelling sediment transport needs to be taken

The research question is therefore: *How can the bed load sediment transport be described over a longitudinal-training-dam sill for various flow situations and bed configurations?*

A number of sub-questions are defined:

- What is the driving force of sediment transport towards the side channel?
- How is *initiation of motion* influenced by a longitudinal-training-dam sill?
- How is *sediment movement* influenced by a longitudinal-training-dam sill?
- What recommendations/improvements can be made to modelling sediment transport over longitudinal-training-dam sills based on the findings of this research?

1.4 Methodology

In a conceptual model a plausible alternative to the current used bed load sediment transport formulations over longitudinal-training-dam sills. This conceptual model seeks to capture the underlying physical concepts rather than empirical relations is proposed. Qualitative validation of this model is performed by subjecting the model to a uniform flow field. In other words, assuming a uniform water level, flow velocity and flow angle.

A numerical flow and transport model is used to create a flow field that varies spatially. Spatially varying flow fields improve the description of reality. Combining the information of the non-uniform flow fields with the conceptual model, it is assessed how and why sediment is transported over the sill.

Finally, recommendation are made for implementation of the results in numerical models. Implementation of the results aim at predicting the bed load sediment transport over longitudinal-training-dam sills more accurately.

1.5 Related research

Currently other researchers from various institutions are concerned with the longitudinal training dams project in the Netherlands. A list of related research is presented below:

- The RiverCare program is part of the Netherlands Centre for River studies and includes private and public organisations that work together to gain insight into river engineering developments in the Netherlands. In this program PhD students are involved, who also do research on the longitudinal training dams each from a different perspective.

- Frank Collas (Radboud University Nijmegen) is one of these PhD students. He aims at gaining ecological knowledge for a management strategy that creates opportunities for ecological rehabilitation.
- Timo de Ruijscher (Wageningen University) is another PhD student who focuses on the hydrodynamic and morphodynamic effects of the longitudinal training dams. With the use of a laboratory scale model he investigates the regeneration of dunes.
- Bart van Linge (Delft University of Technology) is a graduate student who works in collaboration with HKV Consultants. His work focuses on the flow patterns around the longitudinal training dams.
- Rijkswaterstaat is the executive body of the Dutch ministry for Infrastructure and the Environment. They are responsible for the construction and maintenance of the longitudinal training dams. In addition the Central Information Service department investigates and records flow characteristics, bed topography data and dune developments.

1.6 Reading guide

In chapter 2 an introduction is presented to the reader about the state of the art knowledge related to the design of the longitudinal training dam, the flow situation in the area of interest and sediment transport in general. The next chapter deals with the set-up of a conceptual model, a so-called particle model.

A qualitative assessment with uniform flow fields is done in chapter 4. Non-uniform flow fields are included in chapter 5. In chapter 6 the results are discussed. Finally, in chapter 7 the conclusions and recommendations of this thesis are summarised.

Appendix A provides the reader with more information related to initiation of sediment motion for various bed configurations and flow alignments. In Appendix B the formulas that are presented in the previous appendix, are derived in more detail. Then, Appendix C provides the reader with additional information related to the particle model. Finally, Appendix D presents the reader with information concerning the numerical model set-up and the coupling with the particle model.

Chapter 2

Background information

2.1 Introduction

The configuration of the inlet sill is expected to be important for the long-term morphological effects of both river channels. The previous chapter described that the sediment transport processes over the longitudinal-training-dam sills are not thoroughly understood. This chapter provides the reader with the current state of the art knowledge concerning longitudinal training dams, flow situations, sediment transport in general and related situations.

2.2 Design of longitudinal training dams

As part of the Room for the River project the longitudinal training dams have been constructed in 2015. According to Rijkswaterstaat this project is an example of an integrated hydraulic engineering design, since it serves multiple functions at once, such as high-water safety, ecology and recreation. Four different objects can be distinguished in the design: main channel, longitudinal training dam, side channel and longitudinal-training-dam sill.

Construction of these objects is likely to have an effect on the hydrodynamic and morphodynamic behaviour of the river system. The physical mechanisms that determine this behaviour are investigated by de Ruijsscher et al. (2015). He also investigates the formation, regeneration and evolution of subaqueous dunes. By separating the channel into a main and side channel, a sheltered area is created in which species might find refuge from the dynamics of the water in the main channel. Collas et al. (2015) investigates the effect of the longitudinal training dams on ecology.

The longitudinal training dams have been constructed at three locations: Wamel, Dreumel and Ophemert, see Figure 2.1. Upstream of Wamel the river is 260 m wide and this reduces to 230 m at the downstream side of the longitudinal training dams at Wamel. However, in further computations the main channel is assumed to be 230 m wide over the full length of the river. The side channel width measures approximately 90 m over the full length. According to Rijkswaterstaat (2011), the crest of the longitudinal training dam is based on a discharge at Lobith (River Rhine) of 2606 m³/s. The rubble stones that are used for the top layer of the longitudinal training dam and the construction of the sills are 40-200 kg. Both the longitudinal training dam and the sills are designed with a transverse slope of 1:2.5 on both sides.

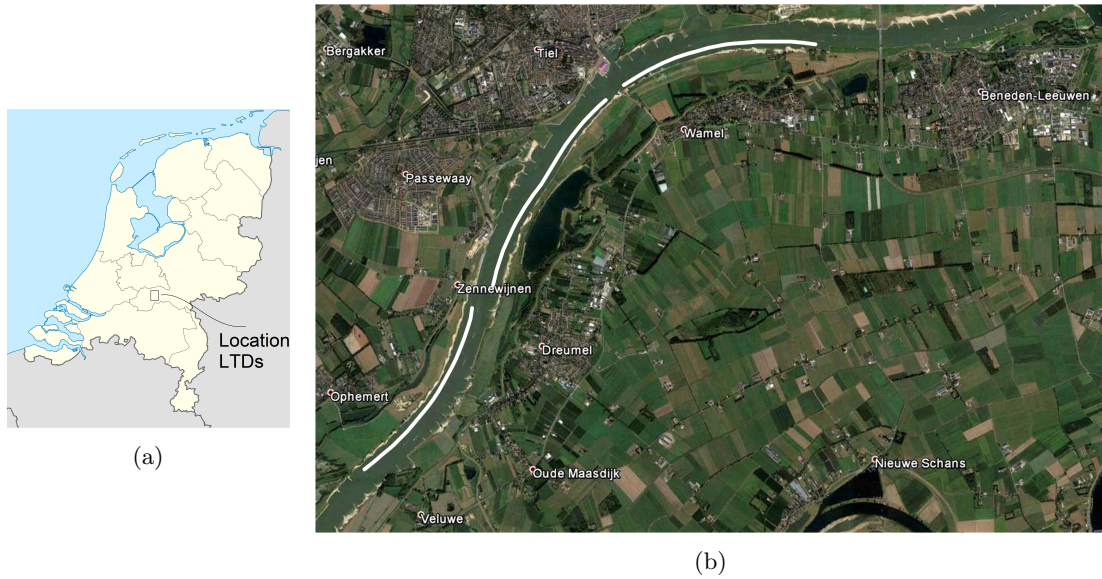


Figure 2.1: (a) shows the locations of the longitudinal training dams (LTDs) in the Netherlands. (b) shows three locations (Ophemert, Dreumel and Wamel) where the longitudinal training dams have been constructed, thick white lines. The main flow is from Wamel towards Ophemert. (Source a: (Graph Atlas, 2016)) and (Source b: Google Earth).

The longitudinal training dam at Wamel is used as an example in further explanations concerning the longitudinal training dams, it is schematically represented in Figure 2.2. The blue arrows in Figure 2.2 indicate that there is a flow from right to left.

Upstream of the inlet sill the flow is aligned with the river banks. The side channel causes a sudden widening of the river and the flow needs to adapt to this widening. Behind the inlet structure the flow decelerates and an eddy is formed at the start of the side channel. Besides a longitudinal flow component a transverse flow component causes a flow over the inlet sill. At the start of the longitudinal training dam the river bifurcates and the flow is separated. In Figure 2.3 a close-up of the inlet structure is presented showing schematically a possible streamline (dashed line), eddy pattern behind the inlet sill (circled arrow) and the bifurcation (split arrow).

In Figure 2.2 three vertical lines are drawn indicated by (a), (b) and (c). At these locations a cross-section has been drawn, which is presented in Figure 2.4. The first cross-section (a) is of the longitudinal training dam. This structure is non-porous and for an average discharge the dam is emerged, see Figure 2.4a. Cross-section (b) and (c) are both porous structures, the difference is caused by the crest height of the sill. Figure 2.4b is a cross-section that is situated downstream of the inlet and emerges only occasionally. At cross-section (c) the inlet sill is drawn, which is generally submerged, this cross-section is drawn in Figure 2.4c.

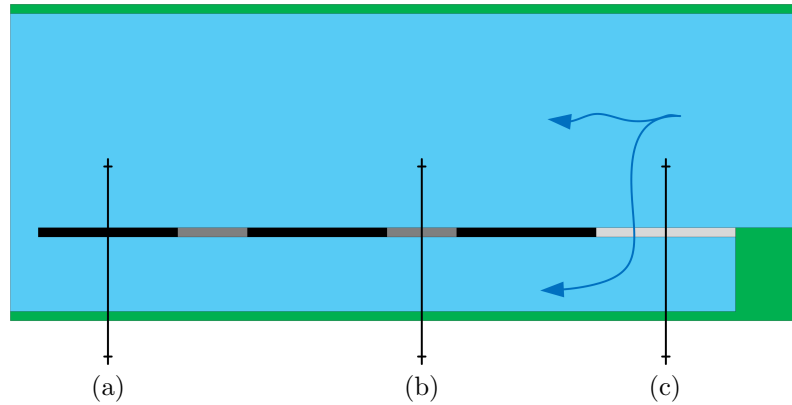


Figure 2.2: Schematisation of longitudinal training dams near Wamel. Three different structures can be distinguished in this drawing: (a) longitudinal training dam, (b) longitudinal-training-dam sill that is emerged for an average discharge and (c) longitudinal-training-dam sill that is submerged for an average discharge. The blue arrows indicate that the flow is from right to left and that at the inlet sill water is entering the side channel. In Figure 2.4 the cross-sections of each letter is drawn. Typical length of the inlet structure is 200 m and total length of the longitudinal training dams is 3 km. The width of the side channel is typically 90 m and the main channel is assumed to be 230 m over the full length.

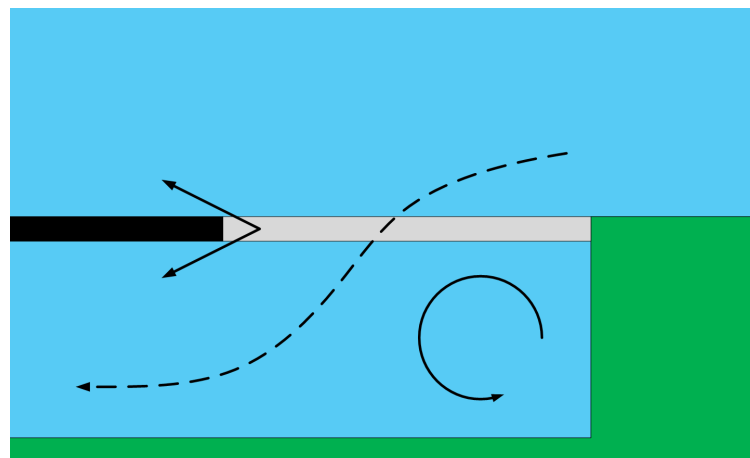


Figure 2.3: Close-up of the inlet structure of the longitudinal training dam, showing typical stream patterns. The dashed line is a possible streamline where water from the main channel enters the side channel. Eddy formation just behind the sill and bifurcation where the longitudinal training dam starts.

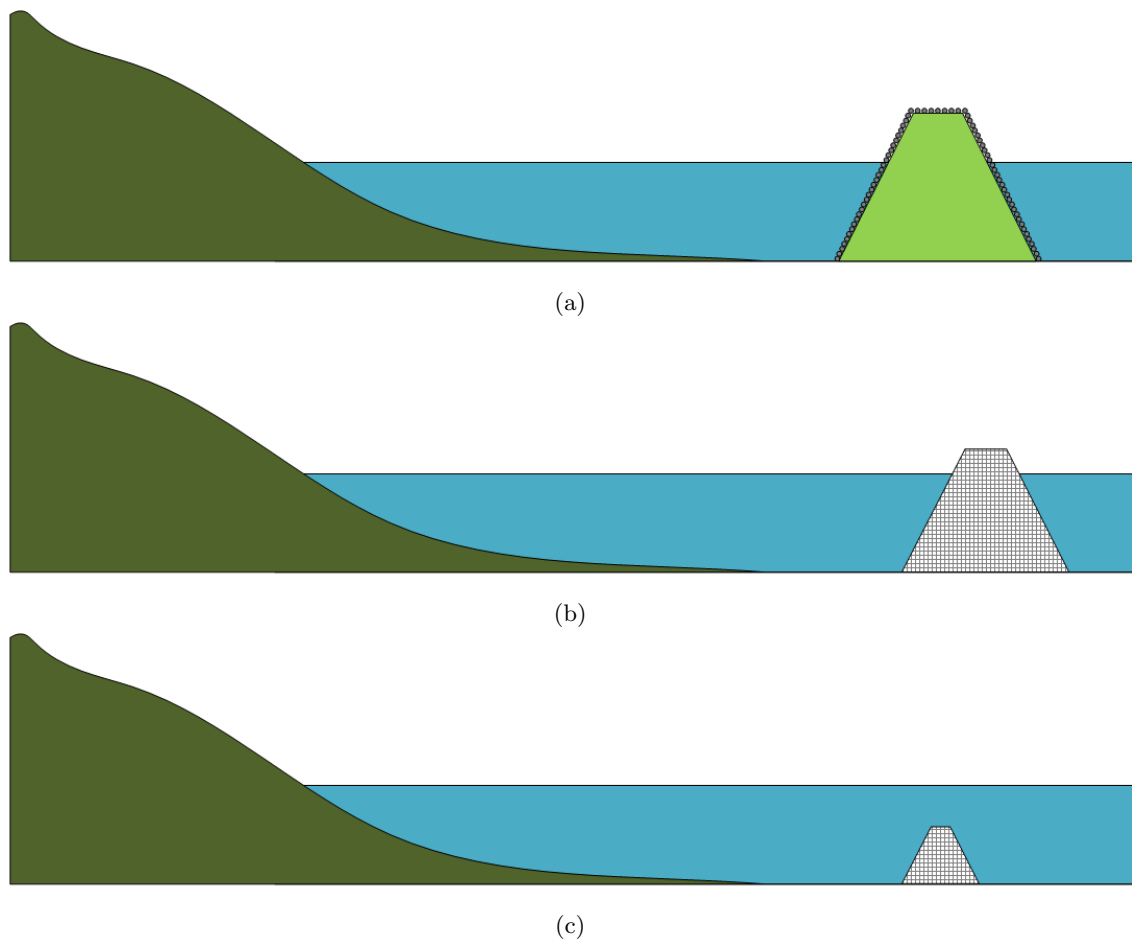


Figure 2.4: Cross sections of the longitudinal training dam and the longitudinal-training-dam sills as indicated in Figure 2.2: (a) the longitudinal training dam, (b) the emerged longitudinal-training-dam sill and (c) submerged longitudinal-training-dam inlet sill.

2.3 Flow situation in River Waal

Discharge variations in the River Waal follow a similar pattern as the River Rhine, due to the bifurcation near Lobith with a fixed discharge distribution¹. The discharge is on average 2250 and 1500 m³/s for the Rivers Rhine and Waal respectively. Figure 2.5 shows yearly seasonal discharge fluctuations. According to de Vriend et al. (2011) this river system is classified as a mixed river which means that the discharge is a combination of rainwater and melting glacier water. The river system serves multiple functions, such as shipping, fresh water supply and quality of life.

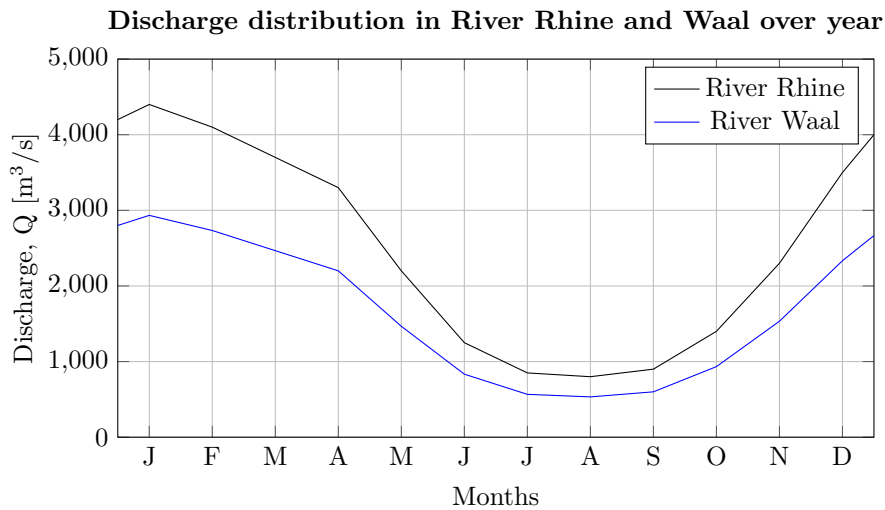


Figure 2.5: Monthly variations of the discharge in the River Rhine and the River Waal. Source: de Vriend et al. (2011).

In the Netherlands a design discharge is defined for each river, which is used as a reference discharge for the design of the primary flood defence structures. At Lobith the River Rhine enters the Netherlands, the design river discharge at this location is 16,000 m³/s. As a result of the fixed discharge distribution the design discharge in the River Waal is 10,165 m³/s. According to Rijkswaterstaat (2011), the return period of this discharge is 1250 years. In the design phase of the longitudinal training dams it was found that during design discharge the longitudinal training dams would induce an additional water level lowering compared to lowering the crest of the groyne² (Huthoff et al., 2011).

2.4 Field data in River Waal

In this section field data of the River Waal is presented. Flow data is presented which shows characteristic discharges in the River Waal. Furthermore, bed topography data is presented to give an insight into the sediment patterns at the river bed near the inlet of a longitudinal training dam.

¹2/3 of the flow is discharged to the River Waal, 1/3 to the Panmerden Canal.

²Lowering of the crest of groynes is a substitutional measure for the longitudinal training dams in the Room for the River project, see subsection 1.1.2.

2.4.1 Flow in River Waal

Rijkswaterstaat³ records the water levels and the discharges in the main rivers of the Netherlands. Figure 2.6 shows an example of the historical data of the discharge in the Rivers Waal and Rhine, at the locations Tiel and Lobith respectively. From this graph it follows that in the period between 1989 and 2014 the minimum measured discharge in the River Waal was $584 \text{ m}^3/\text{s}$, the maximum discharge was $7309 \text{ m}^3/\text{s}$ and the average discharge was $1584 \text{ m}^3/\text{s}$. Note that the design discharge in the River Waal is $10,165 \text{ m}^3/\text{s}$, which has never occurred since 1989.

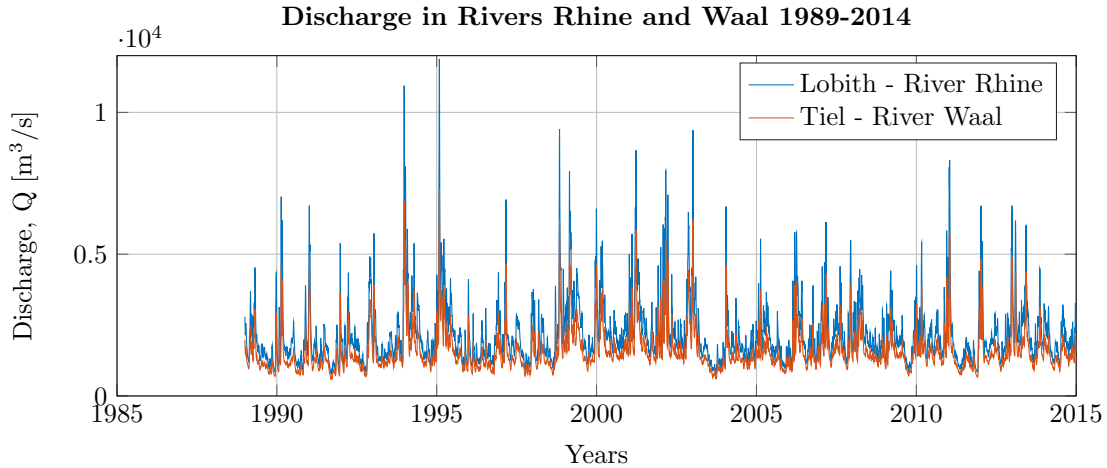


Figure 2.6: Discharge in the River Rhine and the River Waal between 1989-2014. Source: Waterbase.

Flow measurement data of Rijkswaterstaat is done in the River Waal on a frequent basis. Close to the inlet of the longitudinal training dam the flow varies along the inlet. Realistic values of the flow angles vary between 0 and 15° at the inlet of the side channel.

2.4.2 Bed topography River Waal

Rijkswaterstaat performs bed topography measurements in the River Waal on a frequent basis. In Figure 2.7 the most upstream longitudinal training dam near Wamel is presented, this is kmr^4 911-912. The irregularities in the main channel indicate bed forms on the river bed. Colours indicate the height of the river bed: blue indicate that the river bed is deeper with respect to NAP⁵, red means that the river bed is higher with respect to NAP. In this figure it can be seen that the side channel is on average higher than the main channel. Note that the recording of this figure was made on February 17th, 2017. The water level was at that moment $+4.4 \text{ m}$ and the discharge $1450 \text{ m}^3/\text{s}$.

In Figure 2.8 a close-up is presented of the inlet sill. Two lines indicate the approximated sill direction and the approximated sediment direction. The latter means that a clear sedimentation pattern is observed at the start of the side channel. The upstream side is blue coloured, which indicate that the bed is situated deeper. This deeper part is exactly at the location where an eddy is expected to occur. The angle between the sill direction and the sediment direction is approximately 20° .

³The executive body of the Dutch ministry for Infrastructure and the Environment.

⁴'kmr' is the abbreviation for the Dutch word 'kilometerraai'. This is a length scale indicating the distance (in kilometres) to the entrance of the waterway.

⁵NAP is a Dutch vertical datum, approximately equal to Mean Sea Level (MSL).

Bed topography of River Waal kmr 911-912

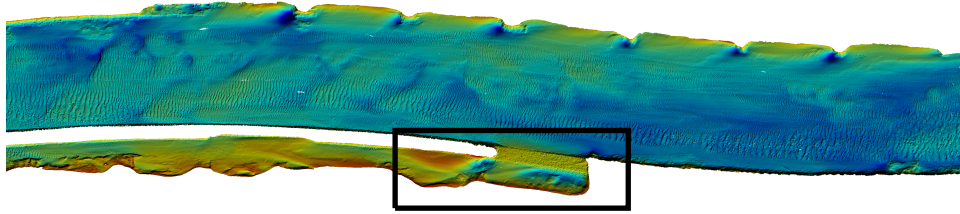
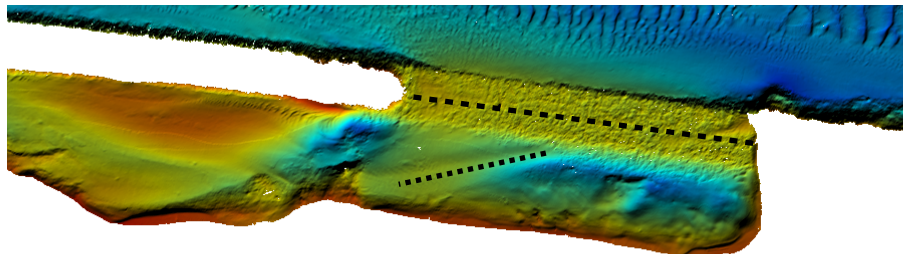


Figure 2.7: Rijkswaterstaat bed topography data in River Waal at kmr 911-912, near Wamel. The flow in this figure is from right to left. In Figure 2.8 a close-up of the inlet sill is presented, see black box in this figure. Recording was done on February 17th, 2017. Source: Rijkswaterstaat.

Inlet sill



- Approximation of sill direction
- Approximation of sedimentation direction

Figure 2.8: Rijkswaterstaat bed topography data at inlet structure of longitudinal training dam near Wamel. At the upstream side of the inlet the river bed is deeper and sediments seem to enter the side channel under an angle of approximately 20° . This is the angle between the approximated sill direction and sedimentation direction. Furthermore, until $2/3$ of the sill no sediment seems to enter the side channel. Source: Rijkswaterstaat.

According to Giri et al. (2008) the type of sediment on the river bed in the River Waal is sand with a mean grain diameter of 1-2 mm, which means that the bed consist of coarse sand.

2.5 Sediment transport in general

Natural river systems do not only discharge water, but also transport sediment. Transport of sediment is described in various ways. Many of these formulations exist which find their basis in empirical relations, such as formulated by (Meyer-Peter and Müller, 1948), (Engelund and Hansen, 1967) and (van Rijn, 1993). However, others suggest to use semi-empirical formulations, which are based on physical processes, but still need to make unavoidable assumptions based on empirical relations.

In any sediment transport formulation ‘initiation of motion’ or ‘incipient motion’ plays a role in estimating the amount of transport. Initiation of motion means the point at which the flow exceeds a certain criterion so that the particles can start to move. Once the particles move they can be transported according to four different mechanisms (as seen in Figure 2.9): (a) entraining/suspension, (b) rolling, (c) saltating and (d) sliding. Generally, a distinction is made between the transport type (bed load and suspended load); a sediment particle that is in suspension (above the dashed line in Figure 2.9) is considered as suspended load, whereas below it is called bed load transport.

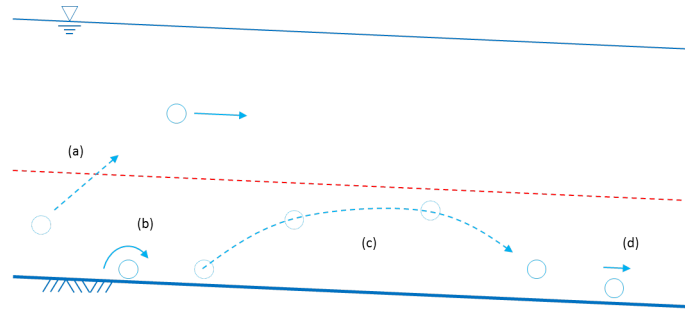


Figure 2.9: Side view showing four different transport modes can be distinguished in this figure: (a) entraining/suspension, (b) rolling, (c) saltating and (d) sliding. Flow is from left to right in this figure. Below the dashed line the sediment is considered as bed load sediment transport, above as suspended load transport.

2.6 Criteria for initiation of sediment motion

Initiation of motion is a result of the interaction between flow and sediment particles and is thereby the start of sediment transport. In (Shields, 1936) a critical Shields parameter (θ_c) has been derived which describes the relation between the load (caused by the friction force of water on the bed) and the strength (weight of grains). Shields found an empirical relation between two dimensionless parameters, namely the critical Shields parameter and the particle Reynolds number⁶ (Re_*). This relation is presented in Equation 2.1⁷. Δ is the submerged relative density, g is the gravitational acceleration, D the particle diameter and u_{*c} the critical shear velocity.

$$\theta_c = \frac{u_{*c}^2}{\Delta \rho g D} = \frac{\tau_{0c}}{\Delta \rho g D} = f(Re_*) = f(u_{*,c}, D, \nu) \quad (2.1)$$

Figure 2.10 shows the Shields diagram, established from the experiments of Shields (1936) and

⁶The particle Reynolds number is a measure that expresses the turbulence around a particle: $Re_* = \frac{u_{*c} D}{\nu}$

⁷The critical bed shear stress τ_{0c} can be found by: $\tau_{0c} = \rho u_{*c}^2$.

adapted by van Rijn (1984). Since the critical shear stress velocity is present in both dimensionless parameters (θ_c and Re_*) u_{*c} has to be found iteratively. A set of analytical formulations for the Shields diagram was derived by van Rijn (1993). Equation 2.2 summarises these analytical formulations. He uses a dimensionless particle diameter instead of the particle Reynolds number that is given by: $D_* = \sqrt[3]{\frac{\Delta g}{\nu^2}} D_{50}$. Note that ν is the kinematic viscosity (typically for water 10^{-6} m²/s) and D_{50} is the median grain size diameter. Although the grain size diameter is 1-2 mm, the

$$\text{van Rijn's formulations} \quad \begin{cases} \theta_c = 0.24D_*^{-1}, & 1 < D_* \leq 4 \\ \theta_c = 0.14D_*^{-0.64}, & 4 < D_* \leq 10 \\ \theta_c = 0.04D_*^{-0.1}, & 10 < D_* \leq 20 \\ \theta_c = 0.013D_*^{0.29}, & 20 < D_* \leq 150 \\ \theta_c = 0.055, & D_* \geq 150 \end{cases} \quad (2.2)$$

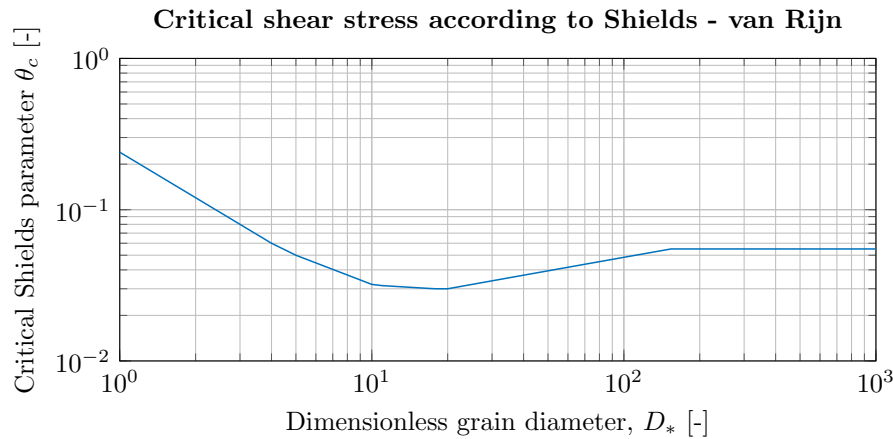


Figure 2.10: Shields diagram - adapted by van Rijn. For horizontal beds the relation holds. Both parameters are dimensionless. Source: van Rijn (1993).

Shields performed experiments to describe initiation of motion for horizontal beds. Yang (1973) used a different approach, he derived criteria for initiation of motion based on force balances acting on a sediment particle that is under influence of a flow. Others, such a Dey (2014), use semi-empirical formulations. He combines the formulation of Shields for horizontal beds with correction factors for different bed configurations.

The longitudinal-training-dam sill can be considered as a side slope⁸ in the river, which means that the approach of Shields (horizontal beds) would not work. Moreover, at the inlet sill the flow is unaligned with the crest of the sill, which means that there is a longitudinal and transverse flow component. In the approach of Dey (2014) the critical Shields parameter is corrected for the bed configuration based on the forces that act on a sediment particle at the moment of initiation of motion. Soulsby (1997) proposed an additional correction factor for the flow alignments on side slopes. In Appendix A correction factors for various bed configurations and flow alignments are explained in more detail. The derivations for each correction factor can be found in Appendix B.

In order to derive the correction factor of the critical Shields parameter, the forces that act on the sediment particle must be known. Due to the interaction between the flow and the sediment particle, a hydrodynamic lift and drag force is created which act on the particle. These forces are

⁸The words side slope, transverse slope or transverse bed slope are interchangeably used.

counteracted by a gravity and a resistance force. Figure 2.11 shows an example of the forces that act on a sediment particle for a horizontal bed and a flow with a logarithmic profile.

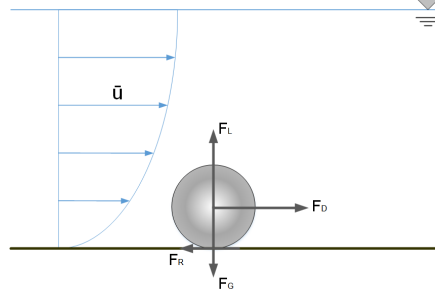


Figure 2.11: Forces that act on a sediment particle that is located on a horizontal bed.

Equation 2.3 shows how the critical Shields parameter is corrected with the method proposed by Soulsby (1997) and Dey (2014). Θ_{cx} is the ‘corrected’ critical Shields parameter. This parameter is corrected for the bed configuration and/or the flow alignment. For a horizontal river bed and aligned flow Θ_{c0} is found. $\tilde{\Theta}_{cx}$ is the ratio between the corrected critical Shields parameter and the Shields parameter for horizontal beds with aligned flow.

$$\tilde{\Theta}_{cx} = \frac{\Theta_{cx}}{\Theta_{c0}} \quad (2.3)$$

2.6.1 Correction initiation of motion for transverse slope

Figure 2.12 shows an example of a transverse bed slope with an aligned flow. This figure represents one side of the longitudinal-training-dam inlet sill. It is assumed that there is no longitudinal bed slope and the transverse bed slope is called α . In Equation 2.4 the correction factor, as was derived by Dey (2014), is presented. This correction factor contains two unknowns: the transverse bed slope (α) and the natural angle of repose (ϕ)⁹. The natural angle of repose is chosen to be 30° , which is a common value for sand (Verruijt, 2012).

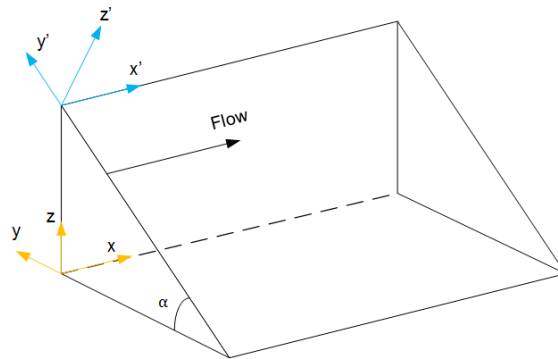


Figure 2.12: Side slope with angle α and flow is aligned with the crest of the sill.

$$\tilde{\Theta}_{c\alpha} = \cos(\alpha) \sqrt{1 - \frac{\tan^2(\alpha)}{\tan^2(\phi)}} \quad (2.4)$$

⁹More information about the natural angle of repose can be found in Appendix A.

The effect of the correction factor is presented in Figure 2.13. It shows the dependence of the correction factor of the side slope angle. An increase of side slope angle results in a lower correction factor, which means that the real critical Shields parameter is lower as well. Steeper side slopes make it ‘easier’ for sediment particles to start moving. An increase in side slope angle causes an increase of the gravity component and thus in a reduction of the critical Shields parameter. Note that side slopes that are steeper than the natural angle of repose are considered to be unstable, from Figure 2.13 it follows that the correction factor for this angle is 0.

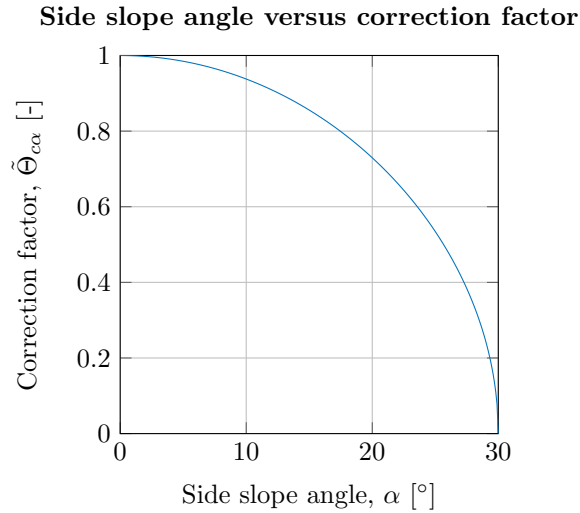


Figure 2.13: Effect of the correction factor for various flow angles. Larger flow angles result in a lower correction factor, which consequently lead to a lower critical Shields parameter.

The Shields diagram, which was only applicable for horizontal beds, can with the use of the correction factor be ‘corrected’ for the transverse slope (side slope) angles. The result of this correction is presented in Figure 2.14.

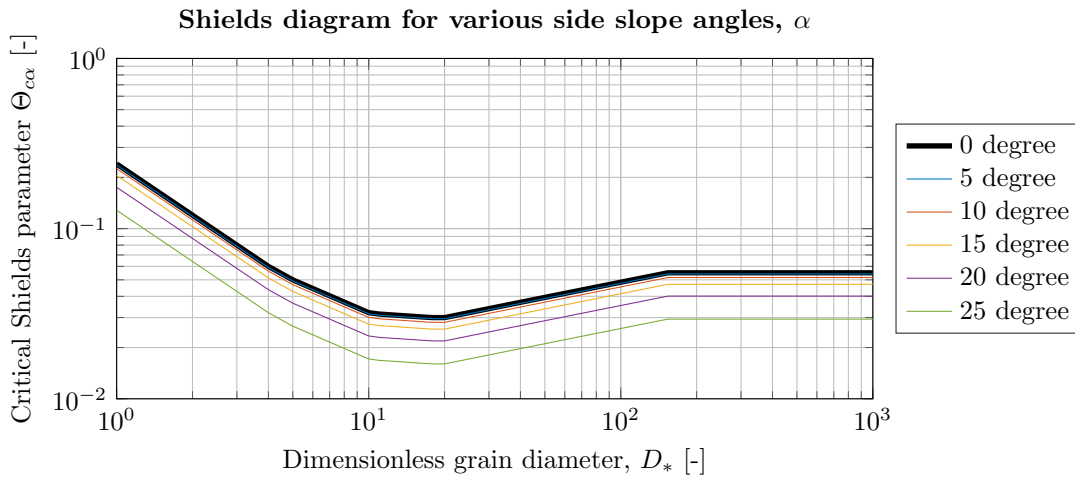


Figure 2.14: Shields diagram corrected for the side slope angle. The critical Shields parameter is thus lower for higher side slope angles, which also results from Figure 2.13.

2.6.2 Correction initiation of motion for flow alignment

The flow over a longitudinal-training-dam sill is unaligned with the crest of the sill. In Appendix A and B the derivations for this correction factor is presented. This result appeared to be similar to what was found by Soulsby (1997)¹⁰. In Figure 2.15 the sill is schematically pictured and the result of the correction factor for an unaligned side slope is presented in Equation 2.5. The side slope has a slope angle α , natural angle of repose ϕ and a flow angle γ . The natural angle of repose is still 30° , the slope angle is chosen to be 20° since this value is similar to the slope of the sill in practice.

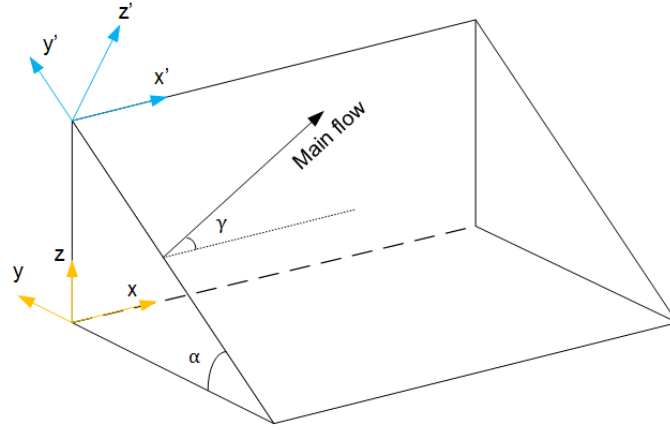


Figure 2.15: Side slope with angle α and a flow that is unaligned with the crest of the slope. The flow angle is indicated with angle γ .

$$\tilde{\Theta}_{c\gamma} = \frac{\Theta_{c\gamma}}{\Theta_{c0}} = \frac{\sin(\alpha) \sin(\gamma)}{\tan(\phi)} + \cos(\alpha) \sqrt{1 - \frac{\tan(\alpha)^2 \cos(\gamma)^2}{\tan(\phi)^2}} \quad (2.5)$$

The flow causes a drag force that acts on the sediment particle, which is the driving force that causes movement of sediment in the flow direction¹¹. The flow angle is expressed as the ratio between the transverse drag force component ($F_{d,t}$) and the longitudinal drag force component ($F_{d,l}$), see Equation 2.6 and Appendix A for more information. In Figure 2.15 the local coordinate system is defined, the positive x', y' and z' are indicated with the blue arrows. According to this coordinate system an anti-clockwise rotation means a positive flow angle (γ). The coordinate system such as is presented in Figure 2.15 indicates that an anti-clockwise rotation (i.e. positive flow angle) for means uphill and negative downhill. Note that if the side slope angle alpha would reverse an anti-clockwise rotation means downhill, while still being a positive flow angle. Unless otherwise specified a positive flow angle (γ) in combination with a positive slope angle¹² (α) means uphill.

$$\gamma = \arctan\left(\frac{F_{d,t}}{F_{d,l}}\right) \quad (2.6)$$

For a certain flow angle (γ), transverse slope angle (α) and natural angle of repose (ϕ) the effect of the correction factor (see Equation 2.5) can be calculated. Figure 2.16a shows how the correction factors changes for a changing flow angle. It becomes clear that moving uphill (γ is

¹⁰In section B.5 it is proven that these formulas are indeed similar, but use a different coordinate system.

¹¹More detailed information about the drag force is presented in the next section.

¹²Positive α means that the angle is from y to z axis, which is the case in Figure 2.15.

positive) increases the correction factor ($\tilde{\Theta}_{c\gamma}$). The other correction factor ($\tilde{\Theta}_{c\alpha}$) is unchanged, since it does not depend on the flow angle. In other words, the critical Shields parameter is underestimated for positive flow angles and overestimated for negative flow angles if the flow angle would not be included in the correction factor. Moreover, it follows that initiation of motion, for a flow in uphill direction, is ‘harder’ than when the flow is in downhill direction. This effect can be explained by the presence of gravity. This component withholds the sediment motion to be initiated if the flow is in uphill direction and it contributes to the initiation of motion process if the flow is in downhill direction. Note that in this figure the side slope angle was assumed to be 20° , similar to the slope of the sill in practice.

Figure 2.16b shows the result of applying the correction factor of Equation 2.4 ($\tilde{\Theta}_{c\alpha}$) and Equation 2.5 ($\tilde{\Theta}_{c\gamma}$) for various side slopes. The first correction factor does not correct for the flow angle and is therefore equal to the correction factor that does include the flow angle only if $\gamma = 0^\circ$. However, the flow angle γ is assumed to be 15° , since this value was found to be realistic according to the Rijkswaterstaat data.

If the absolute value of the transverse slope angle becomes larger or equal to the absolute value of the natural angle of repose particles move without any flow due to a natural instability. It follows from this graph that excluding the flow angle from the correction factor gives an underestimation of the critical Shields parameter for positive side slopes. In other words, adding the flow angle γ to the correction factor leads to a higher required critical Shields values to initiate sediment motion. This can be explained by the fact that correction factor that includes the flow angle considers the transverse direction and the sediment particle has to overcome the gravity force component to be initiated for positive flow angles (uphill). Reversely, if the flow angle is negative on a positive side slope, the drag force works in the same direction as the gravity force and that makes it ‘easier’ for the sediment particle to be initiated.

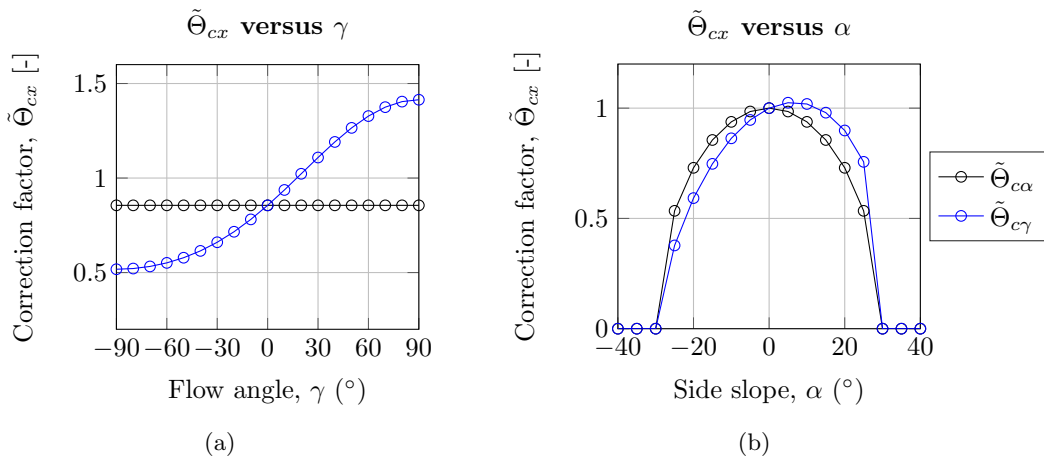


Figure 2.16: In these two graphs the correction factor is presented for various flow angles (γ) and transverse slopes (α). The correction factor that includes the flow angle ($\tilde{\Theta}_{c\gamma}$) is compared with the correction factor that excludes the correction factor ($\tilde{\Theta}_{c\alpha}$). In (a) the side slope is assumed to be 20° and the flow angle is varied. In (b) the side slope is varied and the flow angle is assumed to be 15° .

The results of Figure 2.16a is used to construct the Shields diagram in Figure 2.17. The Shields diagram is presented for various flow situations. In case the flow angle is positive, this means that the flow is directed uphill. Note that a side slope α is assumed of 20° .

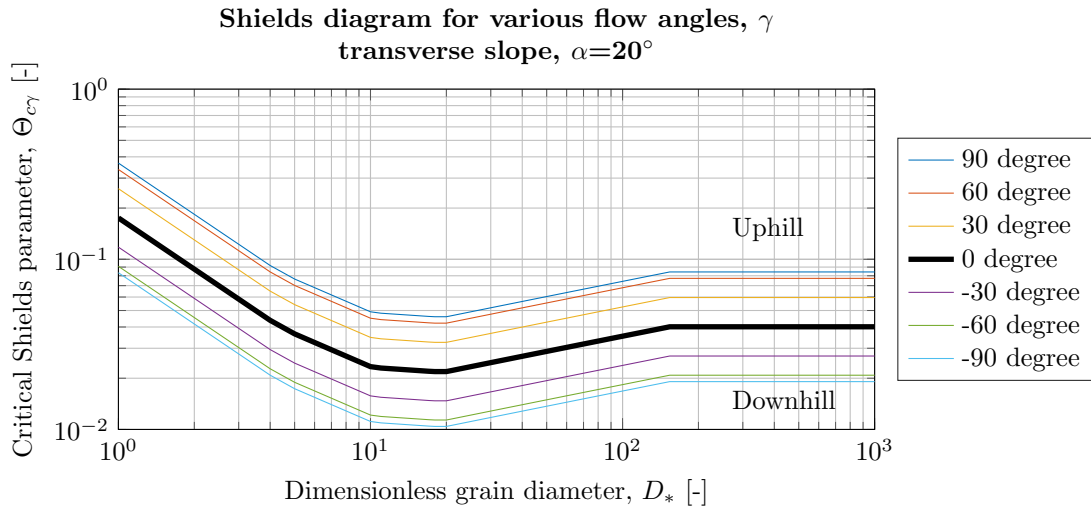


Figure 2.17: Shields diagram that is corrected for various flow situations. Positive flow angles indicate that the flow is directed uphill. The side slope is assumed to be 20° .

2.7 Sediment motion

In Equation 2.5 the correction factor is presented for a side slope with unaligned flow, it is explained that the critical Shields parameter changes. The corrected critical Shields parameter is used as a criterion for initiation of motion on longitudinal-training-dam sills. This section describes the situation when the shear velocity (u_*) has exceeded the critical shear velocity (u_{*c}) and thus sediment is in motion.

Many empirical relations are included in numerical models. However, in the problem description it was already mentioned that the current models are not able to describe sediment transport over the sills of the longitudinal training dam. In other words the available tools are insufficient to model sediment transport over sills. Therefore other available methods are consulted.

Some of the semi-empirical formulations find their origin in force balances acting on a sediment particle in order to describe the movement of the particle. For example, van Rijn (1984, 1993) suggests to solve the equations of motion¹³ of a sediment particle to compute the saltation characteristics (bed load) for a plane bed. Sekine and Parker (1992) created a model to describe saltating grains on a side slope. Nabi et al. (2012, 2013) developed a numerical model to simulate sediment transport by solving the equations of motions.

Equations of motion are in fact a classical mechanic description of the movement of a physical object. By describing sediment motion with the use of equations of motion momentum must be conserved and inertia should play a role. If the flow is considered as laminar (the streamlines would follow a straight pattern) inertia becomes irrelevant since viscous resistance would dominate. The negligibility of inertia can be quantified by a particle Reynolds number. In Appendix C it is described that for the situation in the River Waal inertia plays a role for the sediment particles.

For initiation of motion the critical Shields parameter was corrected based on the forces acting on a sediment particle. In this section it is assumed that the same forces as for initiation of motion act on a sediment particle once the particle is in motion. Note that some parameters in calculation of the forces might differ between initiation of motion and sediment motion. Using the equations of

¹³The equations of motion are a physical concept based on Newton's second law, which states that the motion of an object can be described by the forces that act on that object.

motion a particle trajectory can be calculated, describing the path a sediment particle takes. The slope of the longitudinal-training-dam sill and the flow alignment at the sill have been indicated with the symbols α and γ .

2.7.1 Forces on sediment particle

The forces that act on a sediment particle that is moving are described in more detail here. Forces that are described in this paragraph are based on van Rijn (1993). Figure 2.18 shows the forces that act on the sediment particle that is situated on a side slope. Note that there are two coordinate systems: xyz and $x'y'z'$. The first is with respect to a horizontal bottom ($\alpha=0$) and the other one with respect to a transversal side slope (α).

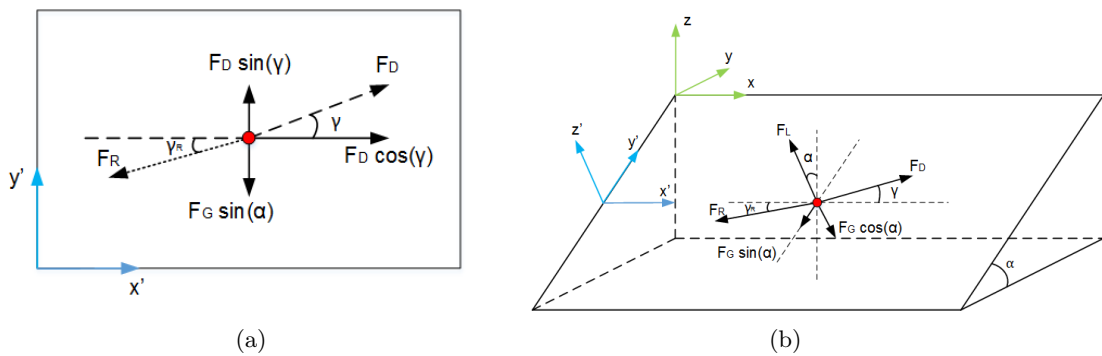


Figure 2.18: In (a) the $x'y'$ plane is sketched and the forces that act on the sediment particle in this plane are drawn in two dimensions. In (b) the forces that act on a moving sediment particle are presented in three dimensions. The forces normal to the $x'y'$ plane are also visible now.

At the top of a sediment particle the streamlines contract which results in a lower pressure at the top and consequently a lift force in upward direction, see Figure 2.19. At the lee side of the sediment particle energy is lost, which finally leads to a force in the flow direction. This is called the drag force. On horizontal beds the drag force is always acting in the flow direction. Equation 2.7 and 2.8 describe these forces mathematically.

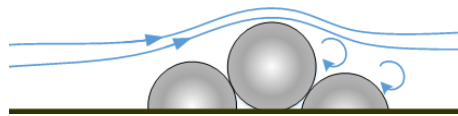


Figure 2.19: The flow in this side view is from left to right. The lines indicate the streamlines around a sediment particle. At the top the streamlines contract and at the lee side small eddies are formed.

$$F_D = C_D \rho u_r^2 A \quad (2.7)$$

$$F_L = C_L \rho u_r^2 A \quad (2.8)$$

C_D and C_L are drag force and lifting force coefficients, which are often empirically determined, ρ is the density of water, A is the particle surface, which for spheres: $A = (1/4)\pi D^2$. The ratio between the longitudinal and transverse drag force is by definition equal to the flow angle γ . $\gamma=0$ means that there is no transverse drag force, positive means that it is directed uphill and negative

downhill. In other words, if γ is negative no sediment particles are transported over the sill. u_r is the relative velocity, which is the difference between the velocity of the fluid and the velocity of the sediment particle.

A submerged weight is present due to the weight and buoyancy of a sediment particle under water. This force can be expressed by the submerged mass multiplied with the gravitational acceleration according to Archimedes' principle, see Equation 2.9. Δ is the relative submerged density $\Delta = \frac{\rho_s - \rho}{\rho}$, ρ_s equals the density of sediment. V indicates the particle volume, which for spheres equals: $V = (1/6)\pi D^3$.

$$F_G = (\rho_s - \rho)gV = \Delta\rho gV \quad (2.9)$$

The friction force depends on the natural angle of repose (ϕ) and the resulting force normal to the bed. The friction always works opposite to the direction of motion, for horizontal beds this is thus opposite to the flow direction, for side slopes with an unaligned main flow it can be found with the use of γ_R , see Figure 2.18a. The angle γ_R is the friction angle found by a combination of the net force in transverse and net force in longitudinal direction.

$$F_R = \tan(\phi)(F_L - F_G) \quad (2.10)$$

2.7.2 Streamwise side slope experiments

Sekine and Parker (1992) described bed load sediment transport under the influence of transverse slopes. In section A.4 initiation of motion is explained for aligned flow ($\gamma=0$). Figure 2.20 shows how a saltating grain starts at the slope and under the influence of gravity tends to move down the slope.

Sekine and Parker performed a thought experiment in which they describe qualitatively how a sediment particle tends to move down a side slope that is under the influence of drag and gravity forces. In order to confirm their thought experiments they developed a saltation model to study bed load sediment transport on such a transverse slope.

With the use of equations of motion they described sediment particles that saltate on a side slope. In addition, they compared their numerical results with experimental data. They appeared to be more accurate than several existing empirical relations. Finally, they derived a relation between the bed load vectors in both longitudinal and transverse direction.

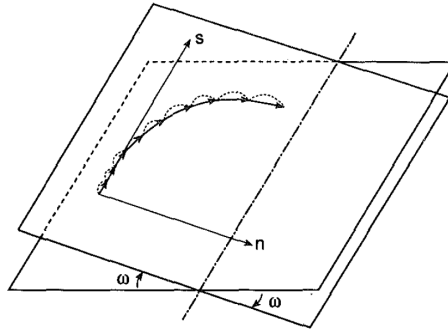


Figure 2.20: Thought experiment with aligned flow ($\gamma=0$) on a sill slope α (in this figure $\omega=\alpha$). The particle starts moving in downstream direction (s), but tends to move downhill in transverse direction (n) as a result of gravity. Source: (Sekine and Parker, 1992).

2.8 Scope of research

In order to make morphological predictions in regions that are currently considered in numerical models as morphologically inactive (i.e. the side channel of the longitudinal training dams), the sediment transport processes over the longitudinal-training-dam inlet sill need to be understood. This research aims at providing insight into these processes for various flow situations. It is assumed that suspended sediment transport does not influence the bed load sediment transport over the sills and suspended sediment is therefore disregarded from this research.

Rivers are naturally dynamic (e.g. variable discharge) while at the same time they are subjected to human interventions (e.g. dredging works). The latter is out of the scope of this research, since this is not one of the physical elements that drives the sediment transport over the sill.

Generally speaking, turbulence or ship waves induce an additional flow, which can result in a different trajectory of a sediment particle. Processes such as turbulence, which are natural phenomena in rivers, are hard to quantify and include in a conceptual model. In the models of van Rijn (1984, 1993) and Sekine and Parker (1992) turbulence was excluded from the equations of motion to reduce complexity. For the same reason it is decided to exclude turbulence in further computations as well. Numerical models, such as Delft3D, are able to approximate turbulence with the use of different turbulent models (Deltares, 2014).

Usually river beds are not flat but consists of bed forms. Bed forms are deformations of the river bed, which can be ripples, dunes or even anti-dunes. Since bed forms migrate over the river bed and bed forms depend on the local flow conditions, they are not constant in space and time. To reduce complexity this effect is left out in further computations.

2.9 Key points of this chapter

This chapter provided the reader with information regarding the processes that play a role in sediment transport over sills of longitudinal training dams. It is explained that the longitudinal training dams are built near Wamel, Ophemert and Dreumel in the River Waal. The flow in this river varies over the year and characteristic discharges are analysed. Sediment transport starts with initiation of motion, which depends on the bed configuration and flow alignment as is explained in this chapter. Once sediment moves its trajectory can be described based on equations of motion.

It appears that the current models are not able to describe the sediment transport over the longitudinal-training-dam sill with empirical relations. However, movement of sediment particles can be described by equations of motion for either horizontal beds (van Rijn, 1984) and side slopes with aligned flows (Sekine and Parker, 1992). At longitudinal training dams an inlet sill at the river bed forms an obstacle which can be seen as a side slope with an unaligned flow.

In the next chapters the method of equations of motion are applied to find an answer to the question how bed load sediment is transported over the sill of the longitudinal training dam. This is done by using a conceptual model which makes use of force balances.

Chapter 3

Set-up of conceptual particle model

3.1 Introduction

Sediment transport can be modelled in various ways. The conventional empirical methods appear to be insufficient for sediment transport over longitudinal-training-dam sills. Therefore a conceptual model is developed that explores sediment transport over a sill with a different approach.

Criteria for initiation of motion such as presented in section 2.6 are based on forces that act on a sediment particle. In section 2.7 it was explained that sediment movement can be described based on force balances, i.e. with the use of equations of motion. In order to apply this method, momentum must be conserved and inertia has to play a role. The equations of motion give insight into the path a sediment particle follows. Van Rijn (1984), Sekine and Parker (1992) and Nabi et al. (2013) used equations of motions to describe bed load transport.

For this research the equations of motion are used to calculate the movement of a sediment particle over a sill. In this situation the flow is usually not aligned with the crest of the sill. This differs from the model of Sekine and Parker (1992), they only considered sediment transport on side slopes with aligned flows.

At three locations in the River Waal the longitudinal training dams have been built. The dimensions of the river and the longitudinal training dams near Wamel are applied in this model. Figure 3.1 shows a graphical representation of the area and it includes the computational domain that is considered in the particle model. The black dashed line indicates the boundaries of the model, the blue dashed line represents the submerged longitudinal inlet sill.

Unaligned flow on a side slope affects the criteria for initiation of motion, which was explained in the previous chapter. In this chapter it is investigated under which conditions initiation of motion can be expected. In addition, the development of the particle model is explained step-by-step in section 3.5.

In the process of developing a conceptual particle model many assumptions have been made. The conceptual particle model is simplified in order to understand the essence of the system behaviour. These assumptions are extensively described at the end of this chapter. Later in the discussion (chapter 6) these assumptions are reviewed again in combination with the results.

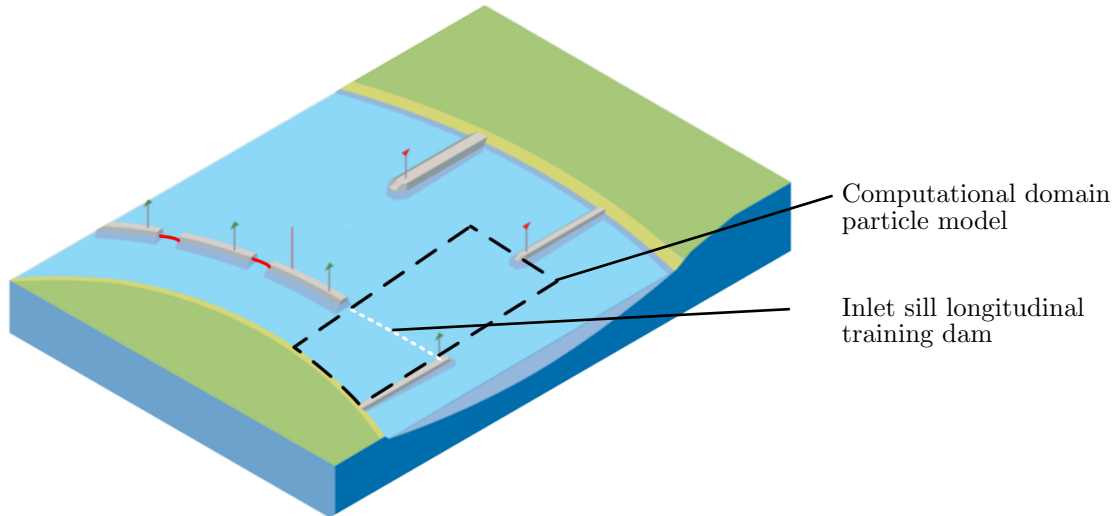


Figure 3.1: Graphically representation of the longitudinal training dams. This figure indicates the computational domain with the black dashed rectangle. Water flow from right to left in this figure and enters the side channel at the location of the inlet sill. Adapted from: Room for the River.

3.2 Schematisation of river bed in particle model

River beds in delta regions have in general a very mild slope¹ in longitudinal direction. However, for small river sections the river is assumed to be flat in this direction. In transverse direction the slopes are often much steeper. Towards the river banks, these slopes can in general become in the order of 10-20°.

The conceptual particle model includes solely the first opening of the longitudinal training dam, where the river bed in the main and side channel is assumed to be flat and in-between there is a sill. Figure 3.1 shows the computational domain (black dashed line) in the sketch of the longitudinal training dam. The white dashed line indicates the location of the sill.

Figure 3.2 shows a cross-section of the river in transverse direction with a side channel (left of the sill) and main channel (right of the sill). In blue the river bed is indicated, the side channel is assumed to be one metre higher compared to the main channel. The sill is the local elevation of the river bed, on both sides it has a slope of 1:2.5 ($\approx 20^\circ$).

¹Mild river slopes are in the order of 10^{-4} , which means that over a river section of 1 km there is a bed level elevation difference of 10 cm.

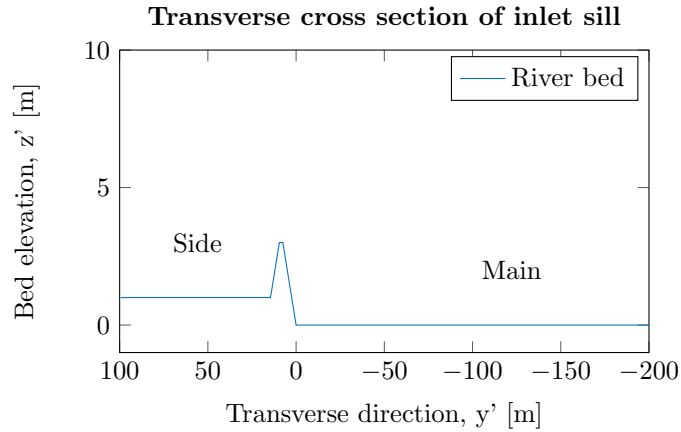


Figure 3.2: Cross section of the river in transverse direction at the inlet sill. The side channel ('Side') is located one metre higher than the main channel ('Main'). Slope of sill is 1:2.5 on both sides.

3.3 Distribution of flow

Figure 3.3 shows a top view of the two channels separated by longitudinal training dams. The black bars indicate the longitudinal training dams, dark gray the emerged opening sill and light gray the submerged opening sill. The blue arrows indicate the flow direction, the flow is thus from right to left and bifurcates at the inlet sill. The transverse flow component is caused by multiple reasons, which are explained below. Currently van Linge (2017) is researching the effect of the flow distribution between both channels.

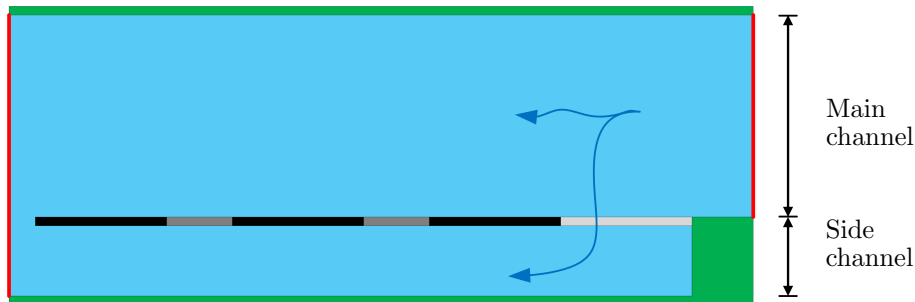


Figure 3.3: A top view of a schematisation of the longitudinal training dam. The main channel and side channel can be distinguished. The blue arrows indicate the flow direction which is from right to left. Note that the bed elevation is indicated with z' and has the bottom of the main channel as reference level.

First, the design of the longitudinal training dam divides the river in a main channel and a side channel. The geometry of the inlet structure is likely to cause an energy reduction, which consequently leads to a reduction of the discharge to the side channel. This means that the specific discharge (discharge per unit width) is not equal for both channels. A difference in specific discharges between both channels lead to a water level difference.

This water level difference is explained by using backwater curves in the system. In the work of van Linge (2017) the domain that is presented in Figure 3.3 is considered. At the left side of this figure a red line indicates the downstream boundary condition, which is equal for the entire cross-section. At the upstream side a discharge boundary is specified. Based on weir formulations

at the locations of the sills he calculates the backwater curves. In backwater curve calculations the equilibrium depth (d_e) and a critical depth (d_c) are calculated, see Equation 3.1. In this equation q is the specific discharge, C is the Chézy roughness coefficient, i_b the bottom slope in longitudinal direction and g the gravitational acceleration.

$$d_e = \left(\frac{q^2}{C^2 i_b} \right)^{1/3} \quad (3.1a)$$

$$d_c = \left(\frac{q^2}{g} \right)^{1/3} \quad (3.1b)$$

A different specific discharge leads to a different equilibrium depth and critical depth. Consequently this causes a different backwater curve in the main channel and side channel and thus eventually a difference in water level. A difference in water level causes a pressure difference and thus a flow in the transverse direction.

Second, longitudinal training dams are situated at the inner side of the river bend. The curving of the river causes a difference in length of both channels, the side channel is shorter than the main channel. This also affects the backwater curves, since these have to be considered over a different length. Therefore the relative distance upstream is considered in Figure 3.4², which is the length with respect to the length of the channel.

Third, both channels might have a different roughness. The roughness value is incorporated in the equilibrium depth, which thus leads to a different evolution of the backwater curves in both channels.

The model of van Linge (2017) calculates the water levels at the inlet structure. The difference in water level in Figure 3.4 is approximately 10 cm between the main and side channel. As explained above, this water level difference causes a pressure difference which results in a transverse flow.

Assuming that the flow over the longitudinal training dam sill is mainly driven by the water level difference leads to an approximation of the discharge over the sill by Equation 3.2. The discharge over the sill q_{sill} depends on the water level in the main channel (h) and the height of the sill (w). α_{sw} and β_{sw} are coefficients depending on the type of equation that is used and which flow regime is applicable. The water level difference is often included in these coefficients.

$$q_{sill} \sim \alpha_{sw} (h - w)^{\beta_{sw}} \quad (3.2)$$

However, note that other aspects - besides water level differences - might play a role in the flow over the longitudinal training dam sill. For example the fact that the longitudinal velocity in the main channel is higher than in the side channel. This might cause a transfer of momentum in longitudinal direction from the main to the side channel. But also in transverse direction a transfer of momentum might occur. Due to the secondary flow in the main channel a difference might occur between the transverse velocities. All these effects might contribute, but in van Linge (2017) only the water level differences are considered.

²The upstream discharge boundary condition in this case is 2000 m³/s.

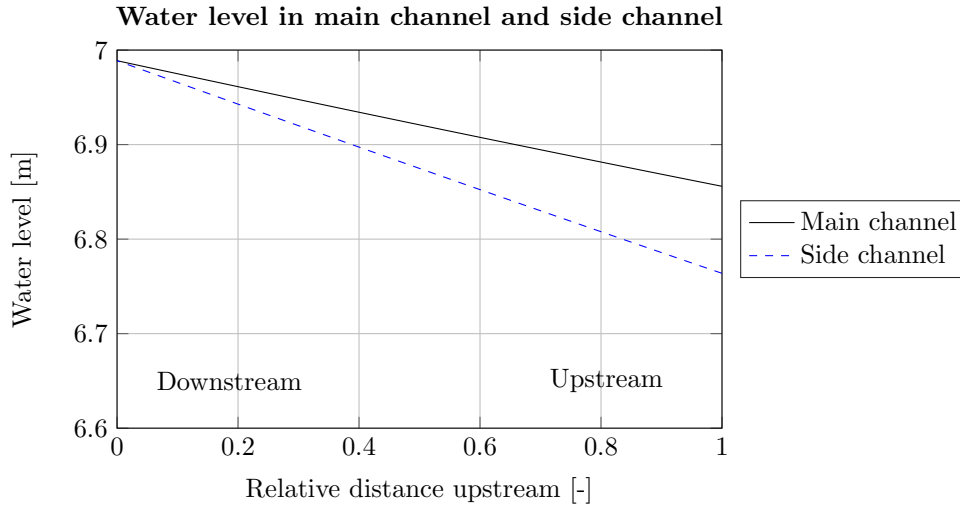


Figure 3.4: Results of backwater curves in the main channel and side channel. The distance is relative to the length of the channel. The length of both channels differs due to the curving of the river. Relative distance 0 means downstream and 1 means at the inlet. The water level difference at the inlet is approximately 10 cm in this case. This figure shows an arbitrary situation Water level downstream is 6.85 m and upstream a discharge boundary of 1500 m³/s is imposed.

3.4 Initiation of motion of sill slope

Initiation of motion is in fact the critical moment at which sediment starts moving. Therefore, it is interesting to investigate under which conditions, bed configurations, depths and flow alignments sediment transport can be expected at all. For side slopes with unaligned flow a correction factor for the critical Shields parameter was already presented in the previous chapter, but is repeated here in Equation 3.3. This section focusses solely on the side slope, the area of interest of this section reaches from the toe of the sill to the crest of the sill, see dashed box in Figure 3.5.

$$\tilde{\Theta}_{c\gamma} = \frac{\Theta_{c\gamma}}{\Theta_{c0}} = \frac{\sin(\alpha) \sin(\gamma)}{\tan(\phi)} + \cos(\alpha) \sqrt{1 - \frac{\tan(\alpha)^2 \cos(\gamma)^2}{\tan(\phi)^2}} \quad (3.3)$$

For every combination of ϕ , α and γ the correction for the critical Shields parameter ($\tilde{\Theta}_{c\gamma}$) can now be calculated. Given a uniform flow velocity and some other assumptions, the real critical Shields parameter is found. Note that all necessary assumptions for this are described in detail in Appendix C. Finally this leads to generic graphs like Figure 3.6 and Figure 3.7, which are explained in more detail below. Note that in further computations a grain size diameter of 3 mm is used, contrary to the real grain size diameter in the River Waal see section 2.4. This assumption was made, because at the time these computations were performed the real grain diameter in the River Waal was unknown.

The computations in this section make use of a depth-averaged flow velocity, which is defined as the depth-averaged flow velocity in the main channel. This flow velocity is converted to a shear velocity with the use of Equation 3.4. The reason for depth-averaged flow velocity is that this is used in the particle model as well.

$$u_* = \frac{\bar{u} \sqrt{g}}{C} \quad (3.4)$$

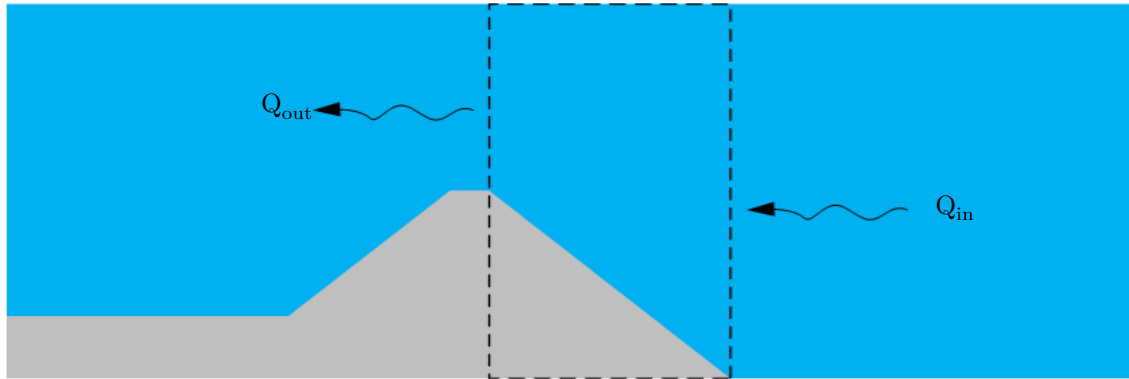


Figure 3.5: Transverse cross section of the river at the inlet of the side channel. The dashed box represents a control volume that is used in the computations. The flow is from right to left, the flow that enters the control volume is indicated with Q_{in} and the flow that leaves the control volume is indicated with Q_{out} . Since the water depth at the top of the sill is smaller than at the toe of the sill, the flow velocity at the top is higher.

3.4.1 Relation between sill slope and flow angle

Figure 3.6 indicates the critical angles at which sediment motions can be expected. In this graph four depth-averaged flow velocities in the main channel are assumed and plotted. The steepness of the slope α and the flow angle γ are varied in this graph. Note that a positive flow angle means that the flow is directed uphill and negative means downhill, see Figure 2.18. The vertical dashed line in Figure 3.7 indicates the division between up- and downhill.

A transverse side slope (α) that is larger than the natural angle of repose (ϕ) creates an unstable situation (above the horizontal dashed line) where sediments move downhill, since the sediment particles are expected to loose grip. However, left of the coloured lines the critical Shields value is exceeded, which means that the sediments start moving. E.g. for a depth-averaged flow velocity of 0.6 m/s, with a side slope of 10° , the minimum flow angle is 15° ; for any flow angle smaller or equal to 15° initiation of motion is exceeded for this transverse bed slope.

Note that if the flow angle is positive (uphill), that does not necessarily mean that a sediment particle, that moves, eventually moves uphill. However, if the flow angle is directed downhill and a particle moves, the sediment particle moves downhill for sure. The experiments performed by Sekine and Parker (1992) showed that for an aligned flow ($\gamma=0$) a sediment particle will eventually move downwards, see Figure 2.20 and subsection 2.7.2. The presence of gravity on a side slope causes a movement downhill eventually.

3.4.2 Relation between sill slope and relative depth

The location at the sill is also important for initiation of motion, since the velocity at each point is different. Assuming that the water level is constant over the sill³, the depth varies over the sill. At the crest of the sill the velocity is higher compared to the toe. This follows from a simple mass balance which is described in more detail below.

In Figure 3.5 a cross section of the river is presented with the side channel on the left side and the main channel on the right. In between there is a sill and the water flows from right to

³In reality there will be a water level difference, which is described in section 3.3. Nevertheless this assumption is made to explain the concept.

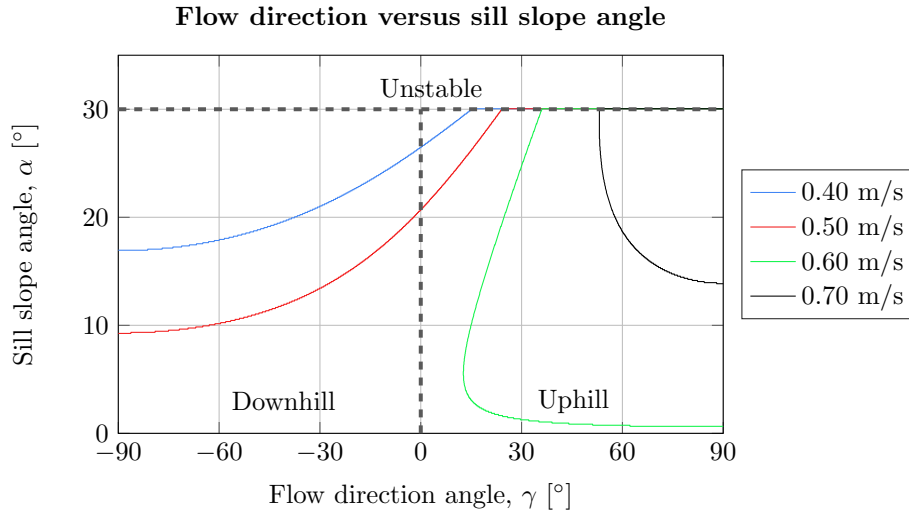


Figure 3.6: Side slope angle versus the flow angle for four depth-averaged flow velocities in the main channel. The lines indicate the critical angles at which sediment motions can be expected. Positive flow angles are in this situation uphill. The area left of a line gives the combination of the sill slope and the flow angle for which sediment motions can be expected. Sill slope angles larger than the natural angle of repose are expected to be unstable. Chézy value is $40 \text{ m}^{1/2}/\text{s}$.

left. The dashed box is the control volume where water flows in and out. Both fluxes are equal. However, the water depth left and right of the control volume is different and thus the velocity must increase.

The velocity at the crest of the sill (left of the control volume) is higher than the velocity at the toe of the sill. The ratio between the depth at the sill with respect to the depth at the toe of the sill is called the relative depth. The local velocity scales with the relative depth. E.g. a relative depth of 0.5 means that the local depth equals half of the depth at the toe of the sill and thus that the local velocity is twice the velocity at the toe of the sill. Equation 3.5 shows the mathematical relation between the fluxes in and out of the control volume and the relative depth.

$$Q_{in} = Q_{out} \quad (3.5a)$$

$$(d \cdot B \cdot u)_{in} = (d \cdot B \cdot u)_{out} \quad (3.5b)$$

$$B_{in} = B_{out} \quad \text{and} \quad d_{rel} = \frac{d_{out}}{d_{in}} \quad (3.5c)$$

$$u_{out} = u_{in} \cdot \frac{d_{in}}{d_{out}} = \frac{u_{in}}{d_{rel}}$$

For a given relative depth and a certain bed configuration it can be investigated if the flow velocity is exceeded or not. Figure 3.7 shows for various depth-averaged flow velocities in the main channel and a fixed flow angle of $\gamma=15^\circ$ the locations at which sediment particles can start moving. Left of the coloured lines the criterion of initiation of motion is exceeded.

If the flow angle is positive the sediment particles are likely to move in a similar direction, however, there is no guarantee that the sediment particles will indeed end up in the side channel. Furthermore, if the transverse slope (α) becomes steeper than the natural angle of repose the system becomes unstable and the sediment particles are expected to move downhill, regardless of the flow angle.

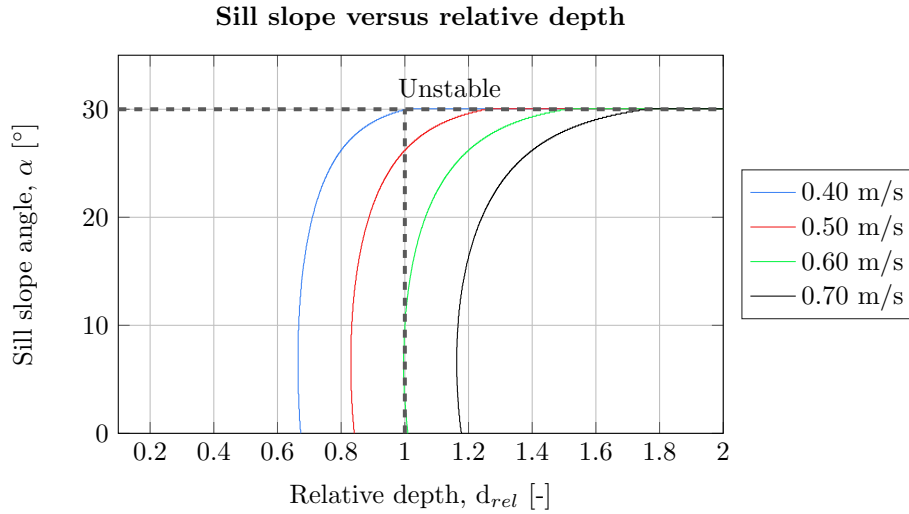


Figure 3.7: Side slope angle versus the relative depth for four depth-averaged flow velocities in the main channel. The lines indicate the critical angles at which sediment motions can be expected. The area left of a line gives the combination of the sill slope and the relative depth for which sediment motions can be expected. Sill slope angles larger than the natural angle of repose are expected to be unstable. The flow angle has been assumed to be 15° (realistic value), which means that the flow is uphill.

3.4.3 Intermediate conclusions

Based on the theory explained above and the presented figures, the following can be said:

- If the transverse slope (α) exceeds the natural angle of repose (ϕ) movement is assumed to be in directed downhill, regardless of the flow angle.
- Only if γ is positive sediments can be transported towards the side channel.
- Certain bed configurations (i.e. some α) do not allow sediment particles to move in the direction of the side channel, e.g. $\alpha=20^\circ$ and depth-averaged flow velocity is 0.5 m/s; movement is only possible if the flow angle is negative and thus directed downhill.
- Depending on the location on the sill, the depth changes and therefore the sediment particles encounter a higher or lower mean flow velocity, which results in a change of the moment at which particles start moving.

3.5 Particle model

A semi-empirical concept is proposed involving calculation of particle trajectories in order to understand the underlying principles of sediment transport at the longitudinal-training-dam sill. Based on the force balances presented in section 2.7, the particle model calculates the path of the sediment particle. In Appendix C additional information on the particle model is provided.

In chapter 2 formulations were derived for incipient motion of sediments on sloping beds. They are based on force balances that act on a sediment particle. This particle model consists of a discretized time and space domain that includes the same forces. For each time step, the forces

are recalculated for each location in the x' and y' -plane, which is the local coordinate system which forms the basis of the model. At each location the local shear velocity is compared with the critical shear velocity. This critical shear velocity is corrected for the bed configuration and the flow angle. Only if the shear velocity is larger than the critical shear velocity sediment transport can start. From the previous chapter it can be concluded that the critical Shields parameter can be underestimated or overestimated if the bed configuration and flow alignment are not included.

A cross-section of the river profile has been implemented in which a sill divides the river into a side channel and main channel as in Figure 3.2. Other used input parameters are the mean flow velocity at the sill, grain properties and dimensions of the river. If the critical shear velocity is exceeded by the shear velocity then the model calculates at each time step the new fluid velocity, the particle velocity and the location of the particle. According to van Rijn (1993) the drag force is calculated with the relative velocity (u_r). This is the fluid velocity (u_f) minus the particle velocity (v_p), see Equation 3.6.

$$u_r = u_f - v_p \quad (3.6)$$

Coordinate systems can be chosen at any location, but for practical reasons a positive x' direction is chosen in downstream direction and positive y' direction is chosen to be directed towards the side channel. From the right-hand rule it follows that the positive z' direction is directed upwards (perpendicular to the bed). The origin of this coordinate system is located at the toe and at the start of the sill. In Figure 3.8 a close-up of Figure 3.3 is presented, it shows the inlet structure and the location of origin of the coordinate system that is used in the particle model and the positive x' and y' directions. The x' is the longitudinal direction and y' is the transverse direction. The origin is located at the toe of the sill in the main channel.

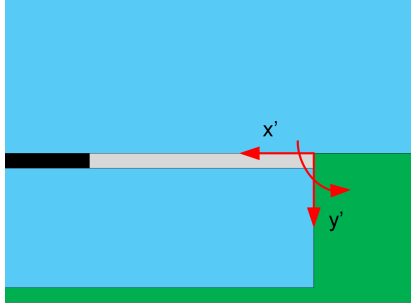


Figure 3.8: Location of origin of coordinate system in particle model. The longitudinal direction is defined as x' and the transverse direction is defined as y' . The origin is located at the toe of the sill in the main channel.

The critical shear velocity depends on the flow angle, transverse slope and the natural angle of repose, as stated in Appendix A. For each location in the spatial domain, the critical shear velocity is calculated according to Equation 3.3 and Equation 3.7. The grain size diameter that is used in the particle model is 3 mm, unless otherwise specified.

$$u_{*,cr} = \sqrt{\tilde{\Theta}_{c\gamma} \Theta_{c0} \Delta g D} \quad (3.7)$$

In order to predict the displacement of the sediment particle, the shear velocity and the near-bed flow velocity need to be calculated. The shear velocity (u_*) is calculated based on the local depth-averaged flow (\bar{u}) (which is a function of the discharge, $Q = \bar{u}hB$), the Chèzy roughness (C) and the gravitational acceleration (g), see Equation 3.4. For the local near-bed fluid velocity

(u_b) a numerical approximation is made: 1% of the local depth above the zero-velocity level (z_0). This assumption was made on a similar approximation that is used for Z-layers in Delft3D, this is discussed further in section 3.6. Equation 3.8 shows that the near-bed fluid velocity depends on the shear velocity and the local depth.

$$u_b = \frac{u_*}{\kappa} \ln \left(\frac{0.01 \cdot d_{local} + z_0}{z_0} \right) \quad (3.8)$$

The near-bed velocity and the particle velocity can be decoupled into a component in x' and y' direction, given a flow angle γ . Note that this flow angle is based on the depth-averaged flow angle. The near-bed fluid velocities are described by: $u_{b,x'} = u_b \cos(\gamma)$ and $u_{b,y'} = u_b \sin(\gamma)$. The direction of the particle velocity is similarly decoupled but then with an angle γ_P , which is discussed later. With the use of this angle the particle velocity can be decomposed in both directions as well. The relative velocity is found by subtracting the particle velocity from the near-bed fluid velocity in both directions.

The drag force is calculated using Equation 3.9a, this force is decoupled into two components (x' and y') by multiplying the drag force with the a ratio for the direction. This ratio is the relative velocity in the direction with respect to the total relative velocity, see Equation 3.9b and Equation 3.9c.

$$F_D = 0.5\rho C_D A u_r^2 \quad (3.9a)$$

$$F_{D,x'} = F_D \frac{u_{r,x'}}{u_r} \quad (3.9b)$$

$$F_{D,y'} = F_D \frac{u_{r,y'}}{u_r} \quad (3.9c)$$

The ratio between the lifting force and the drag force is defined as η . For each calculation step the lifting force is calculated based on this ratio. This ratio is in fact the ratio between the lift coefficient and drag coefficient, see Equation 3.10. The lifting force is perpendicular to the bed. Note that on a slope the lifting force is in a different direction than on a horizontal slope.

$$\eta = \frac{F_L}{F_D} = \frac{0.5\rho C_L A u_r^2}{0.5\rho C_D A u_r^2} = \frac{C_L}{C_D} \quad (3.10)$$

Buoyancy causes a reduction of the gravity force under water (Archimedes' law), which results in a submerged force. This submerged force is always present, even if there is no flow. As explained in subsection 2.7.1, this force equals the weight of the sediment particle minus the buoyancy force. This force can be decoupled in y' and z' direction⁴. Note that the latter is in the same direction as the lifting force. However, the lifting force always has a component in the positive z' direction, while $F_{G,z'}$ is always directed in the negative z' direction, which explains the negative sign in Equation 3.11c.

$$F_G = (\rho_s - \rho)gV \quad (3.11a)$$

$$F_{G,y'} = F_G \sin(\alpha) \quad (3.11b)$$

$$F_{G,z'} = -F_G \cos(\alpha) \quad (3.11c)$$

⁴If there would be a longitudinal slope, the submerged force would have a component in x' direction as well.

The direction of the resistance force is in the opposite direction as the direction of particle motion, i.e. the angle between the resistance force and the direction of motion is 180° . The direction of motion (γ_P) can be found by the active forces that act on a grain, namely drag and gravity, see Equation 3.12a. From this definition it follows that the frictional angle is given by γ_R in Equation 3.12b.

$$\gamma_P = \arctan\left(\frac{F_{D,y'} + F_{G,y'}}{F_{D,x'}}\right) \quad (3.12a)$$

$$\gamma_R = \gamma_P + 180^\circ \quad (3.12b)$$

To find the magnitude of the frictional force the sum of the forces normal to the bed need to be multiplied with a friction factor⁵ μ_f . Decoupling of the frictional force is done with the use of γ_R , see Equation 3.13

$$F_R = \mu_f(F_L - F_G) \quad (3.13a)$$

$$F_{R,x'} = F_R \cos(\gamma_R) \quad (3.13b)$$

$$F_{R,y'} = F_R \sin(\gamma_R) \quad (3.13c)$$

Finally the local acceleration and velocity can be calculated according to Newton's second law. This law states that the sum of all forces balances the mass of the object multiplied with the acceleration. The mass that is used is the submerged mass⁶. Equation 3.14 shows the approximations that were made to describe the local acceleration, velocity and location. Note these description are characteristics of the sediment particle, i.e. the particle acceleration, particle velocity and the location of the particle. t_0 is the start of the computation, the next time step equals $t_1 = t_0 + dt$.

$$\sum F_i = m' a_i \quad \rightarrow \quad a_i(t) = \frac{\sum F_i}{m'} \quad (3.14a)$$

$$a_i(t) = \frac{dv_i}{dt} \approx \frac{v_i(t+dt) - v_i(t)}{dt} \quad \rightarrow \quad v_i(t+dt) = a_i(t) \cdot dt + v_i(t) \quad (3.14b)$$

$$v_i(t) = \frac{dx_i}{dt} \approx \frac{x_i(t+dt) - x_i(t)}{dt} \quad \rightarrow \quad x_i(t+dt) = v_i(t) \cdot dt + x_i(t) \quad (3.14c)$$

with $i = x', y'$

Initial conditions are $x_i(t_0) = x_i(t_1) = 0m$ and $v_i(t_0) = v_i(t_1) = 0m/s$

In Equation 3.14a the acceleration in direction x' or y' is determined based on the sum of all forces in one of these directions. The force balances in both directions are presented in Equation 3.15.

$$\sum F_{x'} = F_D \cos(\gamma) - F_R \cos(\gamma_R) \quad (3.15a)$$

$$\sum F_{y'} = F_G \sin(\alpha) + F_R \sin(\gamma_R) - F_D \sin(\gamma) \quad (3.15b)$$

⁵ $\mu_f = \tan(\phi)$, this is discussed in chapter 6.

⁶The submerged mass is calculated as follows: $m' = (\rho_s - \rho)V$.

3.6 Reflection on particle model

In the previous sections the causes of flow distribution and the theory behind the particle model were presented. A simplified approach has been taken to answer the research question how sediment is transported under various conditions and bed configurations. The advantage of a simplified approach is that the essence of the system behaviour becomes clear.

The approach to apply equations of motion to describe sediment transport is considered by others, e.g. van Rijn (1984), Sekine and Parker (1992) and Nabi et al. (2013). The uniqueness of this model is that it can easily investigate what the effect of a changing flow situation or bed configuration is on the sediment transport.

One of the effects that is excluded is the variability in transport modes. The model calculates the trajectory of a sediment particle based on force balances, while not considering in which mode the particle travels. In section 2.5 four sediment transport modes are described. Sliding is the transport mode that approaches the prediction of this particle model best, since the particle is subjected to a constant friction force and in constant contact with the bed. Considering other transport modes might be possible if the forces in the z' direction are considered as well, in this model they are disregarded to first understand the sliding mode. Only bed load transport is considered in this model, since it was assumed that suspended sediment is transported over the sill anyway (no settling) and that the suspended particles do not affect the bed load particles. This is similar to the assumption that other bed load grains do not influence the bed load particle trajectory.

In reality, bed forms, differences in grain size and interaction with other particles might influence the particle trajectory. This model does not consider any perturbations of the bed, a constant Chézy roughness factor is assumed and a frictional force is calculated. Presence of other particles and the interaction between these particles is ignored. Incorporating this interaction can be done by considering multiple particles at once. If particles collide they affect each others trajectory, nevertheless for a first understanding of the problem one particle is considered.

Turbulence is excluded from this particle model, but could be included by adding a spatially varying flow field to the particle model. Furthermore, including the natural dynamics of the river could be done by implementing a time varying flow field to simulate what happens during a variable discharge. Note that in this case also the supply of sediments upstream should be incorporated to investigate this effect.

Some assumptions are made related to the flow field. At each point in the computational domain the flow is assumed to be in the same direction (γ) and scales linearly with the relative depth. This means that for example at the top of the sill the flow is higher compared to the flow in the main channel, but that the flow direction is the same everywhere. In order to give an approximation of the near-bed flow velocity it is assumed to be at 1% of the local depth above the zero-velocity level. This assumption was made, since no other physical determination of the near-bed flow velocity was found. Nevertheless, a similar approximation of the near-bed flow velocity is assumed in Delft3D.

Finally, a logarithmic velocity profile in the vertical is assumed. However, this profile might be deformed in reality due to the presence of a longitudinal-training-dam sill. Lauchlan (2001) performed experiments with perpendicular sills⁷. In her report she mentioned that the critical shear stress would change as a result of the sill structure and that accelerations at the sill would deform the velocity profile. Consequently this would lead to different shear stresses at the sill.

⁷Perpendicular sills have a crest which is perpendicular to the flow direction.

3.7 General applicability of particle model

The method that is used in the particle model is generic and therefore applicable for many situations. Bed load sediment transport is described by the model for any bed configuration and flow situation based on equations of motion. This section discusses within what limits the model is generally applicable. For example, the transport mode that is considered in the model is best described by sliding, since the particles are in constant contact with the river bed. However, it is possible to adapt the particle model to vertical velocity variations and thereby including other transport modes as well.

Initiation of motion is corrected for the flow alignment and transverse bed slope. Longitudinal bed slopes are considered to play a minor role in initiation of sediment motion, since these slopes are usually very mild (order 10^{-4}). Note that in case steeper longitudinal bed slopes are present, a different correction factor of the Shields parameter should be derived. However, since rivers usually have a very mild slope in longitudinal direction, the particle model is applicable for most rivers with mild longitudinal slope.

The current bed configuration (more details in section 3.2) is assumed to be constant in longitudinal direction. Nonetheless, any other bed configuration of the computational domain is possible. This makes the model flexible and generally applicable. The influence of the height, length and slope of the sill can easily be changed and the effect can be investigated. The particle model provides the opportunity to test the parameters that are used in the particle model.

Two flow situations are considered in this thesis: (I) uniform (chapter 4) and (II) spatially varied (chapter 5). In both situations the flow is assumed to be steady, which means that the flow is constant in time. Numerical models (e.g. Delft3D) can be used to generate a steady non-uniform flow field for any situation. On the assumption that a steady flow field is investigated, this model is applicable for any spatially varying flow situation.

The particle model can easily be extended with spatially varied parameters, such as flow fields or roughness coefficients. In this way better approximations of the near-bed flow velocity and flow angle can be made. Also the roughness of the sill can be varied. Note that the flow field might be affected by variable roughness. In other words, flow fields that are generated by numerical models should then also include a spatially variable roughness.

3.8 Key points of this chapter

This chapter started with explaining the causes of a transverse flow component in the river. This transverse flow component is in fact the driving force behind the flow and thus also the sediment transport over the sill. Generic results have been established from the criteria for initiation of motion on a sill slope. Graphs were made for depth-averaged flow velocities and varying side slopes. These graphs explain under which conditions the criteria of initiation of motion is exceeded or not on a side slope with unaligned flow.

This result was used in the particle model that has been developed in this chapter. If the shear stress exceeds the critical shear stress sediment particles start moving and the particle trajectory is calculated based on equations of motion.

The model made several assumptions and simplifications, which have been discussed in section 3.6. In the next chapter the model is verified with a uniform flow field. In this thesis it is also investigated how a spatially varying flow field can be added to the particle model.

Chapter 4

Verification of particle model with uniform flow field

4.1 Introduction

Local geometry influences the distribution of water and sediment between both channels. In the previous chapter a particle model is developed, which is subjected to a uniform flow field. In this case this model is verified for various uniform flow fields. Figure 4.1 shows the computational domain of the particle model in the black dashed box. The arrows in this figure represent the uniform flow field. Inducing a uniform flow field is done to understand the essence of the system behaviour. In other words, to find out why sediment is transported into the side channel or not.

The flow field is not likely to be uniform at the inlet sill, but is likely to adapt gradually along the sill to the widening of the river. The measurements of Rijkswaterstaat show that the flow angle near the inlet is in the order of 15° . In practice the flow angle can vary 0 to 90° along the sill. Note that if the flow angle (γ) is 0 there is no transverse flow, whereas if the flow angle is 90° all the water goes via the side channel. In practice both scenarios are not likely to happen, but for conceptual purposes these situations are verified in the model as well.

Each discharge has its own characteristic velocity, water level and probably also flow angle along the sill. Four different discharges are tested in this chapter: low, average and design discharges in the river. Rijkswaterstaat provided hydrodynamic and bed topography data that are used to assess the model in a qualitative way.

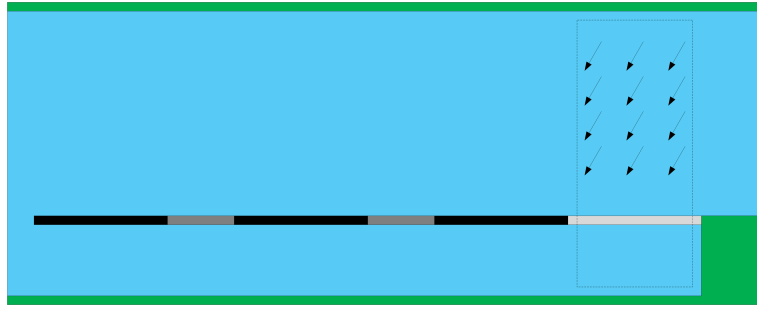


Figure 4.1: A uniform flow field is used for verification of the model. This figure shows the computational domain in the dashed box, the arrows indicate the initial flow field.

4.2 Verification cases of particle model

Rivers are naturally dynamic; dry and wet periods alternate and therefore the discharge in the rivers fluctuates. In this chapter four discharges are assessed during the verification of the particle model. Based on the findings of section 2.3 it is assumed that a low discharge in the River Waal corresponds to $750 \text{ m}^3/\text{s}$, average discharge corresponds to $1500 \text{ m}^3/\text{s}$ and high discharge $3000 \text{ m}^3/\text{s}$. In addition the Rijkswaterstaat's flow measurements are given for for a discharge in the River Waal of $1100 \text{ m}^3/\text{s}$.

With the use of historical data the water levels for each discharge were computed, see Figure 4.2. From design graphs of the longitudinal training dam it was found that the average river bed in the main channel is situated at -3.25 m NAP^1 .

The particle model is subjected to a number of test situations. In these situation a uniform flow velocity and flow angle are assumed. Although this is not very realistic, it is expected to give a better insight into the essence of the system behaviour. In the tests four different discharge are applied: low ($750 \text{ m}^3/\text{s}$), average ($1500 \text{ m}^3/\text{s}$), high ($3000 \text{ m}^3/\text{s}$) and measurement of Rijkswaterstaat ($1100 \text{ m}^3/\text{s}$).

For each situation the flow angle is varied and the critical flow angle for which sediment is transported over the sill is determined. In addition two extra situations are are tested given an average discharge: (I) when there is no transverse flow ($\gamma=0$), i.e. the flow is aligned with the longitudinal-training-dam sill, and (II) when the flow angle is 90° , i.e. there is no longitudinal flow component. This results in six cases which are summarised in Table 4.1.

The flow velocity cannot be retrieved from historical data, therefore the velocity that was measured by Rijkswaterstaat together with the discharge was used as a reference value. All parameters apply for the measurement station Tiel. With the use of the Chézy formula: $u = C\sqrt{hi_b}$ the Chézy coefficient is determined. According to the data the mean velocity was 1.04 m/s , the longitudinal bottom slope (i_b) was assumed to be 10^{-4} and according to the historical data a corresponding water depth of 6.68 m (water level at $+3.43 \text{ m NAP}$, bottom at -3.25 m NAP) was assumed. Applying these parameters in the Chézy formula, it follows that the Chézy coefficient is $40 \text{ m}^{1/2}/\text{s}$. Using this roughness value, flow velocities for other discharges can be determined as well.

The location of the computational domain of the particle model is indicated in Figure 4.1 with the dashed box. This domain contains only the inlet sill which is 200 m long, the width of the main channel is 230 m and the width of the side channel is 90 m .

¹NAP is a Dutch vertical datum, approximately equal to Mean Sea Level (MSL).

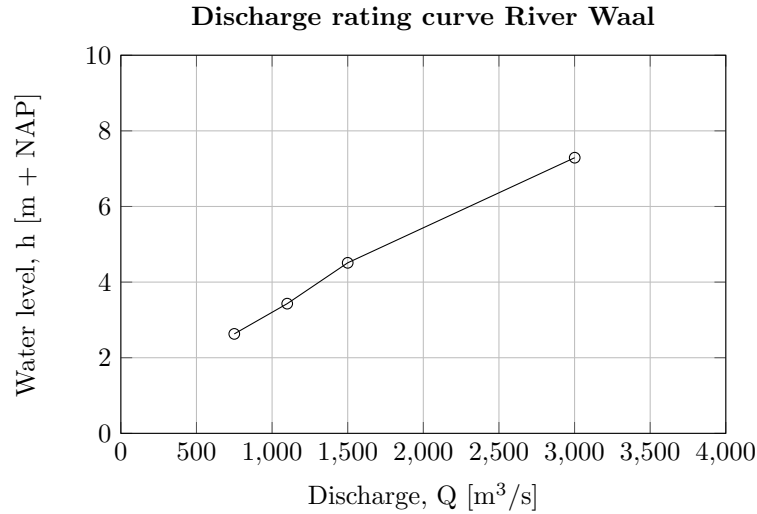


Figure 4.2: Discharge rating curve of the River Waal. This relation expresses the relation between the discharge in the river and the corresponding water level. These values were computed from the measurement station Tiel. Source: Waterbase data.

Table 4.1: Situations that are used for verification of the particle model. The discharge corresponds to a water level at the measurement station of Rijkswaterstaat. Depth-averaged flow velocities are calculated based on the reference discharge (1100 m³/s).

Discharge River Waal (m ³ /s)	Water level at measurement station Tiel(m + NAP)	Water depth in main channel (m)	Depth averaged flow velocity (m/s)	Flow angle (°)
750	2.63	5.88	0.97	Variable
1,500	4.51	7.76	1.11	Variable
3,000	7.29	10.54	1.30	Variable
1,100	3.43	6.68	1.04	Variable
1,500	4.51	7.76	1.11	0
1,500	4.51	7.76	1.11	90

4.3 Minimum flow angle

The initial condition for transport towards the side channel depends on the local flow conditions. The red dashed line in Figure 4.3 indicates possible start locations for a sediment particle in the particle model. From each location flow minimum flow angle can be determined. Figure 4.4 shows that there is a minimum flow angle to reach the side channel. If the flow angle is smaller than this minimum angle the streamlines do not reach the side channel.

The sediment particles are likely to follow the flow. If the flow angle is smaller than the minimum flow angle, sediment particles are not likely to be transported over the sill. Therefore, the minimum flow angle is also a measure for the minimum angle the flow must have in order to transport sediment particles over the sill.

For every possible start location on the red dashed line Figure 4.3 shows the minimum flow angles to reach the side channel. From this figure it follows that in the middle of the main channel the minimum flow angle to reach the side channel is 30°.

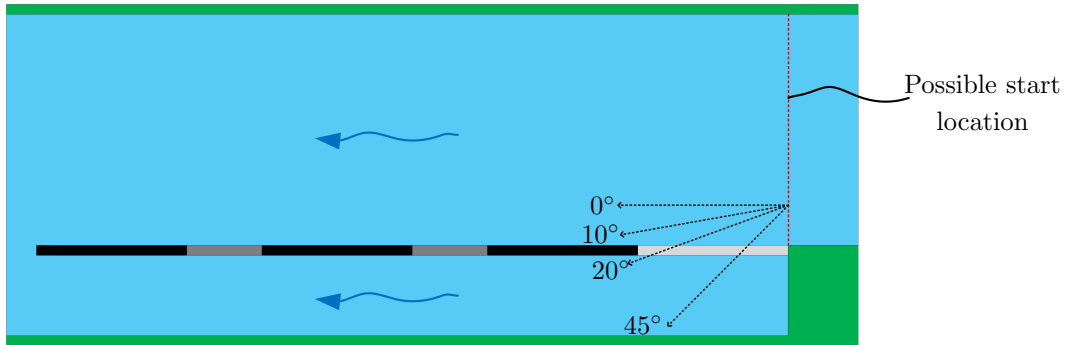


Figure 4.3: At each location on the red line a minimum flow angle can be found. This figure shows for an arbitrary location four flow angles. It shows that for this location the minimum flow angle is approximately 20° .

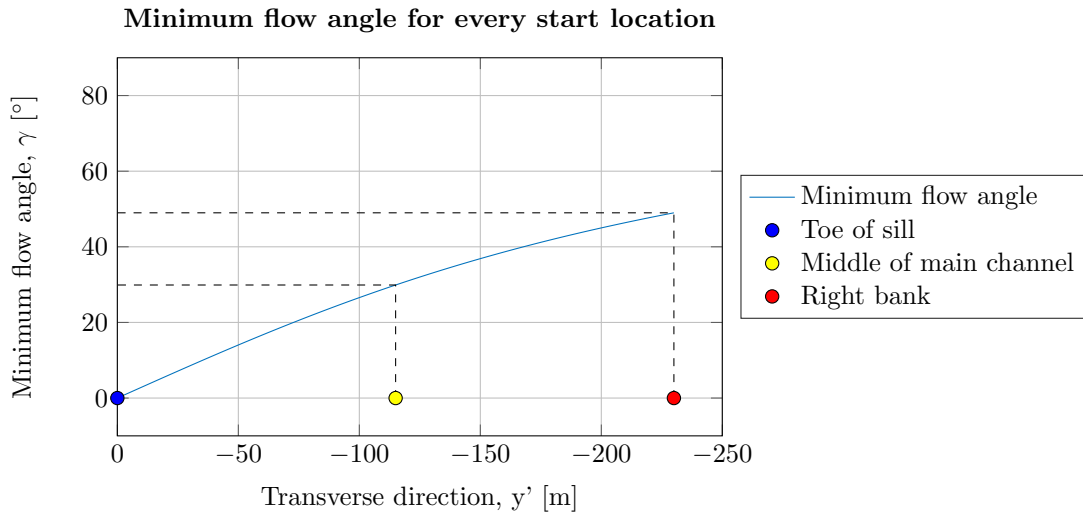


Figure 4.4: For each start location in the main channel the minimum flow angle is calculated. The left side of graph shows the toe of the sill, the right side is the right bank. The dots indicate three locations in the main channel: blue=toe of sill, yellow =middle of the main channel and red=right bank.

4.4 Initiation of motion

Generic graphs for initiation of motion have been presented in the previous chapter. In these graphs the flow angle is varied with the sill slope. The Chézy value is $40 \text{ m}^{1/2}/\text{s}$ in this case, since that followed from the flow measurements of Rijkswaterstaat.

Figure 4.5 shows that for all discharge left of the yellow line initiation of motion occurs. Note that all lines are on top of each other, therefore only the yellow line is visible. Note that this does not prove that there is also movement towards the side channel. It can only be seen from this graph that whatever bed configuration is chosen, sediment movement is possible for every flow angle in the domain of -90 to 90° .

In the previous section the minimum flow angle for every location has been explained. In combination with a minimum required flow regime (this section) causing initiation of motion, a first estimate can be made under which sediment transport over the sill can be expected. However,

Flow angle versus sill slope angle for various discharges

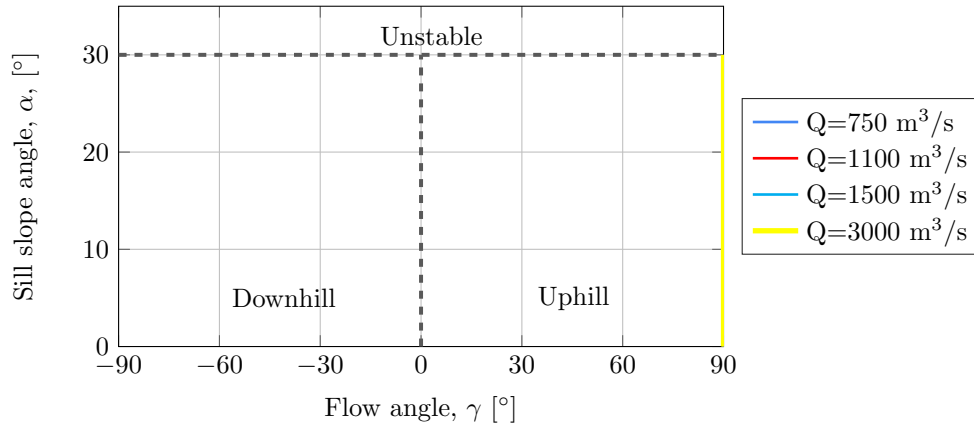


Figure 4.5: Initiation of motion takes place left of the yellow line. All lines are on top of each other, therefore only the yellow line is visible. Chézy value in this case is $40 \text{ m}^{1/2}/\text{s}$. In this figure the first four test cases from Table 4.1 are presented.

a sediment particle does not necessarily follows a streamline. This means that a positive flow angle is no guarantee for sediment transport over the sill.

4.5 Results

4.5.1 Combining initiation of motion with transport over sill

The particle model is applied to different discharges. The results of this particle model are combined with Figure 4.5 in Figure 4.6. For all discharges that are considered in Figure 4.5 the lines are on top of each other. Therefore, they have been combined in one thick blue line representing initiation of motion for all discharges.

The dashed lines in Figure 4.6 indicate the minimum combination of flow angle and sill slope angle. The initial condition was chosen at the toe of the sill. The areas between the thick blue line and the dashed lines are the areas in which sediments are transported over the sill, with initial location the toe of the sill. An increasing discharge leads to more combinations of α and γ for which sediment is transported over the sill.

If initial conditions are selected inside the main channel (see section 4.3), the dashed lines in Figure 4.6 would shift to the right, because less sediment is transported over the sill. If the initial condition is chosen at the slope of the sill itself the reverse occurs, sediment transport towards the side channel is likely to occur for more combinations of α and γ .

Furthermore, at steps of 5° of the sill slope angle, the minimal flow angle is determined. Sill slope angle of 0 is not considered. This would mean that the bottom is flat and that there would be no sill. However, the side channel is one metre higher than the main channel, which causes problems in the bed topography of the particle model. Sill slope angles larger than 30° are considered to be unstable.

Given a discharge of $3000 \text{ m}^3/\text{s}$ a similar minimum flow angle is required for a side slope of 5 and 10° . However, it would be expected that for a smaller sill slope angle also a smaller flow angle

would be necessary to transport sediment particles over the sill. This might have to do with the geometry of the sill. The sill has a fixed length in the particle model. The height of the sill is kept constant, which means that the width of the sill is larger for a milder slope. Therefore, a stronger transverse flow component or a longer sill is necessary to eventually transport the sediment particle over the sill. Additionally, a mild slope of 5° stretches towards the left bank of the river and thus influence the flow possibly more than a steeper slope.

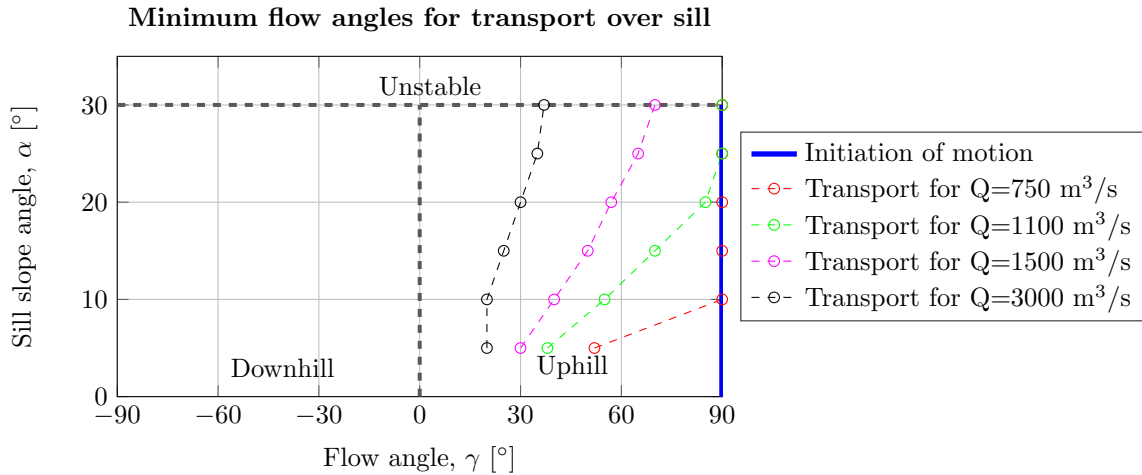


Figure 4.6: These results are the first four case studies from Table 4.1. Minimum flow angles for transport of sediment particle over the sill for four different discharges. Initiation of motion occurs for all sediment discharges. The area between the dashed lines and the line for initiation of motion gives the possible combinations of sill slope angles and flow angles for which sediment particles are transported over the sill.

4.5.2 Test cases aligned flow and unaligned flow

For the final test cases a depth-averaged flow velocity of 1.11 m/s and a water depth in the main channel of 7.76 m, corresponding to average discharge of $1500 \text{ m}^3/\text{s}$ in the River Waal. An arbitrary side slope was assumed of 10° . The reason for selecting this slope is that the particle trajectory is better visible for this slope angle. Verifying the results can be done more effectively.

Aligned flow

Sekine and Parker (1992) have investigated sediment transport on a side slope with an aligned flow. They described qualitatively that due to the presence of gravity a sediment particle on a slope will eventually move down slope. This is in fact similar to the fifth test case of Table 4.1. The initial condition has been selected at the crest of the sill.

Figure 4.7a and Figure 4.7b show the particle trajectory of a sediment particle located at the top of the sill with an aligned flow. It shows that the particle indeed moves down the slope, even though the flow is directed in the longitudinal direction. The reason for this is that there is a transverse force as a result of the gravity. The path seems to be different from the thought experiments by Sekine and Parker (1992) in Figure 2.20. The exact reason for this is unknown, but it might have to do with the chosen initial velocity condition or the different transport mode (sliding in particle model versus saltation in thought experiment).

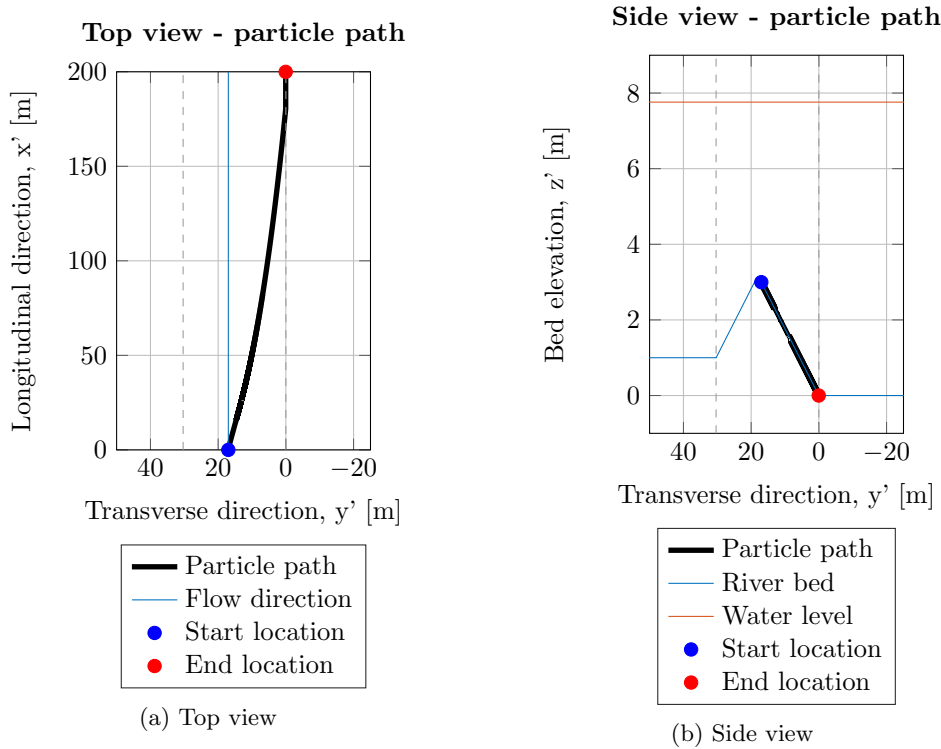


Figure 4.7: This result is the fifth case study of Table 4.1. Transport of sediment particle starting at the top of the sill with slope ($\alpha=10^\circ$). Flow is aligned ($\gamma=0$). Dashed lines indicate the toe of the sill on both sides. Particle moves down the slope under influence of gravity.

The initial velocity might influence the path as well. It seems that the transverse component in the particle model is larger than the longitudinal component. If the particle starts from standstill, it takes some distance before the longitudinal component is larger than the transverse component, which seems to be the case in the experiments of Sekine and Parker (1992).

Sliding causes a constant contact with the bed, which means a constant friction force from the bed. Saltation causes the particle to ‘jump’ over the bed and is thereby not in constant contact. If a particle is in constant contact with the bed it experiences a constant gravity force pulling the particle down the slope.

Unaligned flow

The particle model predicts the particle trajectory, which is shown in Figure 4.8. The start location that is selected for this case study is 20 m left of the toe of the sill (inside the main channel). According to Figure 4.4 the minimum flow angle for the streamline to reach the side channel from the selected initial condition is 6° and according to Figure 4.6 the minimum flow angle for a given side slope of $\alpha=10^\circ$ and an average discharge is 40° . Note that the latter is defined for a start location at toe of sill). Therefore, a flow angle larger than 40° is selected, namely $\gamma=45^\circ$, to illustrate how the sediment is transported over the sill.

Figure 4.8a shows a top view of the computational domain with the particle trajectory (red line).

The sill is situated between 0 and -30 m in transverse direction, the toe of the sill (on both

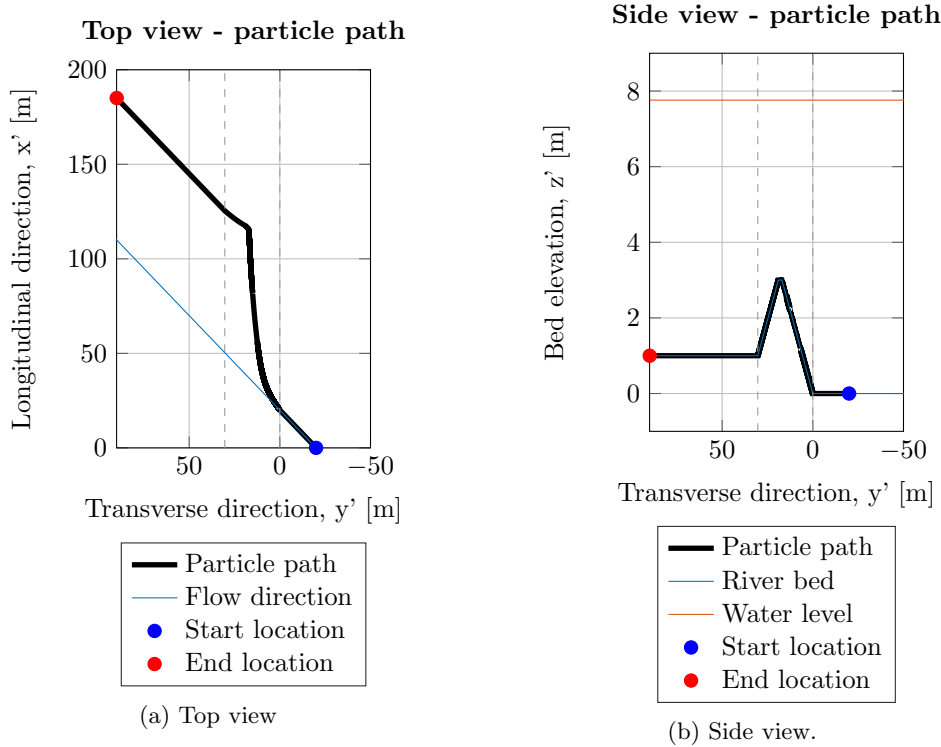


Figure 4.8: Particle path with an unaligned flow ($\gamma=45^\circ$) and a sill slope angle ($\alpha=10^\circ$). Gray dashed lines indicate the toe of the sill. Start location at +20 m in transverse direction, which is in the main channel.

sides) is indicated with the gray dashed line. Left of the sill there is the side channel (positive transverse direction) and to the right the main channel (negative transverse direction).

The particle trajectory shows that the sediment particle starts at the blue dot. Initially the particle follows the streamline, until it reaches the side sill. It takes some distance for the sediment particle to move to the crest of the sill, but once it reaches the top of the sill it follows the direction of the flow again. The particle ends at the left boundary (red dot).

Figure 4.8b shows a side view of the same solution. In this cross section a particle trajectory has been plotted by the thick black line. Note that the red line indicates the water level in this case. From the side view it is observed that the particle starts right of the toe of the sill (blue dot). It moves towards the sill, over the sill and ends at the left bank. The gray dashed lines indicate the toe of the sill on both sides of the channel.

4.5.3 Other results

- Given solely a transverse flow ($\gamma=90^\circ$) the sediment particles are transported over the sill for all discharges that are considered in this study.
- The Rijkswaterstaat data equals a discharge of $1100 \text{ m}^3/\text{s}$ and a representative flow angle is 15° . From Figure 4.6 it follows that for a side slope of 1:2.5 ($\approx 21.8^\circ$) no bed load transport will occur towards the side channel. However, in reality the flow angle changes along the sill and the velocity field is non-uniform. Other factors might also play a role which eventually lead to bed load sediment transport over the sill.

4.6 Key points of this chapter

A uniform flow field is applied to generate generic transport results for six case studies. The first four cases had a variable flow angle (γ), meaning that the minimum flow angle was determined in this chapter. Higher discharges are expected to transport sediment over the sill at lower flow angles. In Figure 4.6 it was observed that an increase in discharge leads to a reduction of the minimum flow angle and thereby creating a wider range for transport over the sill. Furthermore, under the influence of gravity a sediment particle tends to move down the slope for aligned flows. In case there is no longitudinal flow component, sediment particles are transported over the sill for all discharges that are considered in this chapter (750-3000 m³/s).

Initial conditions were described in section 4.3. The initial condition determines the minimum required flow angle that is necessary for a flow to enter the side channel at all. If the streamline does not even enter the side channel, sediment transport over the longitudinal-training-dam sill is not expected. Other initial conditions, such as the initial velocity are chosen to be 0 m/s, although this is in practice not likely to be the case.

Earlier it was found that inside the side channel sedimentation occurs, according to data from Rijkswaterstaat. However, this does not necessarily have to be bed load sediment transport. In section 2.2 and section 3.3 it is explained that neither the flow nor the water level is likely to be spatially uniform in the computational domain. This non-uniformity might be one of the reason why the results of particle model with a uniform flow field do not coincide with the Rijkswaterstaat data. In the next chapter a non-uniform flow field is applied to the model. Improvements of the model are included in the recommendations in chapter 7.

Overall it can be said that the model outcomes seem to coincide with what is expected to happen to a sediment particle that is subjected to a uniform flow field. Therefore the model is considered to be verified. Further development of the model (e.g. implementing non-uniform flow field) is needed for validation of other data.

Chapter 5

Application of particle model with non-uniform flow field

5.1 Introduction

Flow fields are often much more complex in natural dynamic rivers than what can be captured in a uniform flow field. In reality, there might be eddy formation, flow separation or even complicated three-dimensional turbulent situations. In order to approximate the reality better, a two-dimensional depth-averaged numerical model has been made to make an estimate of the plausible two-dimensional flow fields. In these flow fields the water level, flow velocity and flow angle vary spatially. The results of this model are coupled to the particle model. In Appendix D the numerical model set-up is explained in more detail. This chapter only considers the results of the numerical model, the coupling to the particle model and the results of particle model with input of the numerical model.

5.2 Generating a non-uniform flow field

The numerical flow and transport model Delft3D is used to compute water levels and flow fields (Deltares, 2014). A depth-averaged flow model has been created that represents a situation with a longitudinal-training-dam inlet sill. The inlet sill and elevation of the side channel are incorporated in the bed topography of the model. The riverbed of the particle model is thereby similar to the river bed of the numerical Delft3D model. Note that the computational domain of the Delft3D and the particle model differ. The Delft3D model includes part of the upstream river section and part of the longitudinal training dam itself as well.

5.2.1 Boundary conditions

One discharge boundary upstream and two water level boundaries downstream have been imposed in the Delft3D model. In Appendix D it is described that the depth at the crest of the inlet sill should not be too shallow, to prevent indetermination of the model. The computational domain is 230 m wide at the upstream side and 320 m downstream, where it consists of a side channel that is 90 m wide and a main channel of 230 m. The main channel downstream is equal in width to the

channel width upstream. The length of the computational domain is 1.1 km. Figure 5.1 shows the computational domains of the particle model (yellow dashed rectangle) and the numerical model (black dashed rectangle).

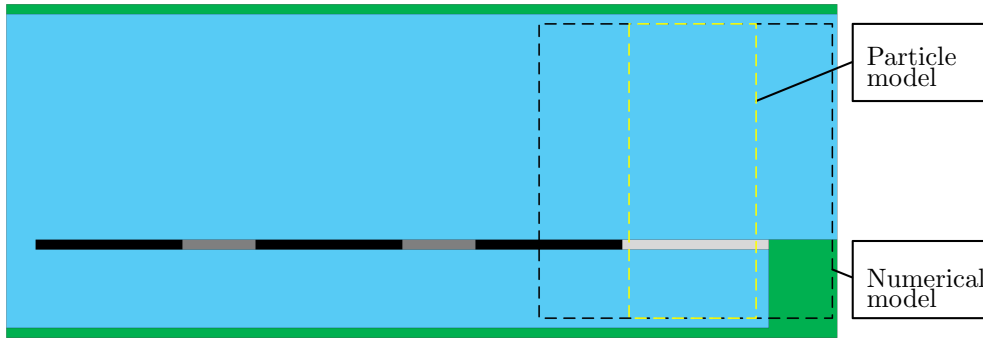


Figure 5.1: The domain of the numerical model (black dashed box) is different from the domain of the particle model (yellow dashed box). The particle model only includes the inlet sill, whereas the numerical model also includes part of the first longitudinal training dam and part of the upstream river section.

5.2.2 Water level field

Figure 5.2 shows the water level field, which is relative to the bottom of the main channel. In the water level field a gradual decrease in longitudinal (or x) direction is noticed which is due to the small bottom slope (order 10^{-4}). The length of the computational domain is 1.1 km, which leads to a change in bottom level of approximately 10 cm. The water level difference is in the same order of magnitude.

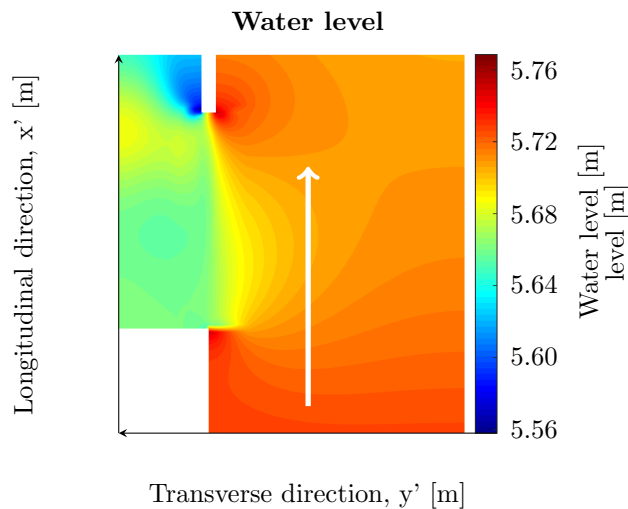


Figure 5.2: Water level field that is generated by Delft3D. Flow is from bottom to top, see white arrow. The length of domain in longitudinal direction is 1.1 km and width of the river at the inlet is 320 m. Left of the sill a water level lowering occurs. The difference in water level in the main channel between downstream and upstream is approximately 10 cm.

5.2.3 Flow velocity field

After the spin-up time Delft3D generates a steady flow velocity field. The flow velocity is depth-averaged and therefore does not consider any vertical velocities. The magnitude of the flow velocity decreases in the left corner of the inlet. Left of the upstream end of the longitudinal training dam the magnitude of the flow velocity decreases as well. Figure 5.3 shows the magnitude of the flow velocity in the entire computational domain of the Delft3D model. Maximum flow velocities occur at the sill and at the start of the side channel. These velocities do not exceed a depth averaged velocity of 1.5 m/s.

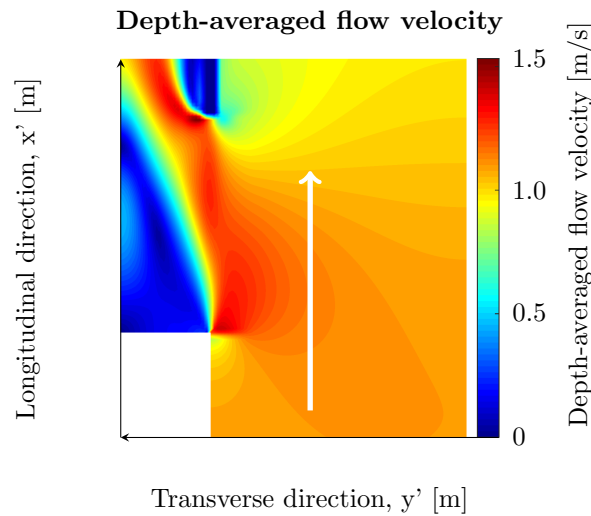


Figure 5.3: Depth-average flow velocity field that is generated by Delft3D. Flow is from bottom to top, see white arrow. The length of domain in longitudinal direction is 1.1 km and width of the river at the inlet is 320 m. At the sill flow velocities increase and left of the inlet the velocity magnitude reduces. Note that the magnitude of the flow velocity is presented.

5.2.4 Flow velocity angle field

Flow velocity vectors indicate the depth-averaged flow direction, which is used later as an input parameter for the particle model to calculate the path a particle takes. In the previous section it was found that the flow velocity magnitude varies spatially. Here the direction of the depth-averaged flow is presented in Figure 5.4. At the end of the sill the longitudinal training dam is situated and the flow is directed towards the side channel.

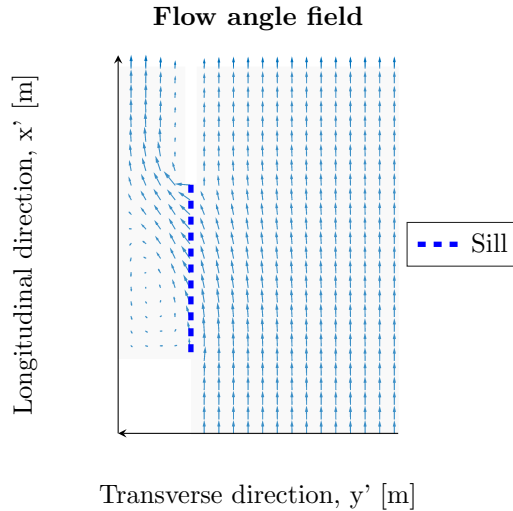


Figure 5.4: Flow angle field that is generated by Delft3D. Flow is from bottom to top, length of domain in longitudinal direction is 1.1 km and width of the river at the inlet is 320 m. Left of the sill a eddy is clearly formed. Left of the longitudinal training dam another eddy is formed.

5.3 Results

In this section the results are presented of the information of Delft3D in the area of interest. This information has been transferred to the domain of the particle model. Three subresults will be discussed, the water level variations, flow velocities and the influence of the bed configuration. In the latter subsection the link with the particle model is made. Note that the model runs, which are presented in the first two sections, use a transverse slope angle (α) of 20° for the longitudinal training dam sill.

5.3.1 Water level

In Figure 5.5 water level differences between the main and the side channel can be observed on the order of a few centimetres. These water level differences cause a pressure difference between both channels. In section 3.3 it was discussed that this water level difference is the driving force behind the flow over the longitudinal training dam sill, towards the side channel. Left of the sill a circular pattern of a water level lowering is noticed. Also left of the longitudinal training dam sill a water level difference occurs.

5.3.2 Flow velocity and flow angle

Figure 5.6 shows the flow velocity information in the area of interest. From these figures it can be seen that left of the sill, where earlier a water level difference was noticed, an eddy is formed. It takes some distance for the flow to enter the side channel. At the end of the sill the flow is directed strongly into the side channel.

In the main channel the flow is mainly in the longitudinal direction, while close to the sill the transverse flow component becomes larger. At the sill the flow angle (γ) can become 90° at the downstream end of the sill, which means completely directed towards the side channel. Averaging

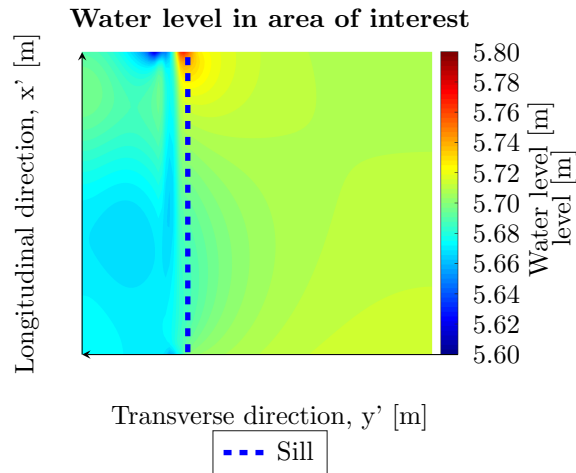


Figure 5.5: Close-up of top view of the water level field in the area of interest. This water level field is coupled to the particle model. Left of the sill a water level lowering is observed, compared to the main channel (green area). Right of sill is the main channel, left of the sill is the start of the side channel. Flow is mainly in longitudinal direction, which is from bottom to top.

the flow angle over the sill in longitudinal direction shows that on average the flow angle is 20-30 degrees at the sill. This is in slightly higher than what was found by the data of Rijkswaterstaat¹. The non-uniform flow field thus gives an indication of realistic values in the field, which might also be applied again in a uniform flow field case study (see chapter 4).

¹Note that the upstream discharge in the Delft3D model is 1500 m³/s and the Rijkswaterstaat measurements the upstream discharge was 1100 m³/s. This might explain that there is a slightly larger mean flow angle at the sill.

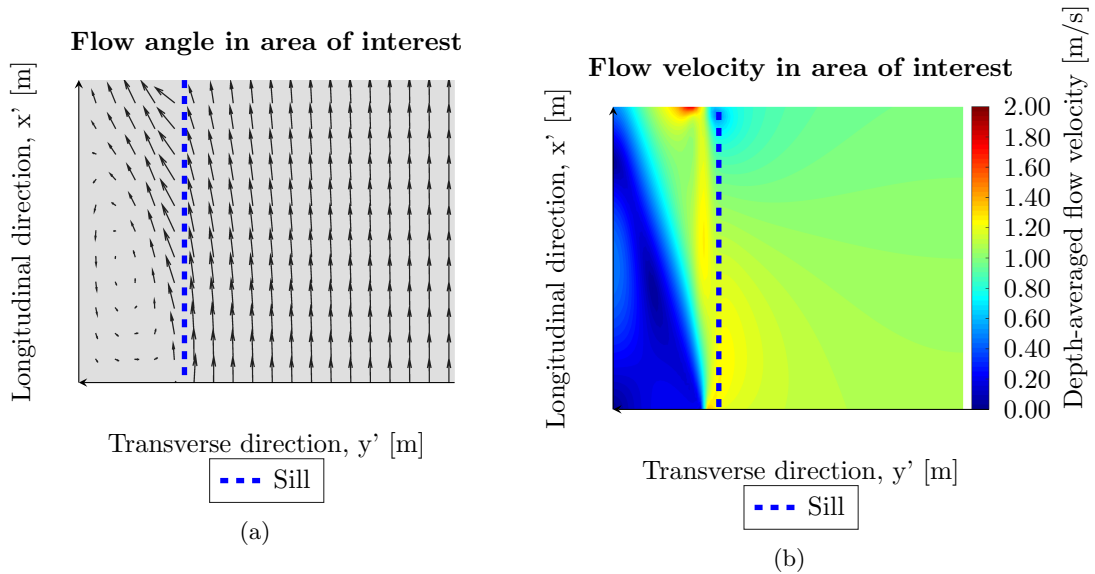


Figure 5.6: Close-up of top view of the flow field in the area of interest. (a) shows the flow angle and (b) flow velocity magnitude in the area of interest. Note that the flow velocity is depth-averaged. Left of the sill an eddy is formed, which causes a reduction in the flow velocity magnitude. Along the sill the flow is not uniformly distributed, at the upstream side of the sill there is almost no transverse flow component, while at the downstream side the transverse flow component is visible.

5.3.3 Bed configuration of the sill

Four different bed configurations of the longitudinal-training-dam sill are imposed. In Figure 5.7 the different bed configurations are presented. Note that solely a section of the river (from $y' = -10$ to 75 m) is presented. It was observed that a different bed configuration of the sill influences the flow close to the sill slightly and therefore the change in flow is not expected to be the main cause of a different particle trajectory. The crest height of the inlet sill can affect the flow more, however, in these computations the crest height has assumed to be constant to investigate the effect of the steepness of the sill.

The discharge boundaries are unchanged; upstream a discharge of $1500 \text{ m}^3/\text{s}$ is imposed, which corresponds to the average discharge in the River Waal. Bed configurations are selected by varying the transverse slope² (α), using 5 , 10 , 15 and 20° .

Increasing the transverse bed slope of the sill makes it harder for the sediment particles to be transported uphill. The gravitational force that acts on the sediment particle scales with the slope of the sill and thus becomes more significant for steeper slopes. This is the reason why the sediment particles on steeper slopes need distance in longitudinal direction to be transported uphill before they reach the side channel. Some particles are not transported over the sill at all.

Figure 5.8 shows the effect of selecting a different transverse slope (α). Steeper slopes affect the hydrodynamics slightly around the sill. In case the mildest slope is selected, most of the sediment trajectories end up in the side channel. Increasing the steepness of the slope of the sill affects the particle trajectory. For a slope of 20° no transport over the sill is observed at all, this is discussed in the next section.

²In reality the transverse slope is 21.8° which corresponds to a slope of 1:2.5.

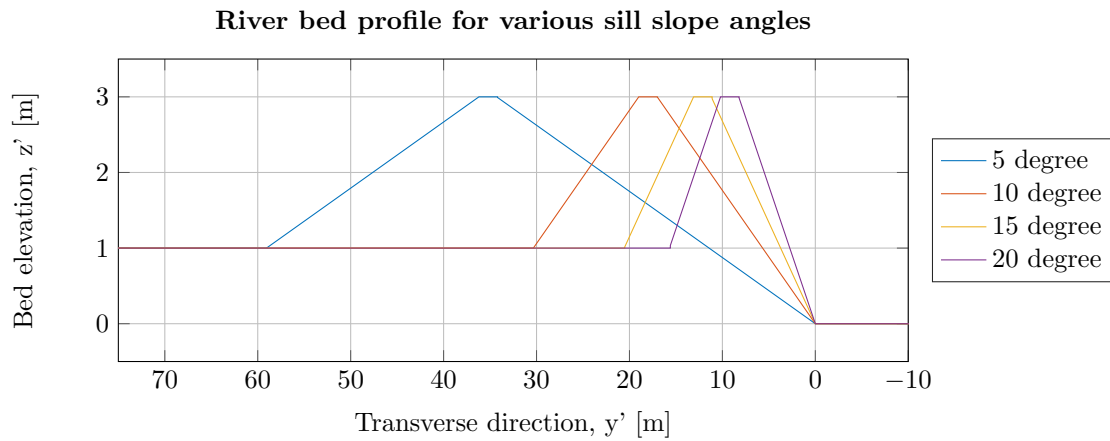


Figure 5.7: Profiles for various slopes, only a section of the transverse direction is presented here. It is shown that milder slopes have larger widths. The height of the sills is kept constant.

5.4 Bifurcation relations

Figure 5.8 shows the trajectories of the sediment particles over the longitudinal training dam sill. It appears that the sill slope (α) has an influence on the distribution of sediments between both channels. The results of the particle model allow to quantify the fraction of the sediments that is transported over the sill. For various initial conditions the sediment trajectory is investigated, similarly to Figure 5.8. The distance between the toe of the sill and the maximum initial condition is used as a measure for the fraction of sediment that is transported over the sill, S_{sill} . The remaining width of the main channel from where sediment is confined in the main channel is called S_{main} .

For example, if the maximum initial condition that causes sediment transport over the sill is 40 m right of the toe of the sill and the main channel is 230 m wide, then ratio of sediment equals $S_{\text{sill}}/S_{\text{main}} = \frac{40}{230 - 40} = 0.21$. This ratio of the sediments over the sill (S_{ratio}) can be related to variable angles of the longitudinal-training-dam sill slope and also to the distribution of flow over the sill.

Figure 5.9 shows the relation between the sediment transport ratio and the slope angle of the longitudinal-training-dam sill. For a mild side slope angle ($\alpha=5^\circ$) the width of the sill is larger and thus a sediment particle takes a longer distance to travel uphill. In the situation with the mild slope it takes a longer distance in transverse direction to reach the crest of the sill. Since the length of the sill is fixed, some particles are still confined in the main channel. This causes a reduction of the sediment ratio for mild slopes, see the difference between the solid and the dashed line in Figure 5.9. If the length of the sill would not be included the ratio of sediment over the sill would increase, which is in accordance with the reasoning in Figure 4.6.

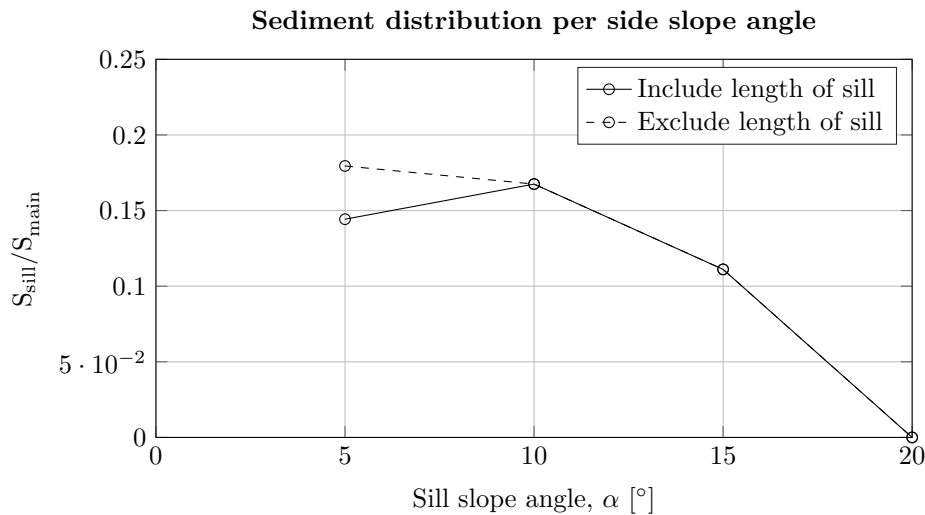


Figure 5.9: Sediment transport ratio expresses the amount of sediment that is transported over the sill with respect to the amount of sediment that is confined in the main channel. This ratio is varied with the steepness of the sill, α . An increase of the steepness leads to a reduction of the sediment ratio. The milder slope causes a wider slope, which causes a reduction of the sediment transport over the sill. If the length of the sill is not included the width effect is not noticed anymore. S_{sill} is the part of the sediment that is transported over the sill and S_{main} is the part of sediment that is confined in the main channel.

The sediment transport over the sill is likely to be a function of the flow distribution between the channels. Figure 5.10 shows that increasing the discharge ratio over the sill this (Q_{ratio}) does

not linearly increase with the sediment that is transported over the sill. Thus, it seems that the sill has an influence on the part of sediment that is transported over the sill and the part that is confined in the main channel. Note that for discharge rates larger than approximately 0.5 only occur under very extreme circumstances. In addition, a discharge rate of 0.5 means that that 1/3 of the discharge is transported over the sill and 2/3 is confined in the main channel.

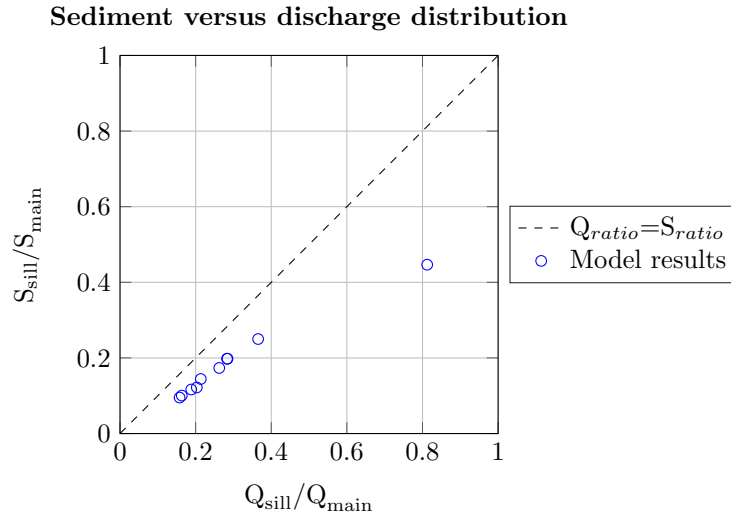


Figure 5.10: Sediment transport ratio with respect to the discharge ratio. These ratios express the amount of the variable that is transported over the sill with respect to the amount that is confined in the main channel. The sediment transport ratio does not follow the discharge ratio, which means that the sill is likely to have an effect on the confinement of sediment in the main channel. S_{sill} is the part of the sediment that is transported over the sill and S_{main} is the part of sediment that is confined in the main channel. Note that the same holds for discharge, Q_{sill} and Q_{main} .

From these results a sediment-discharge relation could be derived, which includes the geometry of the sill. This type of findings could later be used in other models to quantify what the effect of the sill will be on the morphological changes in the entire system. In other words, if erosion or sedimentation will occur behind the sill or in the side channel.

5.5 Key points of this chapter

In reality the flow around a longitudinal-training-dam inlet sill is not likely to be spatially uniform. A two-dimensional depth-averaged Delft3D model was used to generate hydrodynamic information, such as water levels, flow velocities and flow angles, in the area of interest. The sill has been incorporated in the bed topography of the model, in order to assess the situation as good as possible.

At the sill a water level difference is noticed, which causes a pressure difference between both channels and consequently a flow from the main channel to the side channel. This flow tends to increase towards the end of the sill. A reduction of the flow velocity occurs left of the sill, where an eddy has been formed. Non-uniform flow conditions affect the sediment transport over the sill.

The results of the Delft3D model were coupled to the particle model in order to capture this non-uniformity. It was found that the sill slope (α) affects the ratio of sediment that is transported over the sill. It appears that increasing the slope angle leads to a reduction of the bed load sediment

transport. However, at very low slope angles ($\alpha=5^\circ$) the width of the sill increases and this leads to a reduction of the sediment that is transported over the sill. If the length of the sill would be excluded, this effect would not be noticed.

The model results show that for a sill slope angle of 20° there is no sediment transport over the sill. In practice the slope of the sill is 1:2.5, which corresponds to an angle of 21.8° . The data of Rijkswaterstaat give indications for sediment transport over the sill for a sill slope of 21.8° . Further research is necessary to determine under which flow conditions bed load sediment transport over the sill is observed in practice to validate the model.

In the next chapter the model is reviewed with respect to the results. Suggestions to further improve the model and also for implementation of the results in numerical software such as Delft3D. If the model is quantitatively validated sediment rating curves (see Figure 5.9 and Figure 5.10) can be used in numerical software to model the ratios of sediment transport over the sill for various parameters.

Chapter 6

Discussion

Longitudinal training dams create a bifurcation of the river. At the bifurcation, a sill is situated at the bottom of the river in order to regulate the water and sediment distribution. Modelling bed load sediment transport over the sill is done in this research. The sills are modelled as side sills with an unaligned flow. This chapter discusses the results by qualitatively describing if the sediment transport over the sill is underestimated or overestimated for various aspects of the model.

Sekine and Parker (1992) investigated bed load sediment transport on side sills with aligned flows. They described that the gravity force which acts on a sediment particle tends to move the particle down the slope. However, it is unknown what happens to a sediment particle that is under the influence of an unaligned flow on a side slope. Therefore, a theoretical framework has been established that is based on equations of motion in order to predict the movement of a sediment particle. In order to grasp the essence of the sediment movement, the situation is simplified and assumptions are made.

Sediment transport is usually described by empirical relations, since there are many factors that play a role which are hard to describe physically. These formulations do usually not consider individual grains, but bulk volumes of sediment instead. If, however, individual grains are considered they are likely to interact with each other. The particle model has been developed in this study does not include the interaction between sediment particles. Because particles collide they might lose momentum and they decelerate. In reality rivers usually consist of graded sediment, which could mean that some particles might be influenced by the shape and size of other sediments, e.g. by hindrance of sediment movement. This effect is ignored, but it is assumed that it does not contribute in understanding essence of why a sediment particle is transported over the sill. However, it is unclear what the effect is of the interaction with other particles. Particles that collide are likely to lose momentum, which would mean that less sediment is transported over the sill.

Particles are assumed to be in constant contact with the river bed, which corresponds to the transport mode called sliding. In reality other transport modes might also be possible. Sediments can be entrained and brought over the sill in suspension. This phenomenon has been observed in experiments by Lauchlan (2001). Lauchlan suggests that the velocity profile deforms at sills. Deformation of the velocity profile affects the shear stress and can therefore lead to a different behaviour of the sediment transport on the sill slope. However, establishing the shear stress and the correct velocity profile is not considered to be within the scope of this research. Note that the velocity profile is important in describing sediment transport over the sill, since the flow is the driving force of the sediment movement. Further research is necessary to quantify the effect

of a different velocity profile and shear stress. However, if acceleration would also occur on side sloping sills, it is likely that more sediment is entrained and transported over the sill.

Water level differences cause a transverse flow over the longitudinal-training-dam sill. In reality, other aspects might contribute or oppose the flow over the sill. A secondary flow in combination with a sill might induce a difference in transversal momentum at the sill. Also the transfer of momentum in longitudinal direction could (indirectly) play a role in the flow over the sill. This study focusses on the essence of sediment transport over the sill, accurate predictions of the flow distribution are disregarded, but can be important. If the processes around the inlet sill are understood in more detail, this could be verified in the numerical software which is used as an input parameter for the particle model.

In this model a static friction force is assumed for sediment particles that move. However, in other studies a dynamic friction coefficient is applied for moving sediment particles. Dynamic friction coefficients are usually smaller than the static one. Applying a static friction coefficient overestimates the frictional force. Since no clear descriptions of the dynamic friction coefficient on side sills was found, the friction coefficient is assumed to be static. More research is necessary to quantify the dynamic friction coefficient on side sills. Moreover, a uniform bottom roughness is assumed in the entire computational domain. In practice the main channel, side channel and sill could have various roughness coefficients. The model could be extended to describe a variable roughness. Note that an overestimation of the friction coefficient could lead to an underestimation of the volume of sediment that is transported over the sill.

In this particle model a near-bed flow velocity is assumed at 1% of the depth above the zero-velocity level. This assumption is very important in estimating the particle trajectory. The near-bed velocity is based on the logarithmic velocity profile assumption. Estimating the near-bed velocity makes use of the local shear velocity. This shear velocity is calculated by the particle model as well and coincides with the shear velocity in Delft3D. The reason for estimating the near-bed flow velocity at 1% of the depth above the zero-velocity level is that Delft3D uses a similar approach. For Z-layers in Delft3D the near-bed flow velocity is based on the flow velocity in the deepest layer. Therefore, 1% of the total depth is assumed to be an appropriate value. Currently no other ways of computing the near-bed flow velocity is found, therefore this '1%' assumption is made. Choosing a higher near-bed velocity leads to more sediment transport over the sill, lower near-bed velocities give a reverse result. In the next chapter recommendations are made to improve the approximation of the near-bed velocity.

The numerical approximation in time and space in the particle model is explicit Euler. Changing the numerical scheme (e.g. from explicit to implicit schemes) might reduce possible numerical errors. It is unclear what the effect of numerical inaccuracies is on the outcomes of the model. However, it is likely that this might influence the particle trajectory. The same holds for the initial conditions (location and velocity). If the sediment particles have a higher initial velocity, the trajectory of the sediment particle is likely to be different.

In this thesis a steady flow situation is considered, which means that the flow is constant in time. On the other hand, in section 2.3 it is described that the flow situation in the River Waal is not constant in time, but varies over the year. It is assumed that the fluctuations in time are irrelevant for understanding how sediment is transported over the sill. If the model is used for other purposes (e.g. prediction of sediment transport over the longitudinal-training-dam sill during flood wave), this aspect should be further investigated.

Two other aspects that are not included are turbulence and secondary flow. Numerical models such as Delft3D are capable of computing these aspects, which might consequently lead to a different water level field and flow field. In this way turbulence and secondary flow are implicitly included in the particle model, by coupling the information of the numerical model to the particle

model. A secondary flow is likely to cause a higher transverse flow component and thus more sediment transport over the sill. The effect of turbulence is difficult to predict in advance.

In this thesis the slope angle is varied and investigated. However, in practice, also the height of the sill can be changed. It is likely that the height of the sill also has an effect on the trajectory of the sediment particle. For a mild slope it appears that the sediment particle needs longer distance to travel in transverse direction over the sill. Similarly for higher sills, the sediment particle needs to overcome a larger width for equal slopes of the sill. Note that higher sills cause a smaller water depth, which might lead to higher flow velocities. Higher flow velocities can compensate for the height-effect.

Chapter 5 made use of a flow field generated by two-dimensional Delft3D model. Depth-averaged flow velocities and flow angles are used to make an estimation of the flow velocity and flow angle near the bed. The flow angle near the bed is assumed to be the same as the flow angle of the depth-averaged flow. With the use of a three-dimensional Delft3D model, a better approximation of the flow velocity and flow angles near the bed can be made. The flow angle near the bed is expected to be smaller (less directed towards the side channel), which would mean that currently an overestimation of the sediment transport is made.

In the next chapter recommendations are made for extending the particle model by doing more research into the discussion points that are described here. Nevertheless, this model forms a first step into modelling bed load sediment transport over longitudinal-training-dam sills. Graphs like Figure 5.10 have a physical background and could be used for implementation in numerical software such as Delft3D, which is also described in the next chapter.

Finally, lighter particles require a lower velocity to follow the same path as heavier particles. This suggests that there is a relation between the weight of the particle and the flow velocity which determines the particle trajectory. Varying this relation with respect to the sediment transport over the sill makes the results of this thesis even more general applicable. Recommendations are made to investigate this relation. Note that in this thesis a relatively large sediment grain size is used, which means that a higher flow velocity is necessary to transport the sediment particle over the sill compared to the sediment particle with the real grain size. This means that the results might underestimate the real sediment transport over the sill, which might explain why for a sill slope angle (α) of 20° no sediment particle is transported over the sill.

Chapter 7

Conclusions and recommendations

7.1 Conclusions

RESEARCH QUESTION 1: *What is the driving force of sediment transport towards the side channel?*

Interventions in a river system usually affect the hydraulic and morphological behaviour of the system. Longitudinal training dams affect the behaviour of the system as well. At the upstream inlet water and sediment can enter the side channel due to a transverse flow. A sill at the river bed regulates the distribution of water and sediment. The configuration of this sill is affecting the distribution of water and sediment.

The transverse flow is a result of the geometry of the system, i.e. the widths of both channels, the curvature of the river and the length of the opening. In addition, the roughness, the channels and the sill play a role in the flow distribution. All factors together lead to a water level difference between the channels, resulting in a pressure difference, which drives the transverse flow.

Sediment usually tends to follow the streamlines of the flow. However, the sill at the entrance of the side channel prevents some parts of the sediment to enter. Since the flow is the driving force of sediment transport, a relation is made between the flow and the sediment that is transported over the sill. It is found that there is not a linear relation between these parameters. An increasing discharge over the sill does not necessarily lead to a proportional increase of the sediment transport over the sill. According to this research the sill influences the distribution of discharge and sediment differently.

RESEARCH QUESTION 2:

How is initiation of motion influenced by a longitudinal-training-dam sill?

An accurate description of the critical shear stress is often necessary to make predictions of sediment transport in empirical formulations. The critical shear stress that was derived by Shields is only applicable for a horizontal bed with a flow in downstream direction. However, the situation at the longitudinal-training-dam sill is much more complex than this situation. The sill is schematised as a submerged side slope with an unaligned flow. Two corrections were applied: (I) for the transverse bed configuration of the sill and (II) for the flow alignment.

For side slopes with an aligned flow, the critical shear stress reduces if the transverse bed slope increases. In other words, sediment particles tend to move at lower flow velocities for steeper side slopes. This reduction is caused by an increasing effect of the gravity component. According to Sekine and Parker (1992), sediment particles on a side slope move downwards due to the presence of gravity.

A change in flow alignment affects the critical shear stress as well. If the same flow is directed uphill the critical shear stress is increased. In other words, sediment particles start moving at higher flow velocities. For longitudinal-training-dam sills the critical shear stress is increased at the slope due to the configuration of the sill and the flow alignment.

RESEARCH QUESTION 3:

How is sediment movement influenced by a longitudinal-training-dam sill?

In order to determine how sediment particles move, a particle model is developed which is based on equations of motion. It is found that the geometry of the sill affects the trajectory of the sediment particle.

Applying a uniform flow field gives insight into the effects of different flow on the critical shear stress. Under certain conditions initiation of motion is induced, depending on the depth-averaged flow, flow angle and steepness of the transverse bed slope of the sill.

The results of the uniform flow field indicate that as soon as the particles reach the slope they deviate from the streamline and the process of transport on the slope starts. Depending on the flow conditions, it takes some distance for the particles to travel over the sill. From the measurements of Rijkswaterstaat it appears that it takes some distance in longitudinal direction for the sediment particles to be transported over sill.

With the use of a numerical flow model (Delft3D) non-uniform flow fields have been generated. These non-uniform flow fields describe the water level, flow velocity and flow angle in the field. It appears that an eddy is formed behind the sill and that it takes some distance for the flow to be directed into the side channel. Consequently, it also takes some distance for the sediment particles to be transported over the sill, which is again in accordance with the measurements of Rijkswaterstaat.

Finally, the sill affects the ratio of sediment that is transported over the sill. With the use of this particle model relations are found for various transverse slopes. These findings can be used in numerical models, see next section. From the model results it follows that the length of the sill is relevant for mild slopes. Mild slopes have a larger width, which requires more in longitudinal direction for sediment particles to be transported over the sill.

7.2 Recommendations

RESEARCH QUESTION 4:

What recommendations/improvements can be made to modelling sediment transport over sills of longitudinal training dam based on the findings of this research?

Improvements and recommendations of modelling sediment transport over sills of longitudinal training dams are twofold: (I) the particle model and (II) implementation of results in numerical software. For the particle model recommendations are made to reduce the uncertainties caused by the assumptions in the model. In addition, it is described how the results can be parametrized in standard software for morphological simulations, such as Delft3D.

Particle model

The particle model is generic and can therefore be applied for sediment transport situations. However, the model includes assumptions and simplifications which result in uncertainties. How the assumptions affect the results is described in chapter 6. Reducing these uncertainties can be reached by the following recommendations.

Models are always a representation of reality and numerical errors might give inaccurate answers. Different space and time discretizations need to be assessed and the stability of the schemes should be investigated. Also the accuracy of the numerical model results could be increased, in other words instead of depth-averaged 2D models, three-dimensional models could be used. In this way the flow velocity and the flow velocity angle near the bed are better approximated. Vertical velocities could be used to calculate the vertical movements of the sediment particles. Laboratory scale experiments or field data could confirm if the model results coincide with reality.

Currently a logarithmic shaped vertical velocity profile is assumed in the entire computational domain. However, due to accelerations at the sill, this assumption might not hold anymore. A non-logarithmic vertical velocity profile might affect the sediment transport over the sill. Near-bed flow velocities are currently based on a logarithmic shaped vertical velocity profile. Changing this velocity profile might result in a different particle trajectory. In addition, the flow over the sill is unaligned with the crest of the sill. It should be investigated how this alignment affects the vertical flow velocity profile. Numerical models (e.g. Delft3D) are able to approximate the velocities accurately in three-dimensions, this information can be used to approximate the near-bed velocities better. The particle model could be extended to use the near-bed flow velocities and the near-bed flow angles that follow from the numerical models.

Moving sediment particles usually interact and might induce hindrance to other particles. This interaction could be implemented in the particle model by formulating interaction between grains mathematically. Furthermore, since it is assumed that the grains are in constant contact with the river bed, it should be investigated how the dynamic friction coefficient evolves at a submerged side sill.

Parametrization for implementation in standard software for morphological simulation

In this thesis it was found that the sill affects bed load transport over the sill. The particle model is able to describe how and how much of the sediment is transported over the longitudinal-training-dam sill, which can help to improve numerical models (such as Delft3D) in modelling these type of sill structures. In section 5.4 sediment transport over the sill had been compared with two other parameters: (I) discharge over the sill and (II) sill slope angle (α). However, before any parametrizations for numerical models can be made more research is advised, which is described below.

Other geometric features of the sill and flow situations should be investigated as well, such as the influence of: upstream discharge ($Q_{upstream}$), width ratio of the channels (B_{ratio}), sill slope angle (α), crest height of sill (w_{sill}), length of sill in longitudinal direction (L_{sill}), water level in main channel (h_{main}) and water level in side channel (h_{side}). Including all these parameters in a formulation such as is presented in Equation 7.1, the sediment transport over the sill can be calculated. Such a formulation could then be implemented in numerical software.

$$S_{oversill} = f(Q_{upstream}, B_{ratio}, \alpha, w_{sill}, L_{sill}, h_{side}, h_{main}) \quad (7.1)$$

In one-dimensional flow models channels are modelled as branches that are connected. From the results of this thesis it is concluded that longitudinal-training-dam sills form an obstacle for sediments to be transported over the sill. Formulations, such as presented in Equation 7.1, can approximate the sediment transport over the sills. The advantage of one-dimensional models is that it does not matter where sediment is transported over the sill, but that the volume of sediment that is transported is most relevant.

For two-dimensional and three-dimensional flow models it is also important to know where sediment is transported over the sill. This information is available in the results of the particle model, but an additional step is needed for implementation in numerical software. The numerical models need information where on the sill sediment transport can be expected to be higher and where lower. A possible solution for this problem is creating a probability distribution (e.g. Rayleigh distribution or gamma distribution) along the sill to describe the volume of sediment that is transported over a part of the sill.

The particle model can further be extended to investigate geometric features of a river system, e.g. the curvature of a river and the bifurcation angle. This makes the parametrization for implementation in standard software for morphological simulations applicable for other situations as well.

Finally, the influence of different grain sizes should be investigated. The ratio between the weight of the sediment particle, which follows from the grain size, and the flow velocity can also be used for parametrization in numerical models. This ratio could be added to Equation 7.1. For a given ratio, in combination with the other parameters, a part of the sediment is transported over the sill. In this way also the type of sediment can be included in the sediment transport over the sill. However, more research is necessary, since in the computations in this thesis solely one grain size is used.

References

- CIRIA, CUR, and CETMEF (2007). *The Rock Manual: The use of rock in hydraulic engineering (2nd edition)*. C683, CIRIA, London.
- Collas, F., Buijse, A., Hendriks, A., and Leuven, R. (2015). The use of species sensitivity distributions and monitoring to predict the ecological effect of longitudinal training dams. In *H.J.R. Lenders, F.P.L. Collas, G.W. Geerling, R.S.E.W. Leuven (Eds.)*. *Bridging gaps between river science, governance and management. Book of abstracts NCR-days 2015*, pages 19–22, Nijmegen.
- de Ruijsscher, T., Dinissen, S., Vermeulen, B., Hazenberg, P., and Hoitink, A. (2015). A1 : Hydraulics and morphology of longitudinal training dams. In *G. Constantinescu, M. Garcia, D. Hanes (Eds.)*, *Proceedings of the International Conference on Fluvial Hydraulics (River Flow 2016)*, pages 379–380, Wageningen.
- de Vriend, H., Havinga, H., van Prooijen, B., Visser, P., and Wang, Z. (2011). *River engineering*. Delft University of Technology.
- Deltares (2014). Delft3D - FLOW, User Manual. Technical report, Deltares.
- Dey, S. (2014). *Fluvial Hydrodynamics*. Springer.
- Engelund, F. and Hansen, E. (1967). Monograph on sediment transport in alluvial streams. Technical report, TEKNISKFORLAG Skelbreggade 4 Copenhagen V, Denmark.
- Giri, S., van Vuren, S., Ottevanger, W., and Sloff, K. (2008). A preliminary analysis of bedform evolution in the Waal during 2002- 2003 flood event using Delft3D. In *D. R. Parsons, T. Garlan, and J. L. Best (Eds.)*, *Proc. of the 3rd workshop on Marine Sandwave and River Dune Dynamics (MARID), 1-3 April 2008, Leeds, UK*, pages 141–148.
- Graph Atlas (2016). Graphatlas.com, the Netherlands. <http://www.graphatlas.com/netherlands> [Online; accessed 20-February-2017].
- Huthoff, F., Paarlberg, A., Barneveld, H., and van der Wal, M. (2011). Rivierkundig onderzoek WaalSamen. Technical report, HKV Lijn in Water, Lelystad. Project number 2096. [in Dutch].
- Ikeda, S. (1982). Incipient Motion of Sand Particles On Side Slopes. *Journal of Hydraulic Division*, 108(1):95–114.
- Lauchlan, C. (2001). Sediment transport over steep slopes, an experimental investigation - Results and analysis. Technical Report August, RWS-RIZA, Delft Cluster, Delft.
- Liefveld, W., Emond, D., and van der Valk, M. (2011). Toetsing in het kader van de Flora- en faunawet, de Natuurbeschermingswet 1998 en de Ecologische Hoofdstructuur. Technical report, Bureau Waardenburg bv, Culemborg. [in Dutch].
- Meyer-Peter, E. and Müller, R. (1948). Formulas for bed load transport. *Proceedings of the 2nd Congress IAHR, Stockholm*, 2:39–64.

REFERENCES

- Nabi, M., de Vriend, H., Mosselman, E., Sloff, C., and Shimizu, Y. (2012). Detailed simulation of morphodynamics : 1 . Hydrodynamic model. *Water Resources Research*, 48(October):1–19.
- Nabi, M., de Vriend, H., Mosselman, E., Sloff, C., and Shimizu, Y. (2013). Detailed simulation of morphodynamics : 2 . Sediment pickup , transport , and deposition. *Water Resources Research*, 49(April):4775–4791.
- Rijkswaterstaat (2011). Integraal Ontwerp Pilot langsdammen Waal. Technical report, Rijkswaterstaat, Oost Nederland. [in Dutch].
- Rijkswaterstaat (2012). Factsheet Cultuurhistorie kribben. https://issuu.com/ruimtevoorderivier/docs/factsheet_cultuurhistorie/c/smqhi24 [Online; Accessed on 20-February-2017; in Dutch].
- Rivercare (2016). Website RiverCare - Netherlands Centre for River Studies. <http://www.ncr-web.org/rivercare/about> [Online; Accessed on 09-August-216].
- Schiereck, G. and Verhagen, H. (2012). *Introduction to bed, bank and shoreline protection*. VSSD.
- Sekine, M. and Parker, G. (1992). Bed-Load Transport on Transverse Slope. *Journal of Hydraulic Engineering*, 118(4):513–535.
- Shields, A. (1936). *Anwendung der Aehnlichkeitsmechanik und der Turbulenzforschung auf die Geschiebebewegung*. PhD thesis, Technischen Hochschule Berlin. [in German].
- Soulsby, R. (1997). *Dynamics of Marine Sands: A Manual for Practical Applications*. Telford.
- van Linge, B. (2017). Flow patterns around longitudinal training dams. Technical report, HKV; Delft University of Technology, Delft. [in press].
- van Rijn, L. (1984). Sediment transport, Part I: Bed load transport. *Journal of Hydraulic Engineering*, 110(10):1431–1456.
- van Rijn, L. (1993). *Principles of Sediment Transport in Rivers, Estuaries and Coastal Seas. Part I : Edition 1993*. Aqua Publications.
- van Rijn, L. (2006). *Principles of Sediment Transport in Rivers, Estuaries and Coastal Seas. Part II : Supplement 2006*. Aqua Publications.
- Verruijt, A. (2012). *Soil Mechanics*. VSSD, Delft.
- Yang, C. (1973). Incipient Motion and Sediment Transport. *Journal of the Hydraulics Division*, 99(10):1679–1704.
- Zijlema, M. (2016). Numerical Approximations. Technical report, Delft University of Technology, Delft.

Appendix A

Incipient motion of sediment particles

A.1 Introduction

This appendix discusses the incipient motion of sediment particles for different bed configurations and flow situations. Initiation of motion is a result of the interaction between a flow and sediment particles. Dey (2014) suggested to correct the critical Shields parameter for other bed configurations based on force balances acting on a sediment particle. In section 2.6 this has been briefly discussed and derived for a side slope configuration with unaligned flow. In this appendix a step-wise approach is taken to derive correction factors for the critical Shields parameter for various bed configurations and flow alignments. Slopes that are considered in this appendix are: horizontal, inclined and side slopes. For the latter a distinction is made between aligned and unaligned flows. Mathematical derivations for all correction factors is presented in Appendix B.

A.2 Incipient motion on horizontal bed

First an introduction is given to all the forces that are included in the determination of the correction factors for the Shields parameter. Later, the results of Shields are presented. For horizontal beds no correction has to be made, since Shields derived his experiments for horizontal beds.

Figure A.1 shows a close-up of three sediment particles on a river bed with a flow over the particles. At the top of the sediment particle the streamlines contract which result in a lower pressure at the top and consequently a lifting force in the upward direction occurs. At the lee side of the sediment particle energy is lost, which finally leads to a force in the flow direction this is called the drag force. Drag force is thus a result of a pressure difference along the surface of a sediment particle. On horizontal beds the drag force is always acting in the flow direction.

The forces at the moment of incipient motion are calculated by the formulae listed from Equation A.1.

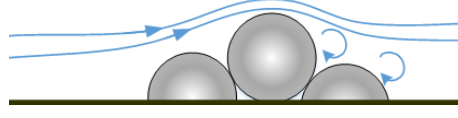


Figure A.1: Streamlines around a sphere, that is situated in between other sediment particles. At the top of the sediment particle the streamlines contract, resulting in an uplifting force. At the lee side energy is lost which causes a drag force in the same direction as the flow direction.

$$F_D = C_D \rho D^2 u_{cr}^2 K_1 \quad (\text{A.1a})$$

$$F_L = C_L \rho D^2 u_{cr}^2 K_2 \quad (\text{A.1b})$$

$$F_G = (\rho_s - \rho) g D^3 K_3 = \Delta \rho g D^3 K_3 \quad (\text{A.1c})$$

$$F_R = \tan(\phi)(F_L - F_G) \quad (\text{A.1d})$$

C_D and C_L are drag and lifting force coefficients, which are often empirically determined, ρ is the density of water and D is the particle diameter. K_1 and K_2 equal A , which is the surface area of a sediment particle, approximated by $A = (1/4)\pi D^2$. K_3 equals V is the volume of a sediment particle, approximated by $V = (1/6)\pi D^3$. u_{cr} is the critical flow velocity.

A submerged force is present due to the weight of and buoyancy on a sediment particle under water. This force can be expressed by the submerged mass¹ multiplied with the gravitational acceleration. Note that the submerged force is defined according to the Archimedes' principle, which states that the submerged force on an object under water is equal to the weight of that object minus the buoyancy force (as a result of the displaced water).

The friction force depends on the angle of repose (ϕ) and the resulting force normal to the bed. The friction always works opposite the direction of motion, for horizontal beds this is thus opposite the flow direction.

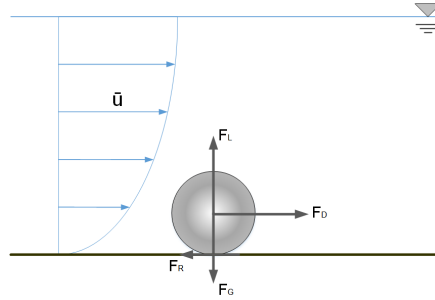


Figure A.2: For a horizontal bed the forces that act on a sediment particle under the influence of a flow are schematised in this figure. In addition, a logarithmic velocity profile is presented.

The force balance in the x-direction is given by Equation A.2, at initiation of motion all balances equal 0.

$$\sum F_{x'} = F_D - F_R = 0 \quad (\text{A.2a})$$

$$\sum F_{y'} = 0 \quad (\text{A.2b})$$

¹Note that $\Delta = \frac{\rho_s - \rho}{\rho}$, ρ_s is the density of sediment and g is the gravitational acceleration.

$$\sum F_{z'} = F_L - F_G = 0 \quad (\text{A.2c})$$

From Equation A.1d it follows that the resistance force is equal to the resulting forces in z -direction multiplied with $\tan(\phi)$. ϕ is often described as the natural angle of repose and means the steepest angle a material can have before sliding. Physically this can be derived from the moment balance of a particle situated between other particles, see Figure A.3 and Equation A.3².

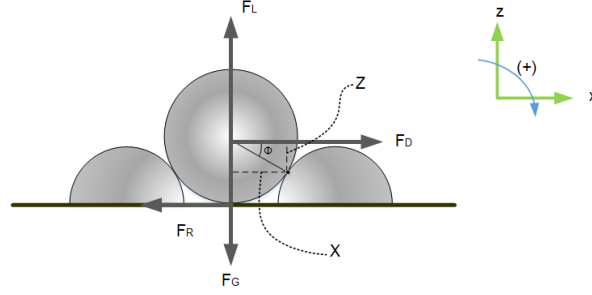


Figure A.3: Definition natural angle of repose (example with horizontal bed)

$$F_D \cdot Z + (F_L - F_G) \cdot X = 0 \quad (\text{A.3a})$$

$$F_D + (F_L - F_G) \cdot \frac{X}{Z} = 0 \quad (\text{A.3b})$$

$$\frac{X}{Z} = \frac{F_D}{F_G - F_L} = \tan(\phi) \quad (\text{A.3c})$$

$$\frac{F_D}{F_G - F_L} = \tan(\phi) \rightarrow F_D = \tan(\phi) (F_G - F_L) \quad (\text{A.3d})$$

From Equation A.2a it follows that $F_D = F_R$, so:

$$F_R = \tan(\phi) (F_G - F_L) \quad (\text{A.3e})$$

Shields (1936) performed experiments and found for horizontal beds critical shear velocities (or dimensionless Shields parameter) for which sediment particles started to move. Van Rijn (1984) presented an analytical approach to describe the Shields diagram, see section 2.6. The Shields parameter (Θ_{c0} , 0 indicates horizontal bed) is presented in Equation A.4 and graphically in Figure A.4. Initiation of motion on horizontal bed are considered as the reference case to which is referred later.

$$\Theta_{c0} = \frac{u_{*c}^2}{\Delta g D} \quad (\text{A.4})$$

²Note that the sign is different for the frictional force, this does not matter for initiation of motion, since the force is equal to zero anyway. In models that will be treated later, the force is always opposite the flow direction, the sign in front of the calculation does not matter anymore.

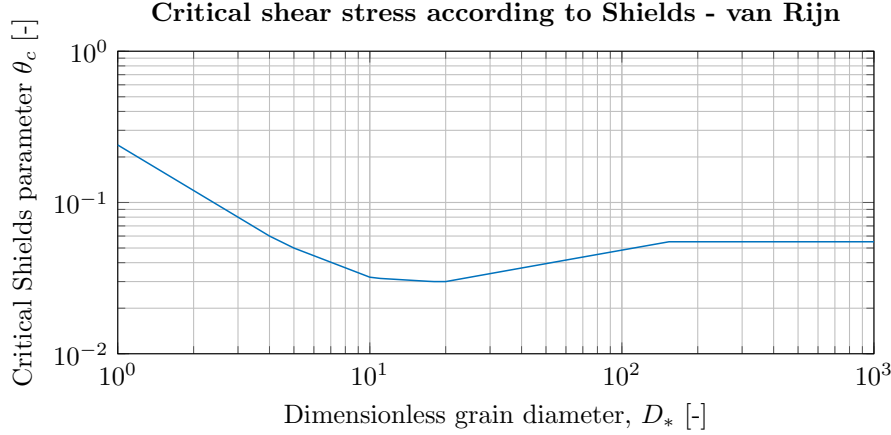


Figure A.4: Shields diagram - adapted by van Rijn. For horizontal beds the relation holds. Both parameters are dimensionless. Source: van Rijn (1993).

A.3 Incipient motion on inclined bed

If the river bed is non-horizontal (inclined at an angle θ) the original coordinate system $[x,y,z]$ -axis (Figure A.5a) change to $[x',y',z']$ -axis (Figure A.5b). At an inclined bed sediment particles encounter an additional force in x' -direction as a result of the gravity. The gravity force can be decoupled in a component along the bed ($F_{G,x'} = F_G \cdot \sin(\theta)$) and normal to the bed ($F_{G,z'} = F_G \cos(\theta)$). Along the river bed there are three forces present in the stream direction (drag, gravitational and frictional force) and two perpendicular to the bed (gravitational and lifting force). The force balance of these forces result in a different threshold condition for initiation of motion compared to the case of a horizontal (flat) bed.

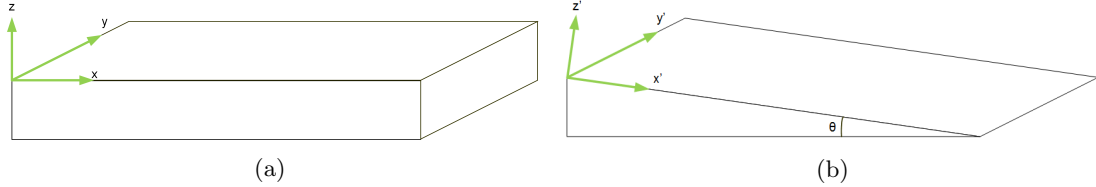


Figure A.5: Definition of coordinate system for (a) horizontal bed and (b) inclined bed. Inclination angle is θ . Flow is in x' direction.

$$\sum F_{x'} = F_G \sin(\theta) + F_D - F_R = 0 \quad (\text{A.5a})$$

$$\sum F_{y'} = 0 \quad (\text{A.5b})$$

$$\sum F_{z'} = F_L - F_G \cos(\theta) = 0 \quad (\text{A.5c})$$

According to the force balance in three directions $[x',y',z']$ a critical condition can be derived for an inclined bed. Note that the effect sideways (y' direction) are assumed to be neglected in this case, since the flow is solely in x' direction. The force balance in the x' direction is at the moment of incipient motion equal to zero. The velocity that is used in the drag and lifting force is at that moment equal to the critical velocity. Dey (2014) proposes to change the critical velocity to a shear velocity divided by a friction factor, i.e. $u_{cr} = \frac{u_{*cr\theta}}{\sqrt{\lambda_f}}$. $*c$ indicates it is the critical

shear velocity and θ means that it holds for inclined beds. Combining this with Equation A.1 and Equation A.5a a critical shear velocity can be derived for initiation of motion on an inclined bed, see Equation A.6.

$$\Delta \rho g D^3 K_3 \sin(\theta) + \frac{C_D \rho D^2 u_{*c\theta}^2 K_1}{\lambda_f} - \left(\Delta \rho g D^3 K_3 \cos(\theta) - \frac{C_L \rho D^2 u_{*c\theta}^2 K_2}{\lambda_f} \right) \tan(\phi) = 0 \quad (\text{A.6a})$$

$$\Rightarrow u_{*c\theta} = \frac{\sqrt{-(C_L K_2 \tan(\phi) + C_D K_1) D \Delta K_3 g \lambda_f (-\cos(\theta) \tan(\phi) + \sin(\theta))}}{C_L K_2 \tan(\phi) + C_D K_1} \quad (\text{A.6b})$$

The critical shear velocity ($u_{*c\theta}$) is incorporated in the determination of a dimensionless Shields parameter ($\Theta_{c\theta}$). Equation A.6b is squared and divided by the terms $\Delta g d$, shown in Equation A.7. If $\theta = 0$ Equation A.7b will reduce to $\Theta_{c0} = K \tan(\theta)$.

$$\Theta_{c\theta} = \frac{u_{*c\theta}^2}{\Delta g d} \quad (\text{A.7a})$$

$$\Theta_{c\theta} = \frac{K_3 \lambda_f}{C_L K_1 \tan(\phi) + C_D K_1} (\tan(\phi) \cos(\theta) - \sin(\theta)) \quad (\text{A.7b})$$

$$\text{with } K = \frac{K_3 \lambda_f}{C_L K_1 \tan(\phi) + C_D K_1}$$

In literature the relative dimensionless Shields parameter on a sloping bed is obtained by dividing $\Theta_{c\theta}$ by Θ_{c0} . This results in Equation A.8, which implies that the critical Shields parameter for horizontal beds Θ_{c0} can be ‘corrected’ for the inclination by a factor $\tilde{\Theta}_{c\theta}$. A derivation of this result is presented in section B.1 and is in accordance with the work of Dey (2014).

$$\tilde{\Theta}_{c\theta} = \frac{\Theta_{c\theta}}{\Theta_{c0}} = \frac{K (\tan(\phi) \cos(\theta) - \sin(\theta))}{K \tan(\phi)} = \cos(\theta) \left(1 - \frac{\tan(\theta)}{\tan(\phi)} \right) \quad (\text{A.8})$$

A correction for the critical Shields parameter implies that initiation of motion occurs for a different flow situations. Figure A.6 shows that the critical Shields parameter is lower for larger inclination angles, which implies that for larger angles, it becomes ‘easier’ to move down the slope. From a physical point of view this is also expected to happen.

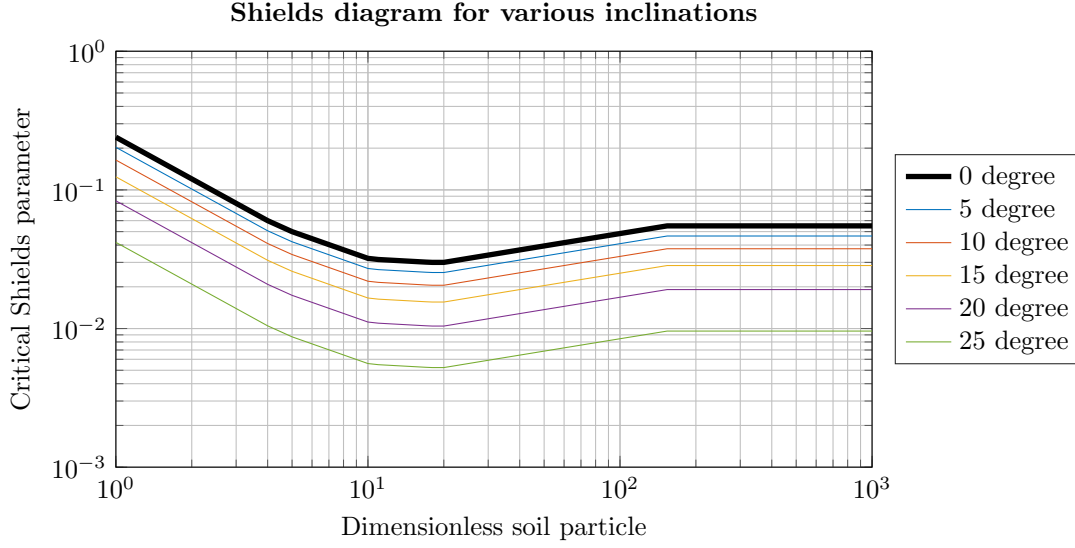


Figure A.6: Adapted Shields diagram for various inclination angles. An increase of the inclination angle reduces the critical Shields parameter. In other words, at lower flow velocities sediment particles start to move.

A.4 Incipient motion on a side slope with aligned flow

In many articles sediment transport on a side slope in streamwise direction has been discussed. Ikeda (1982) described this situation, he assumed a side slope under an angle α and a horizontal river bed, i.e. $\theta = 0$. Figure A.7 shows the new coordinate system $[x', y', z']$ and Equation A.9 shows the force balances for this situation. Figure A.8 shows all forces that act on a sediment particle. Note that β determines the angle the frictional force makes with the x' axis, this can be seen in Figure A.9 where only the x', y' -plane is considered.

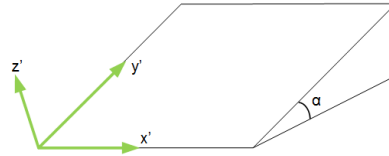


Figure A.7: Coordinate system for side slope. Side slope angle is indicated with α . Flow is in x' -direction.

$$\beta = \arctan\left(\frac{-F_G \sin(\alpha)}{-F_D}\right)$$

$$\sum F_{x'} = F_D - F_R \sin(\beta) = 0 \quad (\text{A.9a})$$

$$\sum F_{y'} = F_G - F_R \cos(\beta) = 0 \quad (\text{A.9b})$$

$$\sum F_{z'} = F_L - F_G \cos(\alpha) = 0 \quad (\text{A.9c})$$

The frictional resistance force is in the opposite direction of the resulting force in the x', y' -plane according to the following equation: $F_R = \sqrt{F_D^2 + (F_G \sin(\alpha))^2}$. In addition, the frictional force

can be found by multiplying the resulting force in z' with $\tan(\phi)$: $F_R = (F_L - F_G \cos(\alpha)) \tan(\phi)$. Balancing both equations leads to Equation A.10.

$$\sqrt{F_D^2 + (F_G \sin(\alpha))^2} = (F_L - F_G \cos(\alpha)) \tan(\phi) \quad (\text{A.10})$$

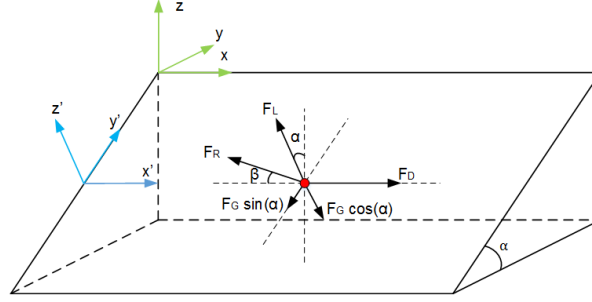


Figure A.8: Forces that act on a sediment particle that is located on a side slope. This figure shows all three dimensions. Flow is in x' direction

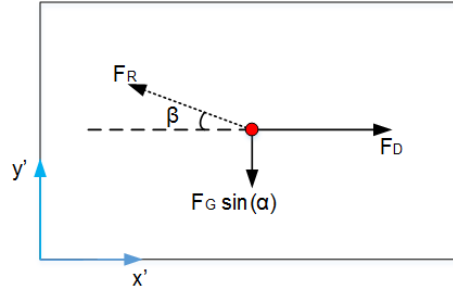


Figure A.9: Forces that act on a sediment particle located on a side slope, flow is in x' direction. This figure only shows the x' - y' plane from Figure A.8.

Drag and lift force has been defined by Equation A.1a and Equation A.1b. η is the ratio between these forces: $\eta = \frac{F_L}{F_D}$. Equation A.11a shows the result of force balance for a sediment particle on a side slope. This result can be rewritten as a function of the dimensionless Shields parameter, similarly to section A.3. Isolating $\Theta_{c\alpha}$ give a quadratic equation. The positive result of the dimensionless Shields parameter is presented in Equation A.11b; a derivation is presented in section B.2.

$$\frac{1}{6} \pi \sqrt{\hat{F}_D^2 D^6 \Theta_{c\alpha}^2 (-\rho_s + \rho)^2 g^2} = -\frac{1}{6} D^3 \pi g \tan(\phi) (-\rho_s + \rho) \quad (\text{A.11a})$$

$$\Theta_{c\alpha} = \frac{-\cos(\alpha) \eta \tan(\alpha)^2 + \sqrt{-\cos(\alpha)^2 \tan(\phi)^2 \eta^2 + \cos(\alpha)^2 \tan(\phi)^2 + \eta^2 \tan(\phi)^2 + \cos(\alpha)^2 - 1}}{(1 - \eta^2 \tan(\phi)^2) \hat{F}_D} \quad (\text{A.11b})$$

At a critical condition the ratio between the lifting force and the drag force is assumed to be zero (i.e. $\eta = 0$), since the sediment particle will not be lifted. The final relative dimensionless Shields parameter is given in Equation A.12. This term is again a 'correction' factor for the side

slope with respect to the reference case where to flow is in the x-direction at a horizontal bed. This formula is in accordance with the findings of Dey (2014).

$$\tilde{\Theta}_{c\alpha}(\eta = 0) = \frac{\Theta_{c\alpha}}{\Theta_{c0}} = \cos(\alpha) \sqrt{1 - \frac{\tan(\alpha)^2}{\tan(\phi)^2}} \quad (\text{A.12})$$

Figure A.10 shows that the critical Shields parameter is lower for larger side slope angles, which implies that for larger angles, it becomes ‘easier’ to move down the side slope. From a physical point of view this is also expected to happen, due to the gravity that acts on a sediment particle.

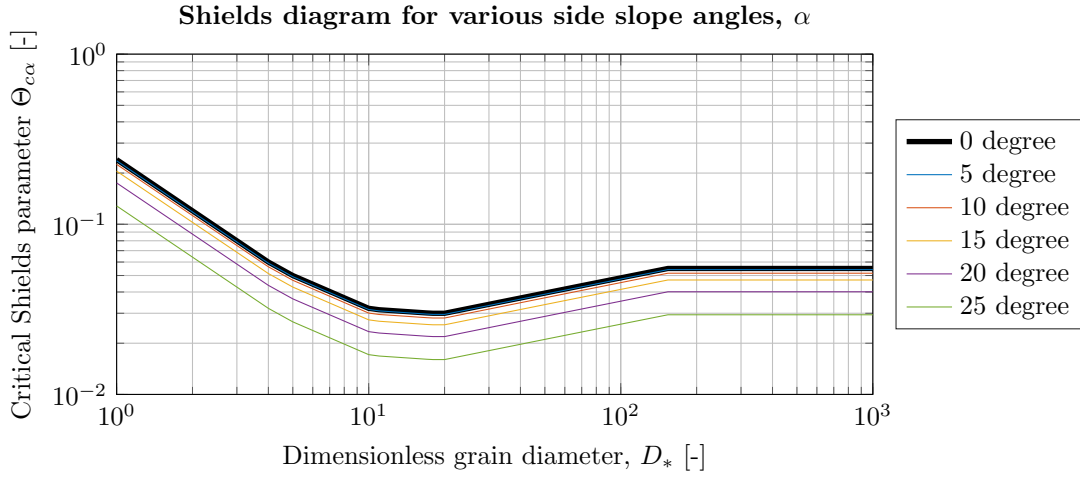


Figure A.10: Adapted Shields diagram for various side slope angles. An increase of the side slope angle reduces the critical Shields parameter. In other words, at lower flow velocities sediment particles start to move.

A.5 Incipient motion on a side slope with unaligned flow

An aspect that is most relevant for longitudinal-training-dam sills is sediment transport on a side slope where the flow is upward or downward the side slope. This means that the flow is not solely in the x' direction, but has a component in both x' and y' direction. Figure A.11 shows the forces that act on the sediment particles in three dimensions. Figure A.12 shows the forces that act on the sediment particle in the x',y' plane. It can be seen that the drag force is now under an angle γ with the x' -direction.

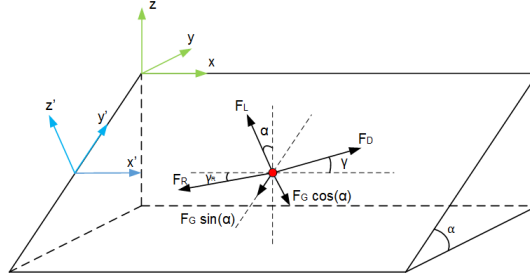


Figure A.11: Forces that act on a sediment particle located on a side slope with flow angle γ . The flow has a component in x' and y' direction.

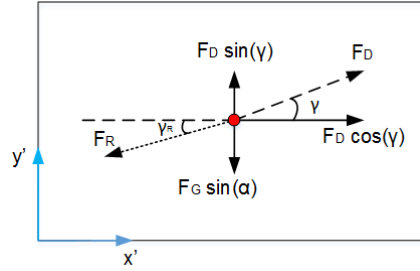


Figure A.12: Forces on a sediment particle located on a side slope with flow angle γ . In this figure only the x',y' plane of Figure A.11 is presented.

The angles that are presented in Figure A.12 are defined in Equation A.13. These angles are used in the force balances of Equation A.14. Note that the derivation for γ_{xy} is presented in section B.3³.

$$\gamma = \arctan\left(\frac{F_{D_{y'}}}{F_{D_{x'}}}\right) \quad (\text{A.13a})$$

$$\gamma_R = \arctan\left(\frac{F_{G_{y'}} - F_{D_{y'}}}{F_{D_{x'}}}\right) \quad (\text{A.13b})$$

$$\gamma_{xy} = \arctan\left(\cos(\alpha)\left(\frac{F_{D_{y'}}}{F_{D_{x'}}}\right)\right) = \arctan(\cos(\alpha)\tan(\gamma)) \quad (\text{A.13c})$$

³This angle is only relevant for special computational purposes .

$$\sum F_{x'} = F_D \cos(\gamma) - F_R \cos(\gamma_R) = 0 \quad (\text{A.14a})$$

$$\sum F_{y'} = F_G \sin(\alpha) + F_R \sin(\gamma_R) - F_D \sin(\gamma) = 0 \quad (\text{A.14b})$$

$$\sum F_{z'} = F_L - F_G \cos(\alpha) = 0 \quad (\text{A.14c})$$

The frictional force is in the opposite direction of the resulting force in the x',y' -plane according to the following equation: $F_R = \sqrt{(F_D \cos(\gamma))^2 + (F_G \sin(\alpha) - F_D \sin(\gamma))^2}$. In addition this force was found by balancing the submerged weight and lifting force: $F_R = (F_L - F_G \cos(\alpha)) \tan(\phi)$. This resulted in a force balance from which the critical Shields parameter was established.

$$\begin{aligned} & \frac{1}{6} \pi \sqrt{D^6 g^2 (-\rho_s + \rho)^2 \left(\hat{F}_D^2 \Theta_{c\gamma}^2 - 2 \hat{F}_D \sin(\alpha) \sin(\gamma) \Theta_{c\gamma} - \cos(\alpha)^2 + 1 \right)} \\ & = \frac{1}{6} \tan(\phi) \pi D^3 g (\eta \hat{F}_D \Theta_{c\gamma} \rho - \eta \hat{F}_D \Theta_{c\gamma} \rho_s - \cos(\alpha) \rho + \cos(\alpha) \rho_s) \end{aligned} \quad (\text{A.15a})$$

$$\begin{aligned} \Theta_{c\gamma} &= \frac{1}{(1 - \eta^2 \tan(\phi)^2) \hat{F}_D} (-\cos(\alpha) \eta \tan(\phi)^2 + \sin(\alpha) \sin(\gamma) \dots \\ & \dots + \sqrt{-\cos(\alpha)^2 \tan(\phi)^2 \eta^2 + \cos(\alpha)^2 \tan(\phi)^2 + \eta^2 \tan(\phi)^2 + \cos(\alpha)^2} \dots \\ & \dots - 1 + \sin(\alpha)^2 \sin(\gamma)^2 - 2 \sin(\alpha) \sin(\gamma) \cos(\alpha) \eta \tan(\phi)^2) \end{aligned} \quad (\text{A.15b})$$

In section B.4 a derivation is given for the relative dimensionless Shields parameter. This equation is presented in Equation A.16. This formula corresponds to the findings in CIRIA et al. (2007), although the coordinate system is different oriented.

$$\tilde{\Theta}_{c\gamma}(\eta = 0) = \frac{\Theta_{c\gamma}}{\Theta_{c0}} = \frac{\sin(\alpha) \sin(\gamma)}{\tan(\phi)} + \cos(\alpha) \sqrt{1 - \frac{\tan(\alpha)^2 \cos(\gamma)^2}{\tan(\phi)^2}} \quad (\text{A.16})$$

Again, this relative dimensionless Shields parameter ‘corrects’ the Shields parameter for horizontal bed Figure A.13 shows an adapted Shields diagram for various flow situations. For an arbitrary situation, the angle of repose was assumed to be 30° and the side slope was assumed to be 15° . The lines above the flow angle $\gamma = 0^\circ$ line are the directed uphill and below downhill.

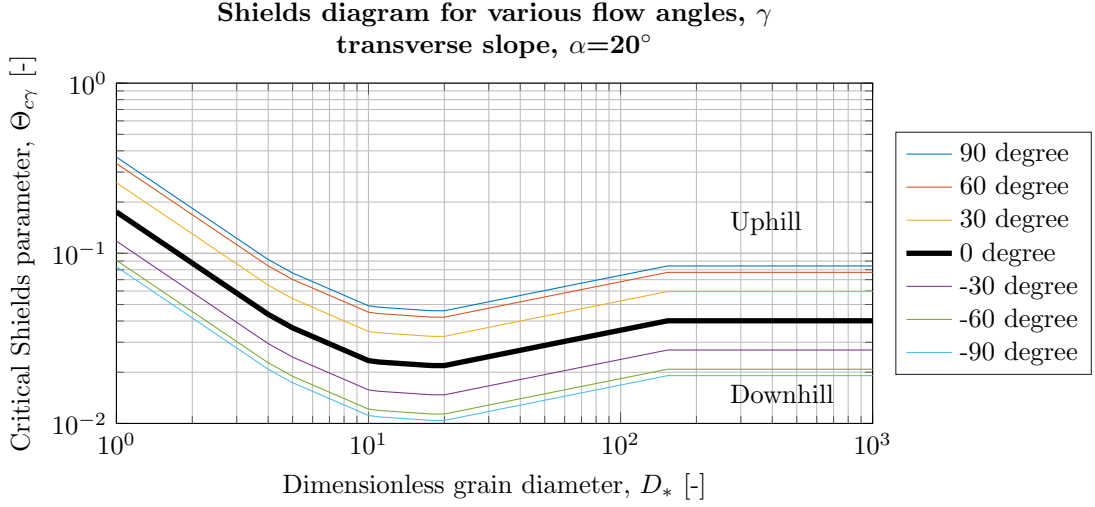


Figure A.13: Adapted Shields diagram for various flow alignments. An increase of the flow angle increases the critical Shields parameter. In other words, if the flow is directed uphill a higher flow velocity is necessary than for a flow directed downhill.

Three situations are described, namely $\gamma = -90^\circ$ (flow is directed downwards the slope; this is similar to section A.3), $\gamma = 0^\circ$ (similar to section A.4) and $\gamma = 90^\circ$ (flow is directed upwards the slope). In which α refers to the situation where there is no flow component in the y' direction, and θ where there is no flow component in the x' direction.

$$\gamma = -90^\circ \quad \rightarrow \quad \tilde{\Theta}_{c\gamma} = \tilde{\Theta}_{c\theta(-)} = \cos(\theta) \left(1 - \frac{\tan(\theta)}{\tan(\phi)} \right) \quad (\text{A.17a})$$

$$\gamma = 0^\circ \quad \rightarrow \quad \tilde{\Theta}_{c\gamma} = \tilde{\Theta}_{c\alpha} = \cos(\alpha) \sqrt{1 - \frac{\tan(\alpha)^2}{\tan(\phi)^2}} \quad (\text{A.17b})$$

$$\gamma = 90^\circ \quad \rightarrow \quad \tilde{\Theta}_{c\gamma} = \tilde{\Theta}_{c\theta(+)} = \cos(\theta) \left(1 + \frac{\tan(\theta)}{\tan(\phi)} \right) \quad (\text{A.17c})$$

Appendix B

Derivations of correction factors for critical Shields parameter

In the previous chapter the results of the correction factors for the critical Shields parameters is explained. This chapter shows the derivations of the correction factors. Van Rijn (1993) and Dey (2014) introduced correction factors for different bed configurations. Soulsby (1997) presented a correction factor for unaligned side slopes, which is similar to what has been derived in this thesis. Dey (2014) introduced new parameters such as η which is the ratio between the lifting force and the drag force. Assuming that $K_1 = K_2$, η is the ratio between the lift- and drag coefficients¹. Θ_{cx} is the dimensionless Shields parameter, x indicates type of bed configuration or flow alignment. Finally \hat{F}_D is a parameter² that is established by Dey (2014) to easily isolate the Θ_{cx} from the force balances. Note that correction factor and relative critical Shields parameter is interchangeably used.

$$\eta = \frac{F_L}{F_D} = \frac{C_L}{C_D} \quad (\text{B.1a})$$

$$\Theta_{cx} = \frac{u_{*cx}^2}{\Delta g d} \quad (\text{B.1b})$$

$$\hat{F}_D = \frac{6F_D}{\pi\rho D^2 u_{*cx}^2} \quad (\text{B.1c})$$

¹Note that K_1, K_2, K_3 are constant factors that include the surface area, volume and/or other constants.

²Considering the elements in this parameter it can be concluded that the parameter itself is dimensionless.

B.1 Relative critical Shields parameter on streamwise sloping bed

Inclined bed slopes have a correction factor for the critical Shields parameter which is found in Equation A.8. The derivation for this correction factor is presented below in is repeated in Equation B.2 and Equation B.3.

$$\tilde{\Theta}_{c\theta} = \frac{\Theta_{c\theta}}{\Theta_{c0}} = \frac{K(\tan(\phi) \cos(\theta) - \sin(\theta))}{K \tan(\phi)} \quad (\text{B.2})$$

$$\tilde{\Theta}_{c\theta} = \frac{K(\tan(\phi) \cos(\theta) - \sin(\theta))}{K \tan(\phi)} \quad (\text{B.3a})$$

$$= \frac{(\tan(\phi) \cos(\theta) - \sin(\theta))}{\tan(\phi)} \quad (\text{B.3b})$$

$$= \cos(\theta) - \frac{(\sin(\theta))}{\tan(\phi)} \quad (\text{B.3c})$$

$$= \cos(\theta) - \frac{(\sin(\theta)) \frac{\cos(\theta)}{\cos(\theta)}}{\tan(\phi)} \quad (\text{B.3d})$$

$$= \cos(\theta) - \frac{\tan(\theta) \cos(\theta)}{\tan(\phi)} \quad (\text{B.3e})$$

$$= \cos(\theta) \left(1 - \frac{\tan(\theta)}{\tan(\phi)} \right) \quad (\text{B.3f})$$

$$(\text{B.3g})$$

$$\tilde{\Theta}_{c\theta} = \cos(\theta) \left(1 - \frac{\tan(\theta)}{\tan(\phi)} \right) \quad (\text{B.4})$$

B.2 Relative critical Shields parameter on streamwise side slope

For side sloping beds with side angle α the derivation of the correction factor is presented below.

$$\Theta_{c\alpha} = \frac{-\cos(\alpha)\eta \tan(\alpha)^2 + \sqrt{-\cos(\alpha)^2 \tan(\phi)^2 \eta^2 + \cos(\alpha)^2 \tan(\phi)^2 + \eta^2 \tan(\phi)^2 + \cos(\alpha)^2 - 1}}{(1 - \eta^2 \tan(\phi)^2) \hat{F}_D} \quad (\text{B.5a})$$

$$= \frac{-\cos(\alpha)\eta \tan(\alpha)^2 + \sqrt{\tan(\phi)^2 \eta^2 (1 - \cos(\alpha)^2) + \cos(\alpha)^2 \tan(\phi)^2 - (1 - \cos(\alpha)^2)}}{(1 - \eta^2 \tan(\phi)^2) \hat{F}_D} \quad (\text{B.5b})$$

$$= \frac{-\cos(\alpha)\eta \tan(\alpha)^2 + \sqrt{\tan(\phi)^2 \eta^2 \sin(\alpha)^2 + \cos(\alpha)^2 \tan(\phi)^2 - \sin(\alpha)^2}}{(1 - \eta^2 \tan(\phi)^2) \hat{F}_D} \quad (\text{B.5c})$$

$$(\text{B.5d})$$

$$\Theta_{c\alpha}(\alpha = 0) = \Theta_{c0} = \frac{-\eta \tan(\phi)^2 + \sqrt{\tan(\phi)^2}}{(1 - \eta^2 \tan(\phi)^2) \hat{F}_D} \quad (\text{B.6a})$$

$$= \frac{-\eta \tan(\phi)^2 + \tan(\phi)}{(1 - \eta^2 \tan(\phi)^2) \hat{F}_D} \quad (\text{B.6b})$$

$$= \frac{\tan(\phi)(1 - \eta \tan(\phi))}{(1 - \eta^2 \tan(\phi)^2) \hat{F}_D} \quad (\text{B.6c})$$

$$= \frac{\tan(\phi)(1 - \eta \tan(\phi))}{(1 - \eta \tan(\phi))(1 + \eta \tan(\phi)) \hat{F}_D} \quad (\text{B.6d})$$

$$= \frac{\tan(\phi)}{(1 + \eta \tan(\phi)) \hat{F}_D} \quad (\text{B.6e})$$

$$\tilde{\Theta}_{c\alpha} = \frac{\Theta_{c\alpha}}{\Theta_{c0}} \quad (\text{B.7a})$$

$$= \frac{-\cos(\alpha)\eta \tan(\alpha)^2 + \sqrt{\tan(\phi)^2 \eta^2 \sin(\alpha)^2 + \cos(\alpha)^2 \tan(\phi)^2 - \sin(\alpha)^2}}{(1 - \eta^2 \tan(\phi)^2) \hat{F}_D} \quad (\text{B.7b})$$

$$= \frac{\tan(\phi)}{(1 + \eta \tan(\phi)) \hat{F}_D} \quad (\text{B.7c})$$

$$= \frac{-\cos(\alpha)\eta \tan(\alpha)^2 + \sqrt{\tan(\phi)^2 \eta^2 \sin(\alpha)^2 + \cos(\alpha)^2 \tan(\phi)^2 - \sin(\alpha)^2}}{(1 - \eta \tan(\phi))(1 + \eta \tan(\phi)) \hat{F}_D} \quad (\text{B.7c})$$

$$= \frac{\tan(\phi)}{(1 + \eta \tan(\phi)) \hat{F}_D} \quad (\text{B.7d})$$

$$= \frac{-\cos(\alpha)\eta \tan(\alpha)^2 + \sqrt{\tan(\phi)^2 \eta^2 \sin(\alpha)^2 + \cos(\alpha)^2 \tan(\phi)^2 - \sin(\alpha)^2}}{(1 - \eta \tan(\phi)) \tan(\phi)} \quad (\text{B.7d})$$

if $\eta = 0$

$$\tilde{\Theta}_{c\alpha}(\eta = 0) = \frac{\sqrt{\cos(\alpha)^2 \tan(\phi)^2 - \sin(\alpha)^2}}{\tan(\phi)} \quad (\text{B.7e})$$

$$\tilde{\Theta}_{c\alpha}^2(\eta = 0) = \frac{\cos(\alpha)^2 \tan(\phi)^2 - \sin(\alpha)^2}{\tan(\phi)^2} \quad (\text{B.7f})$$

$$= \cos(\alpha)^2 - \frac{\sin(\alpha)^2}{\tan(\phi)^2} \quad (\text{B.7g})$$

$$\frac{\tilde{\Theta}_{c\alpha}^2}{\cos(\alpha)^2}(\eta = 0) = 1 - \frac{\tan(\alpha)^2}{\tan(\phi)^2} \quad (\text{B.7h})$$

$$\tilde{\Theta}_{c\alpha}(\eta = 0) = \cos(\alpha) \sqrt{1 - \frac{\tan(\alpha)^2}{\tan(\phi)^2}} \quad (\text{B.7i})$$

B.3 Translation between two coordinate systems

In case the force F_D is under an angle γ , which is defined in the x',y',z' -coordinate system this can be translated into a x,y,z -coordinate system. The new angle is called γ_{xy} . Figure B.1 shows where the angles γ and γ_{xy} are located.

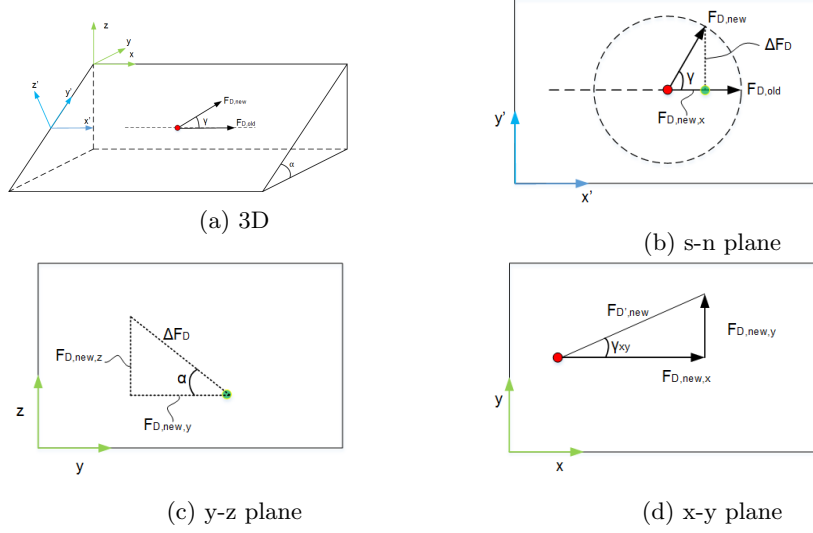


Figure B.1: Example of a drag force vector solely in x' -direction and in x' and y' -direction, see (a)

Since the a 'new' drag force vector must have the same norm³, a circle can be drawn such as is presented in Figure B.1b. The x -component of the new vector can be found by finding by $F_{Dx} = \cos(\gamma)F_D$ and $\Delta F_D = \sin(\gamma)F_D$. See Figure B.1c that this ΔF_D is then used to compute F_{Dy} and F_{Dz} . Combing F_{Dx} and F_{Dy} the angle γ_{xy} is found. Equation B.8 shows mathematically the derivation and solution for γ_{xy} .

$$F_{D_{snb}} = \begin{bmatrix} F_{D,s} \\ F_{D,n} \\ F_{D,b} \end{bmatrix} = \begin{bmatrix} F_D \\ 0 \\ 0 \end{bmatrix} \quad (\text{B.8a})$$

γ = angle s,n,b-coordinatesystem

$$F_{D_{xyz}} = \begin{bmatrix} F_{D,x} \\ F_{D,y} \\ F_{D,z} \end{bmatrix} = F_D \cdot \begin{bmatrix} \cos(\gamma) \\ \cos(\alpha) \sin(\gamma) \\ \sin(\alpha) \sin(\gamma) \end{bmatrix} \quad (\text{B.8b})$$

γ_{xy} = angle x,y,z-coordinate system

$$\tan(\gamma_{xy}) = \frac{F_{D,y}}{F_{D,x}} = \frac{\cos(\alpha) \sin(\gamma) F_D}{\cos(\gamma) F_D} = \cos(\alpha) \tan(\gamma) \quad (\text{B.8c})$$

$$\tan(\gamma) = \frac{\tan(\gamma_{xy})}{\cos(\alpha)} \quad (\text{B.8d})$$

³Mathematical expression for the length of a vector.

B.4 Relative critical Shields parameter on non-streamwise side slope

Side slope with angle α and a flow alignment γ have a correction factor which is presented below. This result is similar to what has been derived by Soulsby (1997), see next section.

$$\Theta_{c\gamma} = \frac{1}{(1 - \eta^2 \tan(\phi)^2) \hat{F}_D} (-\cos(\alpha)\eta \tan(\phi)^2 + \sin(\alpha) \sin(\gamma) \dots) \dots + \sqrt{-\cos(\alpha)^2 \tan(\phi)^2 \eta^2 + \cos(\alpha)^2 \tan(\phi)^2 + \eta^2 \tan(\phi)^2 \dots} \dots + \cos(\alpha)^2 - 1 + \sin(\alpha)^2 \sin(\gamma)^2 - 2 \sin(\alpha) \sin(\gamma) \cos(\alpha) \eta \tan(\phi)^2) \quad (\text{B.9a})$$

$$= \frac{1}{(1 - \eta^2 \tan(\phi)^2) \hat{F}_D} (-\cos(\alpha)\eta \tan(\phi)^2 + \sin(\alpha) \sin(\gamma) \dots) \dots + \sqrt{\tan(\phi)^2 \eta^2 (1 - \cos(\alpha)^2) - (1 - \cos(\alpha)^2) + \dots} \dots \cos(\alpha) \tan(\phi)^2 (\cos(\alpha) - 2 \sin(\alpha) \sin(\gamma) \eta) + \sin(\alpha)^2 \sin(\gamma)^2) \quad (\text{B.9b})$$

$$= \frac{1}{(1 - \eta^2 \tan(\phi)^2) \hat{F}_D} (-\cos(\alpha)\eta \tan(\phi)^2 + \sin(\alpha) \sin(\gamma) \dots) \dots + \sqrt{\tan(\phi)^2 \eta^2 \sin(\alpha)^2 - \sin(\alpha)^2 + \sin(\alpha)^2 \sin(\gamma)^2 \dots} \dots + \cos(\alpha)^2 \tan(\phi)^2 (1 - 2 \tan(\alpha) \sin(\gamma) \eta)) \quad (\text{B.9c})$$

$$= \frac{1}{(1 - \eta^2 \tan(\phi)^2) \hat{F}_D} (-\cos(\alpha)\eta \tan(\phi)^2 + \sin(\alpha) \sin(\gamma) \dots) \dots + \sqrt{\sin(\alpha)^2 (\tan(\phi)^2 \eta^2 + \sin(\gamma)^2 - 1) + \cos(\alpha)^2 \tan(\phi)^2 (1 - 2 \tan(\alpha) \sin(\gamma) \eta))} \quad (\text{B.9d})$$

The derivation (Equation B.10) for the critical shear stress on a horizontal bed and a streamwise flow ($\alpha = \gamma = 0$) is similar to Equation B.6.

$$\Theta_{c\gamma}(\alpha = 0, \gamma = 0) \Theta_{c0} = \frac{-\eta \tan(\phi)^2 + \sqrt{\tan(\phi)^2}}{(1 - \eta^2 \tan(\phi)^2) \hat{F}_D} \quad (\text{B.10a})$$

$$= \frac{\tan(\phi)}{(1 + \eta \tan(\phi)) \hat{F}_D} \quad (\text{B.10b})$$

The relative critical Shields parameter on non-streamwise side slopes has been derived in Equation B.11. If similar assumptions are made as in section B.2, namely $\eta = 0$ and later $\gamma = 0$ the final result is similar to Equation B.7i.

$$\tilde{\Theta}_{c\gamma} = \frac{\Theta_{c\gamma}}{\Theta_{c0}} \quad (\text{B.11a})$$

$$= \frac{\text{Equation B.9d}}{\tan(\phi)} \quad (\text{B.11b})$$

$$= \frac{(1 + \eta \tan(\phi)) \hat{F}_D}{\tan(\phi) (1 - \eta^2 \tan(\phi)^2)}$$

$$\dots + \frac{\sqrt{\sin(\alpha)^2(\tan(\phi)^2\eta^2 + \sin(\gamma)^2 - 1) + \cos(\alpha)^2 \tan(\phi)^2(1 - 2 \tan(\alpha) \sin(\gamma)\eta)}}{\dots} \quad (\text{B.11c})$$

$$= \frac{-\cos(\alpha)\eta \tan(\phi)^2 + \sin(\alpha) \sin(\gamma)\dots}{\tan(\phi) (1 - \eta \tan(\phi))}$$

$$\dots + \frac{\sqrt{\sin(\alpha)^2(\tan(\phi)^2\eta^2 + \sin(\gamma)^2 - 1) + \cos(\alpha)^2 \tan(\phi)^2(1 - 2 \tan(\alpha) \sin(\gamma)\eta)}}{\dots} \quad (\text{B.11d})$$

if $\eta = 0$

$$\tilde{\Theta}_{c\gamma}(\eta = 0) = \frac{\sin(\alpha) \sin(\gamma) + \sqrt{\sin(\alpha)^2(\sin(\gamma)^2 - 1) + \cos(\alpha)^2 \tan(\phi)^2}}{\tan(\phi)} \quad (\text{B.11e})$$

$$= \frac{\sin(\alpha) \sin(\gamma) + \sqrt{\cos(\alpha)^2 \tan(\phi)^2 - \sin(\alpha)^2 \cos(\gamma)^2}}{\tan(\phi)} \quad (\text{B.11f})$$

$$= \frac{\sin(\alpha) \sin(\gamma) + \sqrt{\cos(\alpha)^2 \tan(\phi)^2 - \tan(\alpha)^2 \cos(\alpha)^2 \cos(\gamma)^2}}{\tan(\phi)} \quad (\text{B.11g})$$

$$= \frac{\sin(\alpha) \sin(\gamma) + \sqrt{\cos(\alpha)^2(\tan(\phi)^2 - \tan(\alpha)^2 \cos(\gamma)^2)}}{\tan(\phi)} \quad (\text{B.11h})$$

$$= \frac{\sin(\alpha) \sin(\gamma) + \cos(\alpha) \sqrt{(\tan(\phi)^2 - \tan(\alpha)^2 \cos(\gamma)^2)}}{\tan(\phi)} \quad (\text{B.11i})$$

$$= \frac{\sin(\alpha) \sin(\gamma)}{\tan(\phi)} + \frac{\cos(\alpha) \sqrt{(\tan(\phi)^2 - \tan(\alpha)^2 \cos(\gamma)^2)}}{\tan(\phi)} \quad (\text{B.11j})$$

$$= \frac{\sin(\alpha) \sin(\gamma)}{\tan(\phi)} + \cos(\alpha) \sqrt{\frac{(\tan(\phi)^2 - \tan(\alpha)^2 \cos(\gamma)^2)}{\tan(\phi)^2}} \quad (\text{B.11k})$$

$$= \frac{\sin(\alpha) \sin(\gamma)}{\tan(\phi)} + \cos(\alpha) \sqrt{1 - \frac{\tan(\alpha)^2 \cos(\gamma)^2}{\tan(\phi)^2}} \quad (\text{B.11l})$$

if $\gamma = 0$

$$\tilde{\Theta}_{c\gamma}(\gamma = 0) = \cos(\alpha) \sqrt{1 - \frac{\tan(\alpha)^2}{\tan(\phi)^2}} \quad (\text{B.11m})$$

In section B.3 a translation formula is established to transform γ to the x-y plane. By substituting Equation B.12 into Equation A.16 it will change to Equation B.13.

$$\tan(\gamma) = \frac{\tan(\gamma_{xy})}{\cos(\alpha)} \quad (\text{B.12})$$

$$\tilde{\Theta}_{c\gamma_{xy}}(\eta = 0) = \frac{\sin(\alpha) \tan(\gamma_{xy})}{\cos(\alpha) \sqrt{1 + \frac{\tan(\gamma_{xy})^2}{\cos(\alpha)^2} \tan(\phi)}} + \cos(\alpha) \sqrt{1 - \frac{\tan(\alpha)^2}{\left(1 + \frac{\tan(\gamma_{xy})^2}{\cos(\alpha)^2}\right) \tan(\phi)^2}} \quad (\text{B.13})$$

B.5 Comparing section B.4 with literature

Soulsby (1997) has derived a similar formula to what has been derived in this derivation. This proves the formulas are equal, but use a different coordinate system. Figure B.2 shows the difference in coordinate systems.

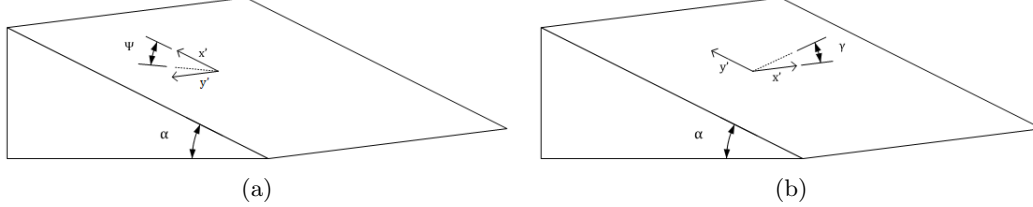


Figure B.2: Difference in coordinate systems between (a) Soulsby (1997) and (b) this thesis.

Soulsby states:

$$\tilde{\Theta}_{c\Psi} = \frac{\cos(\Psi) \sin(\beta) + \sqrt{\cos^2(\beta) \tan^2(\phi) - \sin^2(\Psi) \sin^2(\beta)}}{\tan(\phi)} \quad (\text{B.14})$$

In the previous section (Equation B.11) the following was found:

$$\tilde{\Theta}_{c\gamma} = \frac{\sin(\alpha) \sin(\gamma)}{\tan(\phi)} + \cos(\alpha) \sqrt{1 - \frac{\tan^2(\alpha) \cos^2(\gamma)}{\tan^2(\phi)}} \quad (\text{B.15})$$

From mathematics a shift of the cosine and sine can be described according to Equation B.16.

$$\begin{aligned} \cos(x + 90^\circ) &= \cos(90^\circ) \cos(x) - \sin(90^\circ) \sin(x) \\ &= 0 - \sin(x) \\ &= -\sin(x) \end{aligned} \quad (\text{B.16a})$$

$$\begin{aligned} \sin(x + 90^\circ) &= \cos(90^\circ) \sin(x) - \sin(90^\circ) \cos(x) \\ &= 0 + \cos(x) \\ &= \cos(x) \end{aligned} \quad (\text{B.16b})$$

$$(\text{B.16c})$$

The coordinate system that Soulsby uses (x'_Ψ and y'_Ψ) is in fact a rotation of the coordinate system that was used above (x'_γ and y'_γ) and therefore Ψ can be rewritten as function of γ . x'_Ψ should be rotated towards the x'_γ axis as is indicated in Figure B.3 and then be 'corrected' for γ , since the rotation is not 90° . Finally Ψ is expressed as follows: $\Psi = -90^\circ + \gamma$ or $\gamma = \Psi + 90^\circ$.

Equation B.15 can then be rewritten as follows:

$$\tilde{\Theta}_{c\Psi} = \frac{\sin(\alpha) \sin(\Psi + 90^\circ)}{\tan(\phi)} + \cos(\alpha) \sqrt{1 - \frac{\tan^2(\alpha) \cos^2(\Psi + 90^\circ)}{\tan^2(\phi)}} \quad (\text{B.17a})$$

$$= \frac{\sin(\alpha) \sin(\Psi + 90^\circ)}{\tan(\phi)} + \sqrt{\cos^2(\alpha) \left(1 - \frac{\tan^2(\alpha) \cos^2(\Psi + 90^\circ)}{\tan^2(\phi)} \right)} \quad (\text{B.17b})$$

$$= \frac{\sin(\alpha) \sin(\Psi + 90^\circ)}{\tan(\phi)} + \sqrt{\cos^2(\alpha) \left(1 - \tan^2(\alpha) \frac{\cos^2(\Psi + 90^\circ)}{\tan^2(\phi)} \right)} \quad (\text{B.17c})$$

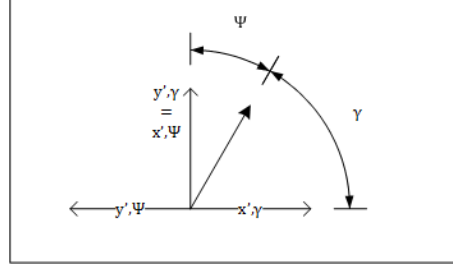


Figure B.3: Ψ and γ indicate the same direction in 2D.

$$= \frac{\sin(\alpha) \sin(\Psi + 90^\circ)}{\tan(\phi)} + \sqrt{\cos^2(\alpha) \left(1 - \frac{\sin^2(\alpha) \cos^2(\Psi + 90^\circ)}{\cos^2(\alpha) \tan^2(\phi)}\right)} \quad (\text{B.17d})$$

$$= \frac{\sin(\alpha) \sin(\Psi + 90^\circ)}{\tan(\phi)} + \sqrt{\cos^2(\alpha) - \sin^2(\alpha) \frac{\cos^2(\Psi + 90^\circ)}{\tan^2(\phi)}} \quad (\text{B.17e})$$

$$= \frac{\sin(\alpha) \sin(\Psi + 90^\circ)}{\tan(\phi)} + \sqrt{\frac{\cos^2(\alpha) \tan^2(\phi) - \sin^2(\alpha) \cos^2(\Psi + 90^\circ)}{\tan^2(\phi)}} \quad (\text{B.17f})$$

$$= \frac{\sin(\alpha) \sin(\Psi + 90^\circ)}{\tan(\phi)} + \frac{\sqrt{\cos^2(\alpha) \tan^2(\phi) - \sin^2(\alpha) \cos^2(\Psi + 90^\circ)}}{\tan(\phi)} \quad (\text{B.17g})$$

$$= \frac{\sin(\alpha) \sin(\Psi + 90^\circ) + \sqrt{\cos^2(\alpha) \tan^2(\phi) - \sin^2(\alpha) \cos^2(\Psi + 90^\circ)}}{\tan(\phi)} \quad (\text{B.17h})$$

with $\cos^2(x + 90^\circ) = \sin^2(x)$ **and** $\sin(x + 90^\circ) = \cos(x)$

$$= \frac{\sin(\alpha) \cos(\Psi) + \sqrt{\cos^2(\alpha) \tan^2(\phi) - \sin^2(\alpha) \sin^2(\Psi)}}{\tan(\phi)} \quad (\text{B.17i})$$

$$(\text{B.17j})$$

From this it follows that Equation B.15 and B.17j are equal. Q.E.D.

Appendix C

Additional information on particle model

C.1 Introduction

This appendix provides some additional information related to the particle model. The set of parameters that were used are described in more detail as well as the velocities that were used for the force calculations. Finally, a description is given of a number of additional boundary conditions that have been implemented in the particle model.

Equation C.1 shows the equation to calculate the particle Reynolds number. Since it was described that inertia should play a role for the equations of motion, it is assessed with this formula. If this parameter is larger than 100 inertia dominates. Assuming that the flow velocity near the bottom (u_b) is 0.5 m/s, the particle diameter (D) is 3 mm and the kinematic viscosity (ν) equals 10^{-6} m²/s, the particle Reynolds number is in the order of 1500. That means that inertia dominates in this region.

$$Re_p = \frac{u_b D}{\nu} \quad (\text{C.1})$$

However, if the grain size diameter of the River Waal is used (1-2 mm), the particle Reynolds number changes as well. For a similar near-bed velocity the particle Reynolds number changes to 500-1000, inertia still dominates. For this grain size diameter inertia dominates if the near-bed velocity is minimally 0.1 m/s.

C.2 Parameters

In the conceptual model generic results were presented, showing under which conditions sediment starts to move. Two parameters were varied, others were assumed to be constant. Below a list is presented with all the assumed constants and formulas.

The relative density is expressed by $s = \frac{\rho_s}{\rho_w} = 2.65$ and the submerged relative density equals

Table C.1: Additional information generic conceptual model

D	Particle diameter	$3 \cdot 10^{-3}$ m
ϕ	Natural angle of repose	30°
ρ_w	Density of water	1000 kg/m ³
ρ_s	Density of sediment	2650 kg/m ³
ν	Kinematic viscosity	10^{-6} m ² /s
C	Chézy coefficient	45 m ^{1/2} /s
g	Gravitational acceleration	9.81 m/s ²
C_d	Drag coefficient	0.5
C_l	Lift coefficient	0.6
k_s	Roughness of Nikuradse	0.15 m
μ_f	Static friction coefficient	$\tan(\phi) \approx 0.58$

$\Delta = \frac{\rho_s - \rho_w}{\rho_w} = 1.65$. To calculate the bed shear stress it is assumed that this varies linearly with the mean velocity (Schierck and Verhagen, 2012), but that it should be corrected with a dimensionless roughness factor. In other words $u_* = \frac{\bar{u}\sqrt{g}}{C}$. Note that the

C.3 Control volume

The control volume that was described in section 3.4 is schematised in Figure C.1. A mass balance between the bottom of the slope (in) and the top (out) is mathematically explained in Equation C.2.

$$Q_{in} = Q_{out} \quad (C.2a)$$

$$(\bar{u} \cdot dA)_{in} = (\bar{u} \cdot dA)_{out} \quad (C.2b)$$

$$(\bar{u}Bh)_{in} = (\bar{u}Bh)_{out} \quad (C.2c)$$

$$(\bar{u}h)_{in} = (\bar{u}h)_{out} \quad (C.2d)$$

$$\bar{u}_{in} = \frac{\bar{u}_{out}h_{out}}{h_{in}} \quad (C.2e)$$

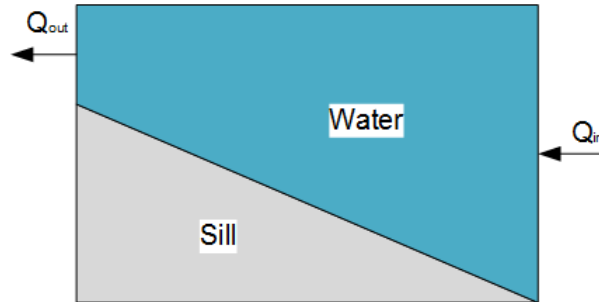


Figure C.1: Sketch of control volume

C.4 Velocities

According to van Rijn (1993, 2006) the flow velocity and particle velocity do not have the same angle. He describes the particle velocity (in the particle direction) and flow velocity (in the flow direction) as vectors. The difference between these vectors is the relative velocity. Decomposing the flow (\vec{u}_f) and particle (\vec{v}_p) vector in two components and summarising them, lead to a relative velocity vector (\vec{u}_r). This decomposition of the velocity vectors has been used in the conceptual model.

$$\vec{u}_f = \begin{bmatrix} u_{f,x'} \\ u_{f,y'} \end{bmatrix}, \quad \vec{v}_p = \begin{bmatrix} v_{p,x'} \\ v_{p,y'} \end{bmatrix} \quad \text{and} \quad \vec{u}_r = \begin{bmatrix} u_{r,x'} \\ u_{r,y'} \end{bmatrix} \quad (\text{C.3})$$

The forces that are described in chapter 2 and 3 use the decomposed velocities. At each location the forces are calculated in the local coordinate system. These forces are then used in the equations of motion.

The near-bed flow velocity is assumed to be at 1% above the zero-velocity level. This assumption is debatable, since the results show that this value is approximately six times larger than the shear velocity in the computational domain. Nevertheless, the 1% is an assumption that can be changed in the future and therefore recommendations are made for this.

C.5 Boundary conditions

In the particle model three boundary conditions were imposed, two related to the computational domain, one to the flow conditions.

- The particle cannot exceed the left or right side of the computational domain.
- The computation is stopped once the particle has reached the downstream end.
- If the flow does not exceed the conditions belonging to initiation of motion, the computation is stopped.

Appendix D

Set-up of numerical Delft3D FLOW model

D.1 Introduction

Numerical computations have been performed in the numerical flow and transport model Delft3D-FLOW (Deltares, 2014). The Delft3D model is used to generate a flow field, which includes water levels, flow velocities and flow angles. This is used as an input for the particle model.

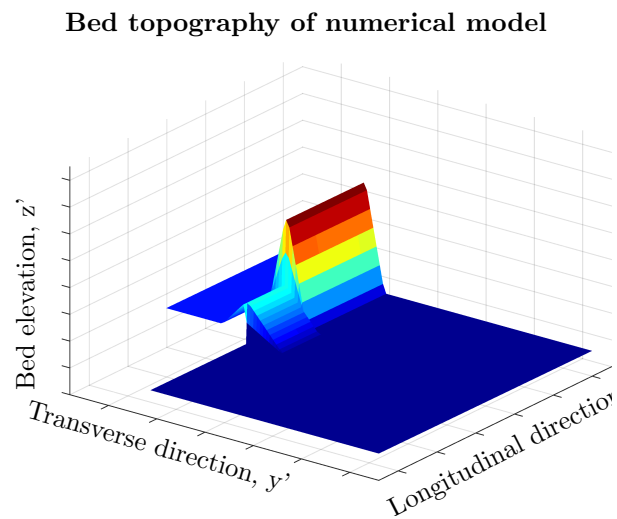


Figure D.1: Numerical grid in Delft3D showing the bed topography that is used. The colours indicate the elevation level. The side channel is light blue, the main channel dark blue, the longitudinal training dam is red and the sill is located in front of the longitudinal training dam. The flow is from right to left.

D.2 Set-up of model

The computational domain was 320 m wide and 1.1 km in length, the width of the upstream part (first 500 m) of the river is 230 m, afterwards it widens to 320 m. At the location where the river widens an inlet sill of 200 m in longitudinal direction has been incorporated in the bathymetry which divides the river in a main and side channel. The final 400 m the river is separated by a longitudinal training dam of 8 m high. Note that the bathymetry of the side channel is 1 m higher than the main channel and that the side slope of the longitudinal training dam sill as well as the longitudinal training dam itself is 1:2.5. Figure D.1 shows the computational domain that was used in 3D.

At first a grid was selected of 10x10 m, a time step of 0.005 min and three boundary conditions. Upstream a discharge boundary of 2000 m³/s was chosen, while downstream two water levels were chosen of 6.27 and 6.37 m in the side and main channel respectively. These boundary conditions are based on a one dimensional approximation of the main and side channel, for more information see van Linge (2017), this one dimensional model makes use of backwater curves. Later the upstream discharge has been reduced to 1500 m³/s, which was assumed to be a better approximation of the average flow velocity in the River Waal. The downstream water levels were used to steer the flow distribution between both channels. Nevertheless, the set-up of the model was done with a upstream discharge of 2000 m³/s.

A trade-off is generally made between accurate answers and reasonable computation time. Therefore, the optimal fineness of the grid and time step were chosen and the spin-up time was estimated.

D.2.1 Grid refinement

The grid has been refined up to 5 times, during the process of grid refinement the boundary conditions were unchanged. In Figure D.2 the grid refinement is plotted versus the depth average velocity at 2/3 of the inlet. This location was chosen because from the model results it was observed that on this location the highest flow velocities occurred. In addition, the relative discharge over the inlet was plotted versus the fineness of the grid. All in all it appears that after a grid refinement of 3 no significant changes occurred anymore.

D.2.2 Time step

Another aspect that has been investigated to reduce the computation time is the timestep. The *Courant number* is used as a first indicator to determine the maximum time step that is allowed so that the physical domain of dependence is within the numerical domain of dependence Zijlema (2016). The Courant number includes the maximum flow velocity u , time step Δt and smallest grid size Δx . In this case the maximum flow velocity will be in the order of 1.8 m/s (according to computations with very small time steps) and the smallest grid size is 3.3 m (grid refinement = 3). This gives a maximum time step in the order of 1.8 s = 0.03 min. The result of time step increase has been plotted in Figure D.3, it becomes clear that increasing the time step up to 4 times $\Delta t = 0.02$ min gives a stable answer. Note that the boundary conditions were unchanged in this optimisation step. Therefore for further computations a time step of 0.02 min and a grid refinement of 3 is used.

$$C = \frac{u\Delta t}{\Delta x} \leq 1 \tag{D.1}$$

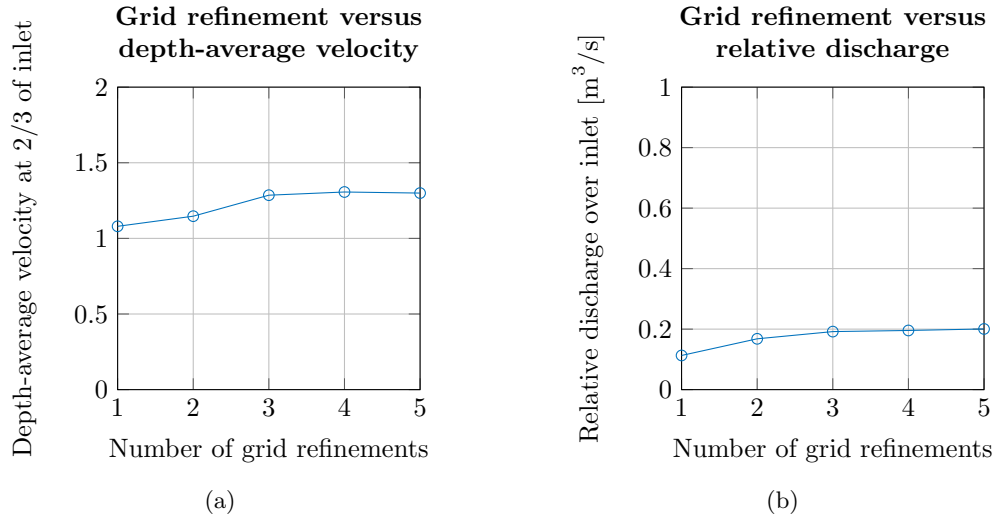


Figure D.2: Grid refinement versus the depth-averaged velocity and the relative discharge over the sill. It is observed that both parameters converged to a fixed value after a certain grid refinement.

D.2.3 Spin-up time

After the grid refinement and timestep were selected the simulation time was determined. In earlier computations the simulation time was assumed to be 1 hr, but to investigate at which time the simulation was well converged a simulation of 5 hrs was tested. It appeared from this test that after 1.5 hr there was no significant spin-up effect noticeable anymore, see Figure D.4.

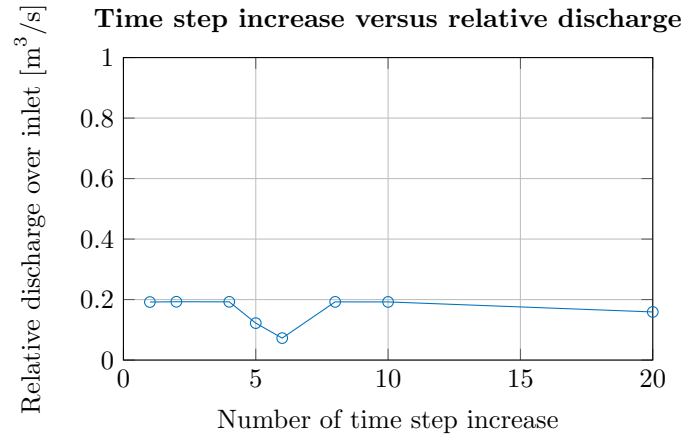


Figure D.3: The time step was chosen at $\Delta t=0.005$ min. This time step has been increased. For an increase up to 4 times the original time step, the relative discharge over the inlet sill does not change.

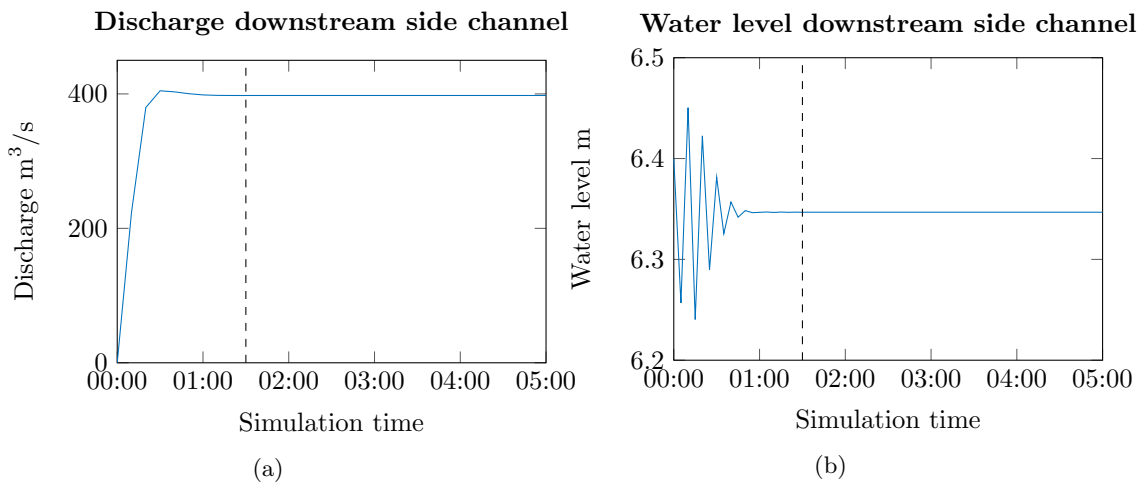


Figure D.4: This figure shows after what time the spin-up disappeared. This test has been performed for a discharge of 2000 m³/s and it appeared that after 1.5 hrs a steady flow field is generated.

D.3 Indetermination

Selecting two water level boundary conditions downstream can become problematic if the inlet longitudinal-training-dam sill is increased. Replacing one of the water level boundary conditions with an appropriate discharge boundary condition can be a solution to that problem. Figure D.5 shows what happens to the water level in case the crest height of the sill is increased and a different boundary condition is chosen. In the case a water level is chosen downstream of the side channel a super critical flow occurs over the sill, while for a discharge boundary downstream of the side channel a subcritical flow occurs. This can be explained by the fact that there are two much degrees of freedom for the model to get to a similar answer as the quasi one dimensional model. Moreover, the particle model is expect to predict given certain conditions (e.g. distribution of water between main and side channel) whether sediment particles enter the side channel. However, for crest heights of the inlet sill of 3 m or lower indetermination did not occur.

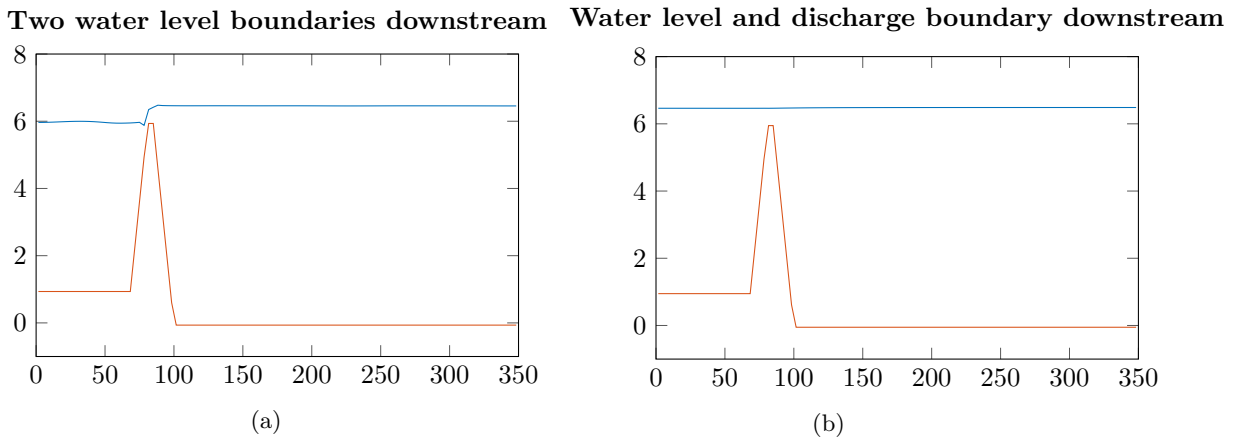


Figure D.5: Cross section with (a) two water level boundaries and (b) a water level and discharge boundary downstream. The crest height of the sill is 6 m in this case, which causes a large water level difference between the main channel and the side channel.

Another solution is to elongate the main channel and side channel to a domain that stretches from upstream to downstream the longitudinal training dams. In this case only two boundary conditions need to be imposed and there is probably no indetermination anymore. This elongation has not been performed, since the sill crest was assumed to be 3 m above the main channel and thus that indetermination would not occur.

D.4 Additional information

Increasing the crest height of the inlet longitudinal training dam sill, the upstream discharge boundary or the bed elevation of the side channel effects the discharge distribution and the water levels in the main and side channel. The reference case has a inlet crest height of 3 m, discharge boundary upstream of $2000 \text{ m}^3/\text{s}$ and a bed elevation of the side channel of 1 m.

Table D.1: Relative discharge for various inlet crest height

Inlet crest height (m)	Water level side channel (m)	Water level main channel (m)	Discharge side channel (m ³ /s)	Relative discharge over inlet (%)
0	6.33	6.34	421.0	21.0
1	6.31	6.35	392.0	20.0
2	6.29	6.36	365.0	18.0
3	6.27	6.36	323.0	16.0
4	6.24	6.38	258.5	13.0
5	6.20	6.40	153.0	8.0
6	6.18	6.43	98.0	2.0
7	6.18	6.44	0.0	0.0

Table D.2: Distribution of discharge for increasing discharge

Discharge upstream (m ³ /s)	Water level side channel (m)	Water level main channel (m)	Discharge side channel (m ³ /s)	Relative discharge over inlet (%)
100.0	0.6	0.9	0.0	0.0
500.0	2.3	2.6	0.0	0.0
750.0	3.1	3.3	33.5	4.0
1000.0	3.9	4.0	106.0	11.0
1500.0	5.1	5.3	221.5	15.0
2000.0	6.3	6.4	323.0	16.0
3000.0	8.3	8.4	507.0	17.0
5000.0	11.7	11.8	750.5	15.0
10000.0	17.6	18.8	1500.0	15.0
15000.0	24.5	24.6	2250.0	15.0

Table D.3: Distribution of discharge for increasing discharge

Bed level elevation side channel (m)	Water level side channel (m)	Water level main channel (m)	Discharge side channel (m ³ /s)	Relative discharge over inlet (%)
0.0	6.25	6.36	364.0	18.0
0.5	6.26	6.36	345.0	17.0
1.0	6.27	6.36	323.0	16.0
1.5	6.28	6.37	299.5	15.0
2.0	6.30	6.38	272.5	14.0
2.5	6.31	6.38	242.0	12.0
3.0	7.70	6.27	800.0	40.0

D.5 Coupling with particle model

In the particle model the water levels, flow velocities and the flow angles are used. For every element it is described how this is implemented in the model.

Water level

The water level is computed at every location, together with the local bottom this gives the water depth. The water depth is used in the computation to compute the near bed flow velocity. In chapter 3 it was described that at 1% of the local water depth above the zero-velocity level the local near-bed velocity has been defined.

Flow velocity

The mean flow velocity of the Delft3D model is used to determine the local shear velocity. This is then used in the calculation of the local near-bed flow velocity as well. The local particle velocity is subtracted from the local near-bed flow velocity, which gives the local relative velocity.

Flow angle

The local flow velocity angle is used to determine the ratio between the near-bed flow velocity in longitudinal and transversal component. Together with the local particle velocities in both directions this gives the relative velocities in both directions as well. Furthermore, in chapter 2 it has been explained that the flow angle influences the critical shear velocity, therefore this flow angle is used to determine this parameter.

